Elasto-Plastic Behavior of Composite Beam Connected to RHS Column

MOHAMMADREZA ESLAMI

(Degree)
博士（学術）

(Date of Degree)
2014-03-25

(Date of Publication)
2015-03-01

(Resource Type)
doctoral thesis

(Report Number)
甲第6074号

(URL)
https://hdl.handle.net/20.500.14094/D1006074

Doctoral Dissertation

Elasto-Plastic Behavior of Composite Beam Connected to RHS Column

角形鋼管柱に接合される合成梁の弾塑性挙動

January 2014

Graduate School of Engineering

Kobe University

Mohammadreza Eslami

Acknowledgement

I must first express my sincere gratitude and thanks towards my supervisor Associate Professor Namba for his patience, motivation, enthusiasm, and immense knowledge. I will forever be thankful for encouraging my research and his invaluable advices on both research as well as on my career. His guidance helped me in all the time of research. He provided the vision necessary for me to proceed through this program and this research would not have been possible without his help and support.

My sincere thank also goes to Professor Tanaka and Professor Otani for the lecturing of courses which helped me develop my structural engineering knowledge. Special thanks for Professor Tabuchi, Professor Tanaka and Professor Taga who kindly arranged several technical visits of under construction projects and steel structural factories. They provided me the opportunity to get familiar with the technologies of steel structures in Japan.

I will forever be thankful to Assistant Professor Asada for all his kindness and encouragement, and other students in the steel structure laboratory of Kobe University for their friendship and help. Special thanks to Fukuoka for his efforts and kind cooperation in experimental tests and data processing of results. Special thanks for Rahimina, my friend for his support during the research.

I would like to appreciate the committee members, Professor Tanaka, Professor Taga and Professor Tani for their time, interest and helpful comments for this dissertation and oral defense.

I gratefully acknowledge the Ministry of Education of Japan (Monbukagakusho) for providing me the opportunity of arrival in Japan and for the financial support during the one and half year period of research student before the start of this Ph.D. course. My sincere thanks to Professor Tabuchi and Professor Takada for their support to start in the Kobe University. Thanks to Takanory Okuyama for his kind tutorial for adaptation to the life during the early months of arrival in Japan. Also thanks to the Kobe University International Student Center (KISC), which provided me this opportunity to make Ph.D. work possible. Especial thanks to Assistant Professor Kawai and Assistant Professor Kuroda for their kind advices and encouragement.

Last, but by no means the least, I thank my family. Words can not express how grateful I am to my parents for their kindness and for letting me through all difficulties and faithfully supported me in my student life. And most of all for my patient and supportive wife for all her efforts and patience during last six years.

Mohammadreza Eslami

January 2014

Abstract

When a steel moment frame is subjected to seismic forces, in positive bending due to the RC slab resisting compression, flexural strength and stiffness of the beam can be increased due to “composite action”. At the same time despite these advantages, composite action increases the strain at the beam bottom flange and it might affect the plastic rotation capacity of beam.

However, in current structural design, rotation capacity of composite beam is supposed to be equal to the bare steel beam. Furthermore, in the case of composite beam-to-RHS column connection, due to effects of out-of-plain deformation of column flange, stress condition of web in the composite beam might be more severe, comparing with bare steel beam.

This research is aimed to clarify the mechanical mechanism how composite action affect to the web connection and what determine web connection behavior. As the first part of this research, elasto-plastic behavior of composite beam is studied through experimental tests on full scale sub-assemblies. Behavior of composite beams which were connected to RHS columns with two different width-to-thickness ratios (*B/t*) of 29 and 22 are studied. Bare steel beam specimen with width-to-thickness ratio of 29 was also prepared as a reference for beam behavior.

Experimental test showed that reduction of RHS column width-to-thickness ratio in composite specimens, did not result to considerable difference in the elastic stiffness and actual plastic strength in positive flexure, but considerable improvement in the cumulative rotation capacity and 10% increase of beam ultimate strength was observed. Experimental test results revealed another specific difference between composite specimens. It was observed that in the specimen with smaller width-to-thickness ratio severe concrete bearing crush happened at the vicinity of column face. Investigations about the contribution of concrete slab on the different strain condition of flanges were conducted and it was observed that following to occurrence of this crush in the slab, reduction in the rate of strain of lower flange happened. However, in the composite specimen with larger width-to-thickness ratio of 29 clear crush was not observed and strain condition was quite higher than the bare steel beam. It is believed that this behavior resulted to significant effect on the improvement of rotation capacity.

During the experimental test, observations regarding the occurrence of damages in the

steel beam and concrete slab were studied, especially focusing on flange fractures which mainly determine rotation capacity of beams. It was observed that in all specimens regardless of existence of concrete slab or width-to-thickness ratio of RHS column, first crack initiation was occurred at the root of weld access hole (scallop). For the composite beam specimen with large width-to-thickness ratio of 29 this occurred at earlier stage with higher progress, comparing with the bare steel beam with same width-to-thickness ratio. Final failure pattern was determined by propagation of this crack. Composite action resulted to 1.27 times increase of actual plastic strength and 1.92 times increase of stiffness in positive flexure, comparing with bare steel beam connected to RHS column with same with-to-thickness ratio. But cumulative rotation capacity of composite beam reduced to half of bare steel beam. Strain study in the first cycle of +2.0 θ_p showed that composite action increased the strain amount of lower flange 2.2 Times of bare steel beam. This strain condition resulted to early crack initiation with higher progress, and finally reduction of rotation capacity of composite beam.

In the composite beam connected to RHS column with smaller width-to-thickness ratio of 22, strain behavior study showed that in the first cycle of +2.0 θ_p , the amount of strain in the lower flange was 0.55 times smaller than composite specimen with width-to-thickness ratio of 29 and 1.2 times more than bare steel beam, but after the occurrence of sever crush in the concrete slab, sudden reduction of strain in the lower flange happened. This resulted to smaller rate of strain increase, even comparing with the bare steel beam. Finally, this resulted to initiation of crack in the later stage of loading. Considerable higher rotation capacity was observed in this specimen.

Occurrence of concrete crush can be considered as the start of removal of composite effect and start of closing to the bare steel beam condition. This showed that further investigation about the mechanism of stress transfer and strain concentration in the composite beam is needed.

Following to the experimental test observations of three full-scale beam-to-RHS column sub-assemblies, further comprehensive understanding of elasto-plastic behavior of composite beam was needed to show the effect of out-of-plain deformation of RHS column on the behavior of composite beam.

In the second part of this research, finite element analysis and limit analysis were carried out to clarify the structural condition of web connection. By the limit analysis, investigations about the ultimate flexural capacity of web connection was conducted.

According to past researches, effect of out-of-plain deformation was mostly considered based on the concern regarding reduction of web flexural capacity. This limit analysis were conducted to clarify the structural condition of web, not only based on the flexural capacity considerations, but also by considering the effect of axial force subjected to the web connection. Actually it is already known that increase of RHS column width-to-thickness ratio results to movement of neutral axis (NA) toward top flange, but according to this research approach interaction of different width-to-thickness ratio and different axial force (N) can be considered simultaneously. Furthermore, FEA study is conducted to understand the mechanical effects of composite action and out-of-plain deformation of RHS column on the elasto-plastic behavior of composite beam. Mechanism of mechanical stress transfer and strain concentration is explained and correspondence between FEA and limit analysis is shown.

It was found that start of concrete bearing crush is corresponding to the start of stress increase of top flange. It was also found that maximum web axial force does not always happen at same time with start of softening of slab concrete. In fact, in large width-to-thickness ratios reduction of axial force is first treated by flange. Top flange yield can be considered as a bench mark in the change of behavior of composite beam.

Mechanism of strain concentration is explained. It is shown that in the bare steel beam and composite beam the difference between strain corresponding to the reduction of web flexural capacity is small. However, difference between strain condition of bare steel beam and composite beam is determined by the axial strain. It is shown that reduction of web flexural capacity does not result to further additional strain concentration, comparing with the bare steel beam. While axial strain due to movement of neutral axis result to more sever condition of strain in the composite beam.

It was shown that effect of composite action to the curvature in not considerable. While effect of width-to-thickness ratio to the curvature and movement of neutral axis is considerable. So, the additional axial strain in the composite beam is strongly depending on the width-to-thickness ratio of RHS column

According to experimental test observations and findings of FEA, it was understood that in composite beam connected to RHS column with large width-to-thickness ratio of 29 effect of axial force to the out-of-plain deformation is considerable and as a result high amount of strain on the lower flange exists and this may result to significant reduction of rotation capacity. In order to prohibit strain concentration on the lower flange, it is recommended to avoid composite action. Application of slit between the column face and concrete slab is recommended in this width-to-thickness ratio which has been proposed by Tagawa et al. The behavior of this type of composite beam is studied in the next part of this research.

According to that proposal, slit may reduce the composite action effects, but comprehensive investigations regarding contribution of studs which are located on transverse beam and loading beam in the composite action has not been carried out yet.

Experimental test results showed that existence of slit could reduce the strain on the lower flange, but improvement of behavior regarding rotation capacity could be obtained by the removal of studs at the vicinity of connection.

Finite element study showed that application of slit result to considerable reduction of axial force on the web connection. But in large width-to-thickness ratio of 29 despite the existence of slit, still web is subjected to axial force. Removal of first stud on the loading beam did not result to reduction of web axial force, but removal of stud on the transverse beam resulted to the reduction of web axial force to almost half.

Studs of transverse beam contribute in the composite action. It could be explained that these studs provide constraint condition for the slab and it may be the reason of contribution in the composite action. It is shown that roll of studs of transverse beam are similar to bearing stress transfer between slab and column face.

Contribution of studs of transvers beam depends on the location of stud. Due to torsional behavior of transvers beam, second stud shear force is considerably smaller than the first stud. So number of studs can be kept according to calculations, and just movement of first stud away from the column face is recommended. Considering the actual seismic loading, removal of studs at the vicinity of connection on both loading and transverse beam is recommended.

Finally, following to experimental test observations and mechanical investigations by FEA, a model is proposed to represent the restraining characteristics of composite beam connected to RHS column. In all specimens acceptable good correspondence obtained from conducted analysis by this model and experimental test results.

Contents

Nomenclature

t_{bw}	Beam web thickness	Mm
d_{bw}	Beam web depth	Mm
A_{bw}	Beam web section area	mm^2
t_{bf}	Beam flange thickness	Mm
B_f	Beam flange width	Mm
A_{bf}	Beam flange section area	mm^2
${}_{bw}\sigma_y$	Beam web actual yield stress	N/mm^2
${}_{bf}\sigma_y$	Beam flange actual yield stress	N/mm^2
${}_{b}\sigma_y$	Beam actual yield stress	N/mm^2
A_s	Cross-sectional area of steel beam section	mm^2
${}_{bf}M_p$	Plastic moment capacity of beam flanges	kN.m
${}_{bw}M_p$	Plastic moment capacity of beam web	kN.m
${}_{bf}Z_p$	Plastic modulus of beam flange	mm^3
${}_{bw}Z_p$	Plastic modulus of beam web	mm^3
${}_{b}K_e$	Beam elastic stiffness	kN.m/rad
${}_{b}K_p$	Beam plastic stiffness	kN.m/rad
$M_{b(1/6)}$	Actual Beam plastic moment by 1/6 stiffness method	kN.m
${}_{b}M_p$	Theoretical beam plastic moment	kN.m
${}_{bw}M$	Moment transferred by beam web	kN.m
θ_b	Beam rotation angle	Rad
${}_{c}\sigma_y$	Column yield stress	N/mm^2
B	Widths of RHS Column section along face transferring load	Mm
t_{cf}	RHS Column flange thickness	Mm
B/t_{cf}	Width-to-thickness ratio of RHS column	-
${}_{cf}Z_p$	Plastic modulus of column flange	mm^3
t_D	Diaphragm plate thickness	Mm
S	Height of beam web weld access hole (scallop)	Mm
s	Nondimensional height of beam web weld access hole (scallop)	-
E_s	Young's modulus of elasticity of steel beam	N/mm^2
G	Material shear modulus	N/mm^2

l	Beam length	Mm
l_b	Beam net length	Mm
M	Beam moment at column face	kN.m
${}_cM_p$	Theoretical composite beam plastic moment	kN.m
${}_jM_{wu}$	Ultimate flexural strength of beam web connection	kN.m
N_w	Axial force acting on beam web connection	kN.m
m_0	Nondimensional ultimate flexural strength of web connection	-
n	Nondimensional axial force of web connection	-
${}_jM_u$	Ultimate flexural strength of connection	kN.m
d_j	Depth of connection	Mm
b_j	Width of connection	Mm
r	Ratio of depth over width of connection	-
α	Nondimensional depth of beam web yield region	-
β	Nondimensional height of location of neutral axis of composite beam	-
Σd_i	Internal energy dissipation in the yield lines of beam-to-RHS column connection collapse mechanism	
${}_vE$	Charpy impact absorbed energy	kJ
δ_{co}	Crack opening near the root of the weld access hole (Scallop)	Mm
ε	Engineering strain in tensile test of material	-
η_b	Normalized cumulative beam plastic rotation	-
θ_b	beam rotation angle	Rad
θ_p	Beam rotation corresponding to the plastic moment capacity	Rad
$\Sigma\theta_p$	Cumulative plastic rotation	Rad
${}_b\delta_p$	Deformation corresponding to the beam plastic moment	Mm
$N_{f\,U}$	Upper flange compression force	kN
$N_{f\,L}$	Lower flange tensile force	kN
σ	Engineering tensile stress in material tensile test	N/mm^2
q_s	The nominal shear strength of one stud	kN
Q_h	The nominal shear force between the steel beam and the concrete slab	kN
f_c	Concrete compressive strength	N/mm^2
t_c	Concrete slab thickness	Mm
B'	Effective width of concrete slab in the composite beam	Mm
A_c	Area of concrete slab within effective width	mm^2

N_c	Concrete slab compression force	N
E_c	Concrete modulus of elasticity	N/mm^2
${}_sI$	Moment of inertia of steel beam section	mm^4
${}_cI_n$	Moment of inertia of the composite beam about the neutral axis of composite beam section	mm^4
x_n	Distance between location of neutral axis of composite beam to the concrete slab surface	Mm
${}_sd$	Distance between composite beam slab surface to the center of gravity of steel beam	Mm
h_r	Nominal Height of rib in the steel deck of composite beam	Mm
h_c	Distance between center of gravity of slab to the center of gravity of steel beam in the composite beam	Mm

1. Introduction

1.1 Background

Commonly in steel frames, steel beam and concrete slab are connected together by shear keys to work as a unit member which is called “composite beam”.

When a composite beam is subjected to positive bending, flexural strength and stiffness of the beam can be increased due to “composite action”. At the same time despite these advantages, composite action increases the strain at the beam bottom flange and it might affect beam plastic rotation capacity.

In Japan, during the 1995 Hyogo ken-Nanbu earthquake, a number of steel moment frame buildings were found to have experienced fracture at beam-to-column connections[1-1)~1-2)]. After the earthquake, based on extensive researches, welding process and weld joint details were revised to improve beam plastic rotation capacity. These extensive researches were mostly conducted on the bare steel beam and limited test data regarding the composite beam is available.

In the case of beam-to-RHS column connection, beam flanges are usually connected to column by through diaphragms to achieve smooth stress transfer from beam flange to column. On the other hand, beam web is connected to RHS column wall (flange) directly without any reinforcement. This might cause local out-of-plane deformation of column flange at the beam web-to-column connection due to flexural moment transmitted by the beam web. It has been already known that in the case of bare beam connected to column with large width-to-thickness ratio, full capacity of beam web cannot be transmitted in the web-to-column connection. This strength reduction due to local out-of-plane deformation causes strain concentration of beam flange at the vicinity of connection, and finally reduction of plastic rotation capacity of beam-to-column connection happen. Actually in Japan these effects have been considered in “Recommendation for Design of Connections in Steel Structures” for design of beam-to-column connections[1-3)], but in the case of composite beam to RHS column connection,

effects of out-of- plane deformation of column flange have not been well understood. In fact, due to the composite action, stress condition of web in the composite beam might be more severe compared to bare steel beam, shown in Figure1.1.
Considering the fact that in the current structural design, rotation capacity of composite beam is supposed to be equal to the bare steel beam, importance of further study on the elasto-plastic behavior of composite beam-to-RHS column can be understood.

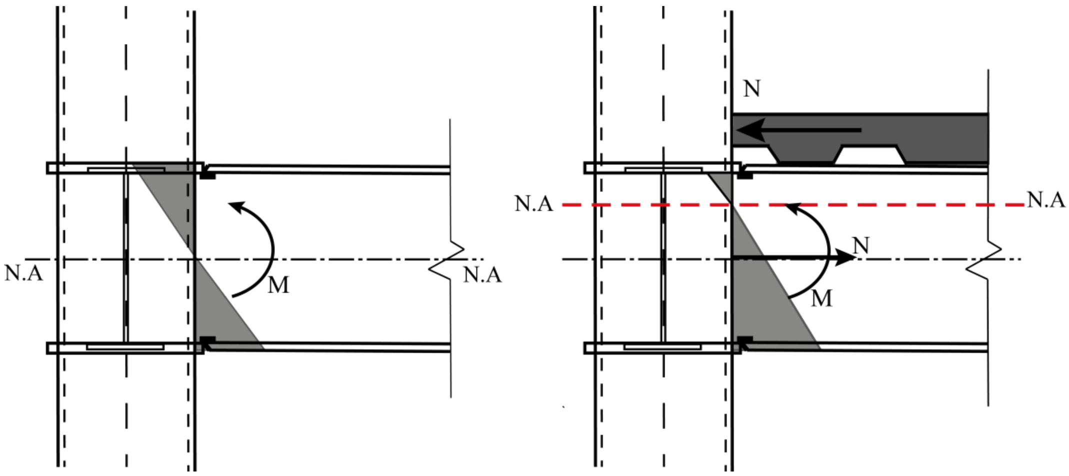

(a) Bare steel beam (b) Composite beam

Fig 1.1 Strain concentration on the lower flange of composite beam in the positive flexure

1.2 Past researches and investigations about rotation capacity of composite beam

According to past researches conducted by Okada et al.[1-4], plastic rotation capacity of composite beam connected to RHS column decrease to almost half of bare steel beam. That investigation was conducted on specimens which were consisted of RHS column with width-to-thickness ratio of 21. Further Research by Okada[1-5] were conducted on the composite beams which were connected to the H-section and RHS columns with larger width-to-thickness ratio of 24 and 38, and it was shown that significant reduction of composite beam rotation capacity will occur in the case of RHS column with large width-to-thickness ratio. Okada showed that out-of- plane deformation of RHS column is affected by reduction of web flexural capacity and movement of neutral axis toward beam top flange. However, in these two investigations, post-earthquake connection details for the beam weld access hole (scallop) geometry were not considered.
Matsuo[1-6] could apply post-earthquake provisions in his study on the rotation capacity of composite beam, but that investigations were just focused on the RHS column with

width-to-thickness ratio of 29. According to his test results, rotation capacity of composite beam specimens were almost half of bare steel beam specimens, shown in Figure 1.2.

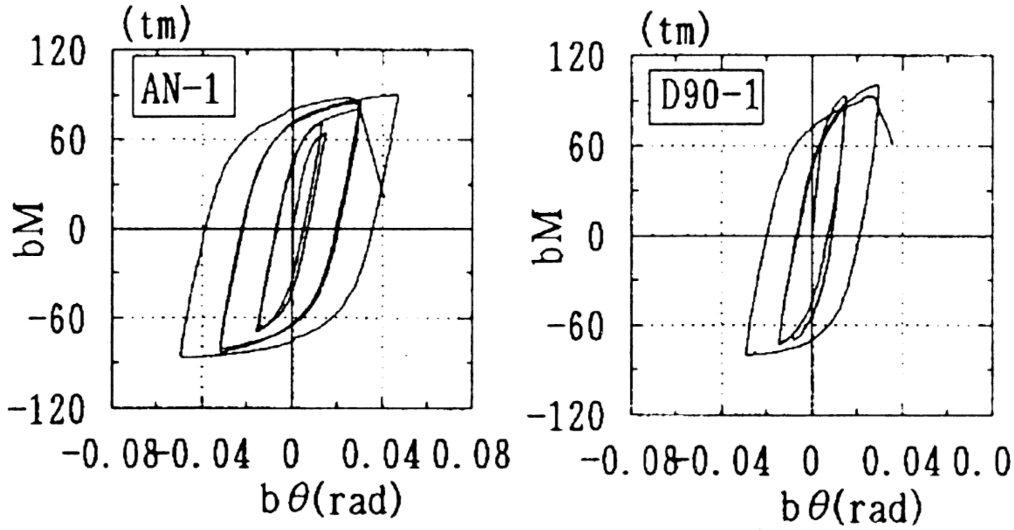

(a) Bare steel beam (b) Composite beam

Fig. 1.2 Results of experimental test on the composite beam conducted by Matsuo [1-6)]

Evaluation of rotation capacity of composite beam connected to RHS column was investigated by Tanaka et al. [1-7)] through series of experimental tests on the specimens with two different width-to-thickness ratios of 16 and 38. Post-earthquake provisions were used in that investigation, but the specimens were subjected to repeated plastic strain and the applied loading protocol in that research had constant amplitudes of 1.2θ_p, 2.0 θ_p and maximum 3.0 θ_p.

Further experimental study on the rotation capacity of composite beam connected RHS column with application of post earthquake provisions and sever loading protocol is needed.

1.3 Features of this research

According to past researches, effect of out-of-plane deformation was mostly considered based on the concern regarding reduction of web flexural capacity. However, effects of axial force subjected to the web connection needs further considerations and investigation. This research is aimed to clarify the mechanical mechanism how composite action affect to the web connection and what determine web connection behavior.

Behavior of composite beam connected to the RHS column with two different width-to-thickness ratios are studied through experimental tests. Results of different strength and

rotation capacity of beams are discussed through the study on the different damages in the steel beam and concrete slab. Also strain studies were carried out to investigate the effects of lower flange strain on the rotation capacity of composite beam.
Following to the experimental test observations, and in order to obtain comprehensive understanding of elasto-plastic behavior of composite beam, finite element analysis (FEA) and limit analysis and were carried out to clarify the structural condition of web connection. Mechanism of mechanical stress transfer and strain concentration is explained and correspondence between FEA and limit analysis is shown.
In the case of composite beam connected to RHS column with large width-to-thickness ratio of 29, recommendations for improvement of seismic behavior and rotation capacity are shown based on the experimental test and finite element analysis study.
Finally, based on the understanding of mechanical behavior, a model for prediction of restraining characteristics of composite beam connected to RHS column is proposed.

1.4 Description of chapters

This dissertation is consisted of six chapters as follows:

Chapter 1. Introduction

Background of previous researches regarding the rotation capacity of composite beam is presented, motivation and features of this study are described.

Chapter 2. Effects of Width-to-Thickness Ratio of RHS Column (B/t) on the Elasto-Plastic Behavior of Composite Beam

Results of experimental study on the elasto-plastic behavior of composite beam connected to Rectangular Hollow Section column (RHS column) in the steel moment resisting frame buildings are presented in this chapter. In order to investigate the effects of width-to-thickness ratio of RHS column on the rotation capacity of composite beam, cyclic loading test were conducted on three full scale beam-to-column subassemblies. Detail study on the different steel beam damages and concrete slab damages are presented. Investigations about the contribution of concrete slab on the different strain condition of top and bottom flanges are also conducted through the study on the strain behavior. Results of different strength, stiffness and rotation capacity of beams are reported. It is shown that lower flange strain condition affect the rotation capacity of composite beam.

It was found that occurrence of concrete crush can be considered as the start of removal of composite effect and start of closing to the bare steel beam condition. This showed the importance of further investigation about the mechanism of stress and strain transfer of composite beam.

Chapter 3. Mechanism of Elasto-Plastic Behavior of Composite Beam Connected to RHS Column

In this chapter, research is conducted to clarify the structural condition of web connection, not only based on the flexural capacity considerations, but also by considering the effect of axial force subjected to the web.

Investigation about the ultimate flexural capacity of web connection is conducted by the limit analysis. Interaction effects of both axial force and flexural moment on the capacity of composite beam web connection is shown simultaneously. Reduction of web connection capacity of composite beam due to increase of RHS column width-to-thickness ratio is shown by equations which are derived by limit analysis. Furthermore, FEA study is conducted to understand the effects of composite action and width-to-thickness ratios of RHS column on the elasto-plastic behavior of composite beam. Mechanism of mechanical stress transfer and strain concentration is described with application of FEA.

Correspondence between FEA and limit analysis is shown and a method for evaluating the ultimate flexural strength of connection is presented by considerations regarding out-of-plane deformation of column flange. Finally the accuracy of proposed method is confirmed by the results of experimental loading tests which were presented in the Chapter 2 and also previous experimental research studies.

Chapter 4. Improvement of Seismic Behavior of Composite Beam Connected to RHS Column with B/t=29

In order to prevent excessive reduction of composite beam rotation capacity, in this part of study “slit” is provided between the concrete slab and column face. It is already known that slit may reduce the composite action effects, but comprehensive investigations regarding contribution of studs which are located on the transverse beam and loading beam in the composite action has not been carried out yet.

In this chapter, results of behavior of composite beam with slit and different arrangement of studs are compared with the behavior of bare steel beam and conventional type of composite beam through a series of experimental test study and finite element analysis.

Chapter 5. Modeling of Composite Beam Connected to RHS Column

Following to experimental test observations and mechanical understandings obtained by finite element analysis, in this chapter a model is proposed to represent the restraining characteristics of composite beam connected to RHS column.

Chapter 6. Conclusions

Observations, results, findings of behavior of composite beam, and new model which is developed during this research are summarized and concluded in this chapter

2. Effects of Width-to-Thickness Ratio of RHS Column (*B/t*) on the Elasto-Plastic Behavior of Composite Beam

2.1 Introduction

It is already well known that in the bare steel beam connected to RHS column with large width-to-thickness ratio, full capacity of beam web cannot be transmitted in the web-to-column connection due to out-of-plane deformation of column web. In composite beam connection, due to the composite action, stress condition of web might be more sever compared to the bare steel beam. Limited experimental test data about the composite beam connected to RHS column exist. Effect of RHS column width-to-thickness ratio were studied by Okada et al.[2-1)], and it was shown that plastic rotation capacity of composite beam connected to RHS column decrease to almost half of bare steel beam. That investigation was conducted on specimens which were consisted of RHS column with width-to-thickness ratio of 21. Further Research by Okada[2-2)] were conducted on the composite beams which were connected to the H-section (representing a RHS column which thickness of wall is infinite) and RHS columns with larger width-to-thickness ratios of 24 and 38, and it was shown that significant reduction of composite beam rotation capacity will occur in the case of large width-to-thickness ratio. But in these two investigations, post-earthquake connection details for the beam weld access hole (scallop) geometry were not considered.Matsuo[2-3)] could apply post-earthquake provisions in his study on the rotation capacity of composite beam, but this investigations were just focused on the RHS column with width-to-thickness ratio of 29. Evaluation of rotation capacity of composite beam connected to RHS column was investigated by Tanaka et al. [2-4)] on the specimens with two different width-to-thickness ratios of 16 and 38. But the loading protocol in that research had constant amplitudes of 1.2 θ_p, 2.0 θ_p and 3.0 θ_p.

Further experimental study on the rotation capacity of composite beam to RHS column with application of post earthquake provisions and sever loading protocol is needed. In this research, results of behavior of composite beam connected to the RHS column with two different width-to-thickness ratios are studied by experimental tests. Differences in rotation capacity of beams are discussed through the study on the steel beam damages and concrete slab damages. Strain studies were carried out to investigate the effects of strain amount on the rotation capacity of beam.

2.2 Experimental test specification

2.2.1 Test specimens

In order to investigate the effects of RHS column width-to-thickness ratio on the rotation capacity of composite beam, cyclic loading test using T-shaped subassembly were conducted on three subassemblies of H-Beam(500×200×10×16) connected to RHS column with two different width-to-thickness ratios of 29 and 22 (□-350×350×12 & □-350×350×16). As shown in Table 2.1, one bare steel beam specimen and two composite beam specimens were prepared. Figure 2.1 illustrates the configuration of specimens, test setups and steel deck geometry, respectively.

Table 2.1 Experimental test specimen specification

Specimen	Concrete Slab	RHS Column width-to-thickness ratio
BS-29	Not	29
CB-29	Existed	29
CB-22	Existed	22
Beam: H-500×200×10×16		Column: □-350×350×12 □-350×350×16

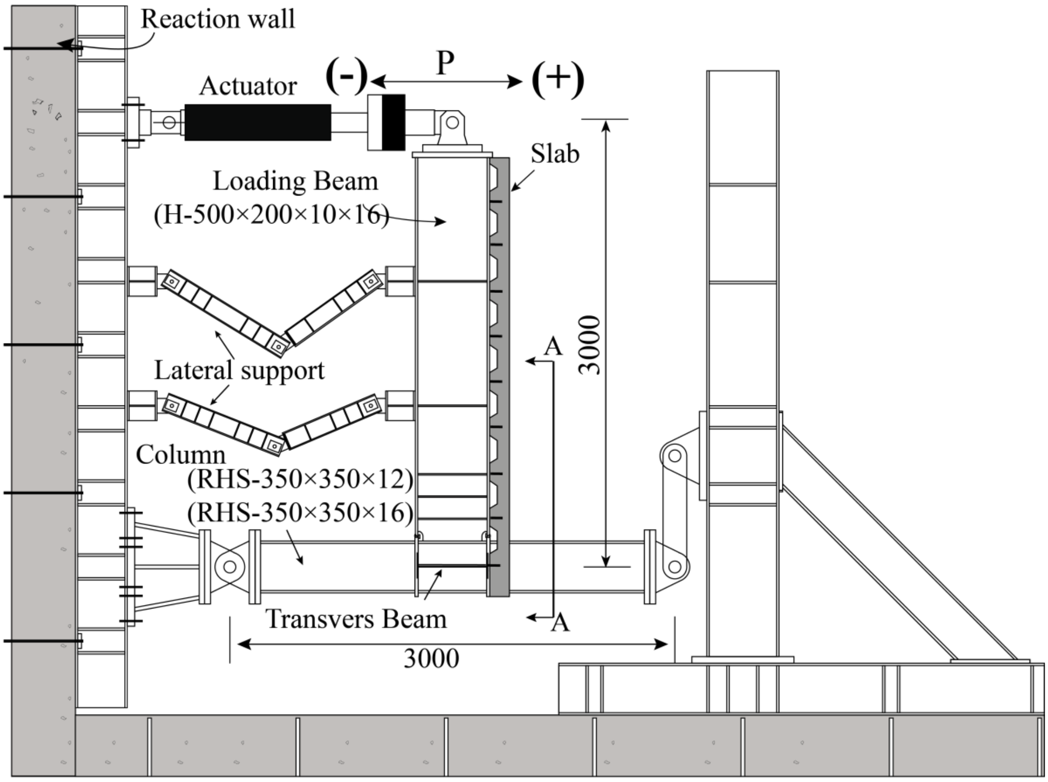

(a) Composite beam Specimen and test setup

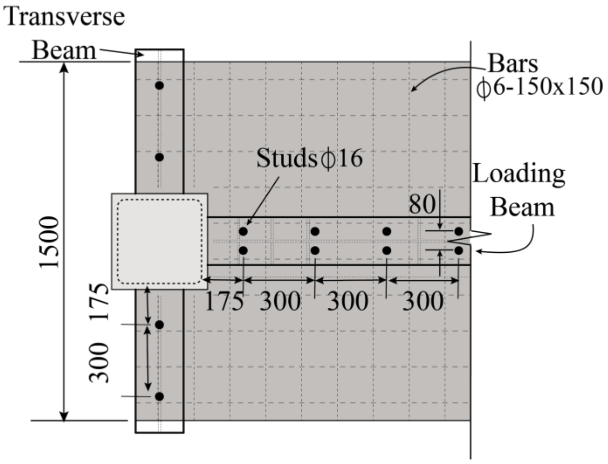

(b) Sec. A-A

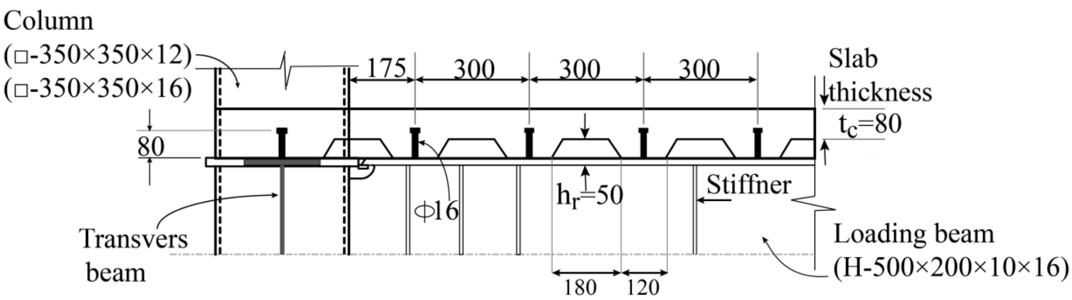

(c) Deck geometry

Fig. 2.1 Configuration and test setups of composite specimens

As shown in Figure 2.1, concrete slab with width of 1500 mm and thickness of 80 mm were used for composite beam specimens. In these specimens, deck plate type QL 99-50-12 applied and two stud bolts of ϕ16 were welded to the beam flange with pitch distance of 300 mm. Transverse distance between studs were 80 mm. The number of shear studs is common to all specimens.

2.2.2 Weld joint details

Weld Joint detail for beam-to-RHS column connection is illustrated in Figure 2.2. Beam flanges are connected to the column by through diaphragm to preventing local deformation of RHS column wall. Beam web is connected to the wall of RHS column without reinforcement, and fillet welds were applied in both sides of the beam. In all specimens shop welded joint type used by complete joint penetration (CJP) groove welds. CO_2 gas shielded metal arc welding method (GMAW) using YGW11 electrodes was conducted. Ceramic run of tabs were used and backing bars left in place. The weld access hole which is known as “scallop”, was consisted of two arcs with radiuses of 35 and 10 millimetres, which is corresponded to post Hyogo ken-Nanbu earthquake scallop geometry type and it is recommended in JASS 6 2007. This type of connection is common in Japan.

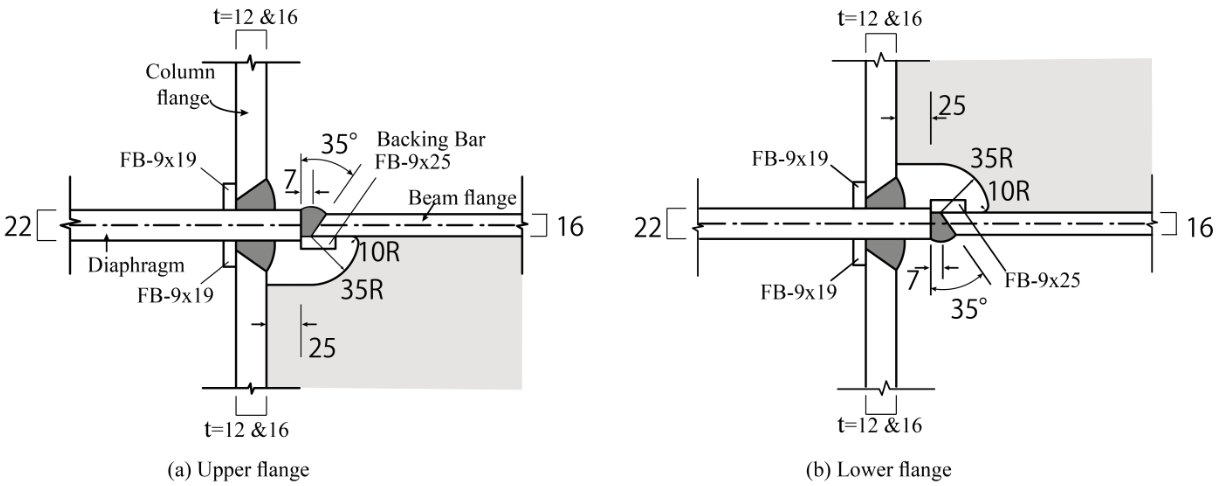

Fig. 2.2 Weld Joint detail

2.2.3 Material properties

The material utilized for the specimens were hot rolled sections with steel grade of SM490A and cold formed BCR295 for beams and columns, respectively. Diaphragm plates material were used with steel grade SM490A. Actual material properties obtained by tensile coupon tests are reported in Table 2.2 and shown in Figure 2.3.

Regarding the beam material toughness, Figure 2.4 plots the values of material Charpy V-Notch (CVN) impact test results associated with "fillet" area, which obtained from coupon tests. Fillet area is defined as the meeting point between the web and the flange which is illustrated in Figure 2.4(a). Studs material were used with steel grade JIS B1198-1995, and push-out tests were also carried out for the purpose of evaluating the shear strength and elastic stiffness of shear studs, summarized in Table 2.3.

The design strength of concrete used for composite beam specimens was 21.0 N/mm^2. The average concrete strength from cylinder tests was 28.4 N/mm^2 .

Table 2.2 Material properties

Member		Material Grade	σ_y (N/mm^2)	σ_u	YR= σ_y/σ_u	EL (%)
Beam	Flange	SM490A	383	551	69.5	40.6
	Web		422	541	78.1	36.6
RHS Column	CB-29	BCR295	328	425	77.0	48.9
	CB-22		369	471	78.3	43.4
Diaphragm		SM490A	370	531	69.7	49.9
Weld Metal		YGW11	420	536	78.3	31.4

Table 2.3 Shear stud push out test results

Elastic Stiffness (kN/mm)	Shear Strength q_y (kN)	Ultimate Shear trength q_{max} (kN)	δ_{max} *(mm)*
347	65.5	88.9	2.36

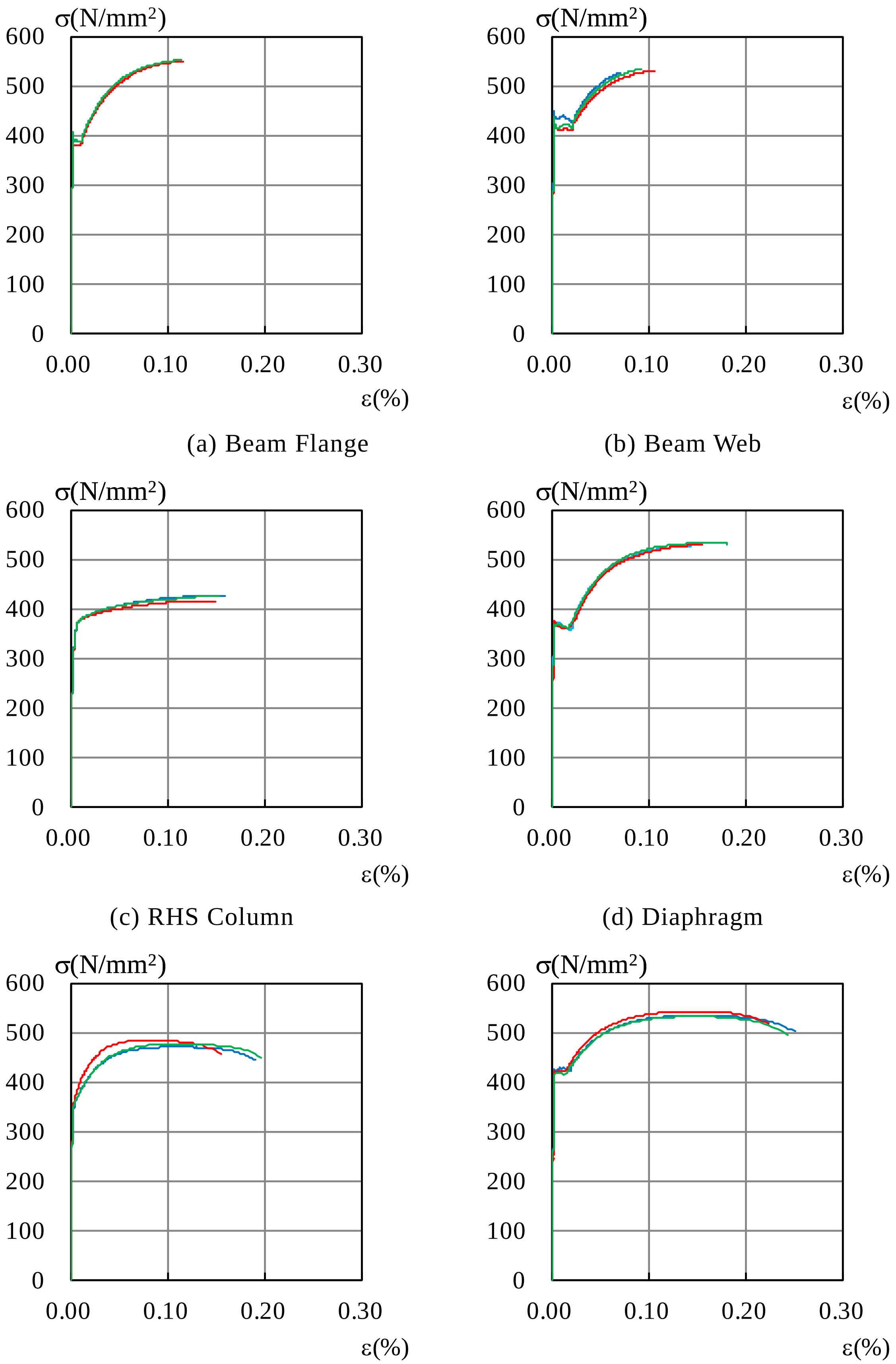

(a) Beam Flange

(b) Beam Web

(c) RHS Column

(d) Diaphragm

(e) Shear stud

(f)Weld metal

Fig. 2.3 Tensile coupon test results

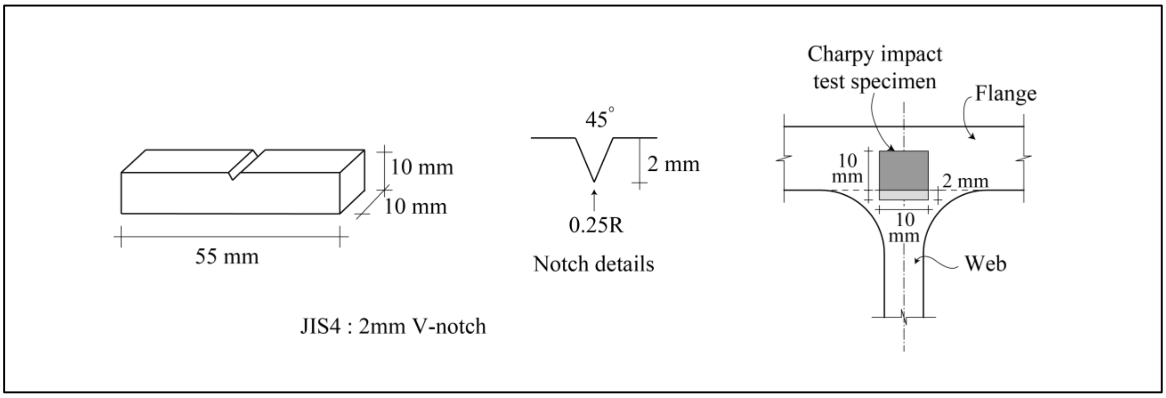

(a) Location of charpy impact test specimen

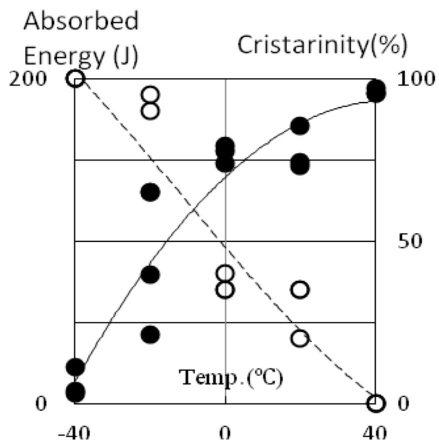

(b) CVN test results

Fig. 2.4 Charpy impact test results for “k” area of beam sections

2.2.4 Design of specimens

Figure 2.5(a) and (b), illustrates the plastic stress distribution in the positive moment for bare steel beam and composite beam, respectively.

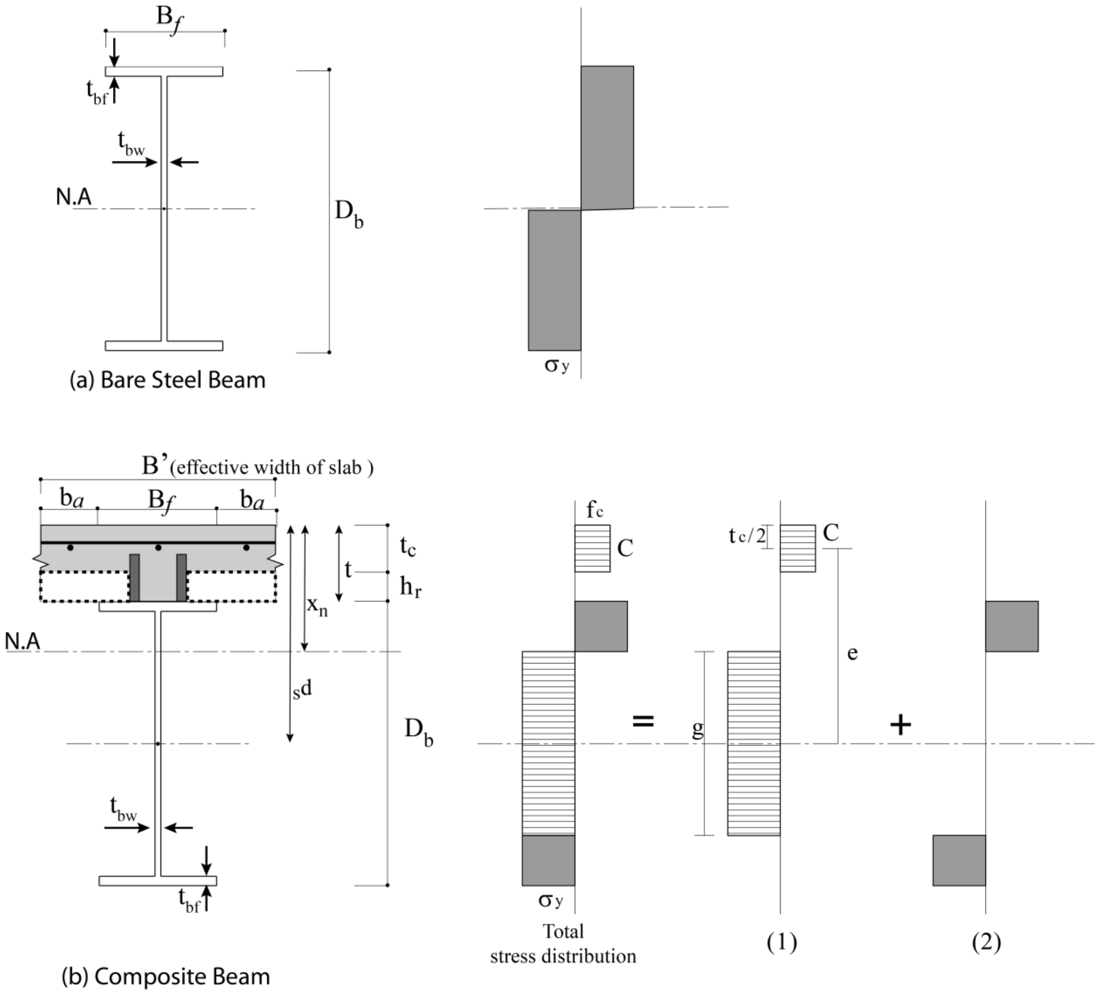

Fig. 2.5 Plastic stress distribution for positive moment in the bare steel beam and composite beam

In the case of bare steel beam[2-5], according to Figure 2.5(a), plastic moment strength of beam ${}_bM_p$, is calculated by:

$$ {}_bM_p = \left[B_f . t_{bf}\left(D_b - t_{bf}\right) + \frac{1}{4}\left(D_b - 2t_{bf}\right)^2 t_{bw} \right] {}_b\sigma_y = \left(D_b - t_{bf}\right) A_{bf} \cdot {}_{bf}\sigma_y + \frac{D_b - 2t_{bf}}{4} A_{bw} \cdot {}_{bw}\sigma_y \quad (2.1) $$

Where, A_{bw} is beam web section area, and A_{bf} is beam flange section area.

θ_p is the rotation corresponding to plastic moment capacity of bare steel beam (${}_bM_p$), which is obtained by dividing beam's plastic moment by its initial stiffness, calculated as:

$$ {}_b\theta_p = \left(\frac{l}{3E_{s} \cdot {}_sI} + \frac{1}{G_s A_{bw} l} \right) \cdot {}_bM_p \quad (2.2) $$

Where

E_s is Young's modulus of elasticity

G_s is Material shear modulus

l is beam length (distance from loading point to the column face)

Deformation corresponding to the beam plastic rotation angle will be obtained by multiplying beam length to the θ_p .

$$ {}_b\delta_p = {}_b\theta_p . l \tag{2.3}$$

In the case of composite beam[2-6], the nominal plastic moment resistance of a composite section in positive bending is given by the following equation:

$$ {}_cM_p = M_1 + M_2 \tag{2.4}$$

Where

$$ M_1 = C \cdot e \tag{2.5}$$

and,

$$ M_2 = {}_bM_p - \frac{g^2 \cdot t_{bw} \cdot {}_{bw}\sigma_y}{4} \tag{2.6}$$

In here, $e = 0.5D_b + h_r + 0.5t_c$ (2.7)

$$ C = 1.3 \times f_c \cdot t_c \cdot B' \tag{2.8}$$

B' is effective width of slab, and determined according to Ref. 2.6: $B' = B_f + 2b_a$ (2.9)

If $p_t = \dfrac{A_s}{B' \cdot {}_sd} \geq \dfrac{t_1^2}{2n(1 - t_1^2)}$, neutral axis (NA) is located in the web (here, $A_s = A_{bf} + A_{bw}$, $t_1 = t_c / {}_sd$, and Young modulus ratio n=15), So, location of Neutral Axis x_n , is calculated by :

$$ x_n = \frac{t_1^2 + 2n \cdot p_t}{2(t_1 + n \cdot p_t)} \cdot {}_sd \tag{2.10}$$

Moment of Inertia of composite beam ${}_cI_n$, is calculated by

$$ {}_cI_n = \frac{B'.t_c}{n} \left\{ \frac{t_c^2}{12} + \left(x_n - \frac{t_c}{2} \right)^2 \right\} + {}_sI + A_s \left({}_sd - x_n \right)^2 \tag{2.11}$$

$$ {}_c\delta_p = \frac{{}_cM_p \cdot l^2}{3 \cdot {}_sE \cdot {}_cI_n} + \frac{{}_cM_p}{G \cdot {}_bA_{bw}} \tag{2.12} $$

and

$$ {}_c\theta_p = \frac{{}_c\delta_p}{l} \tag{2.13} $$

The nominal shear force between the steel beam and the concrete slab transferred by studs, Q_h, shall be determined as the lowest value in accordance with the concrete crushing, or tensile yielding of the steel section. So, Design of studs is conducted by considering the minimum of :

$$ Q_h = \min\left(C, {}_bF_y\right) \tag{2.14} $$

Where: C = Effective compression strength of the concrete slab

${}_bF_y$= The tensile yield strength of steel section($= \sigma_y A_s$)

The nominal shear strength of one stud q_s , shall be determined as follows:

$$ q_s = 0.5 \times {}_{sc}a\sqrt{f_c \cdot E_c} \tag{2.15} $$

Where ${}_{sc}a$ = cross-sectional area of the stud [mm^2]

E_c = Concrete modulus of elasticity [N/mm^2]

f_c = Concrete compressive strength [N/mm^2]

Concrete Young modulus is calculated by :

$$ E_c = 21000 \times \left(\frac{\gamma}{23}\right)^{1.5} \times \sqrt{\frac{f_c}{20}} \tag{2.16} $$

The required number of studs shall be equal to the horizontal shear divided by the nominal shear strength of one stud :

$$ n_r = Q_h / \ q_s \tag{2.17} $$

Table 2.4 summarizes the calculated plastic moment strength, plastic rotation angle and deformation corresponding to the beam plastic rotation angle for the bare steel beam and composite beam specimens.

Table 2.4 Calculated strength and deformation of specimens

Specimen	M_p (kNm)	θ_p (rad)	δ_p (mm)
Bare steel beam	824	0.0088	25.1
Composite beam	1154	0.0064	18.3

2.2.5 Test procedure

As shown in Figure 2.6, specimens were simply supported at both ends of column and the lateral load was applied at the top of beam. θ_b is beam rotation angle based on definition presented in Figure 2.7 and Equation 2.17. The cyclic loading program was applied. The test protocol for this cyclic reverse loading is shown in Figure 2.8 which is consisted of 2 cycles in each ±2.0 θ_p , ±4.0 θ_p and other cycles in ±6.0 θ_p until the failure. θ_p is the rotation corresponding to plastic moment capacity of bare steel beam (M_p), which is obtained by dividing beam's plastic moment by its initial stiffness. Failure was defined as the fracture occurrence or 10% degradation from actual maximum strength obtained during the loading test.

$$\theta_b = \frac{\delta}{h'} = \frac{v_1 - \theta_c.h' - v_c}{h'} \quad [rad] \tag{2.18}$$

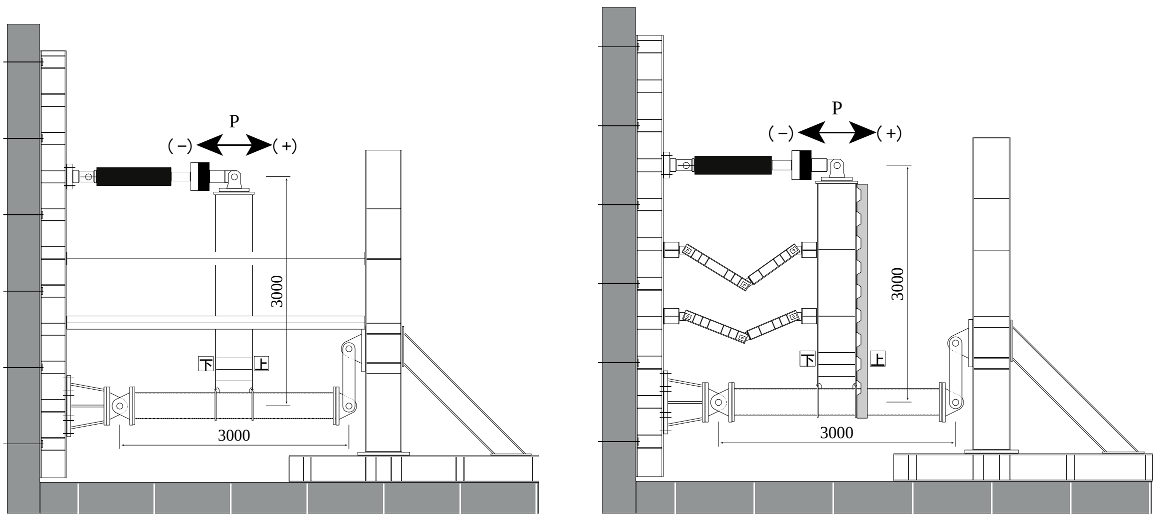

(a) Bare Steel beam specimen (b) Composite beam specimens

Fig. 2.6 Bare steel beam and composite beam specimen test setup

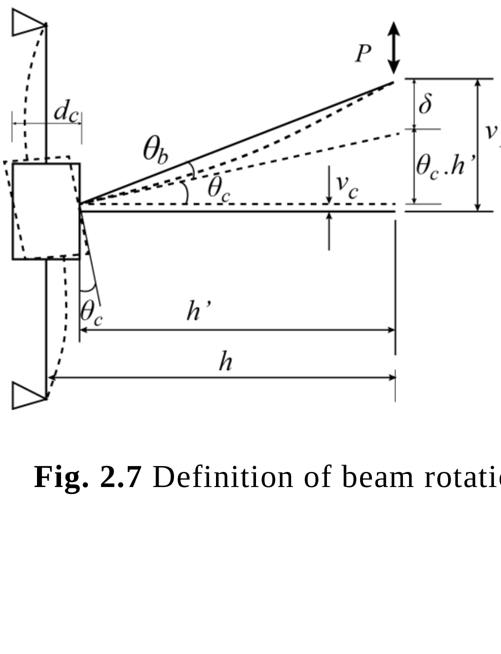

Fig. 2.7 Definition of beam rotation

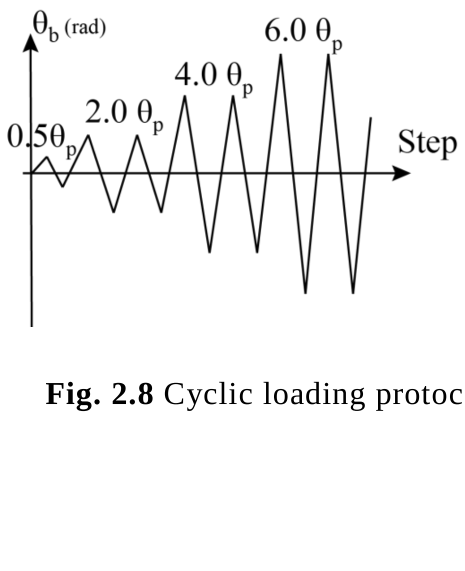

Fig. 2.8 Cyclic loading protocol

2.3 Test results

2.3.1. M_b- θ_b Hysteresis diagrams

M_b-θ_b hysteresis graphs are shown in Figure 2.9. In these graphs M_b represents beam moment at column face and θ_b is beam rotation angle. From the Figure it can be observed that rotation angle of composite beam in the specimen which was connected to the RHS column with large width-to-thickness ratio of 29 (CB-29) was almost half of bare steel beam specimen with same width-to-thickness ratio (BS-29). But in the composite specimen which was connected to the smaller width-to-thickness ratio column (CB-22), considerable improvement of beam rotation angle was observed. It can be seen that in CB-22 specimen, by increase of beam rotation angle, sudden reduction of strength occurred in 0.025 rad. After this drop, strength kept constant until further progress of loading.

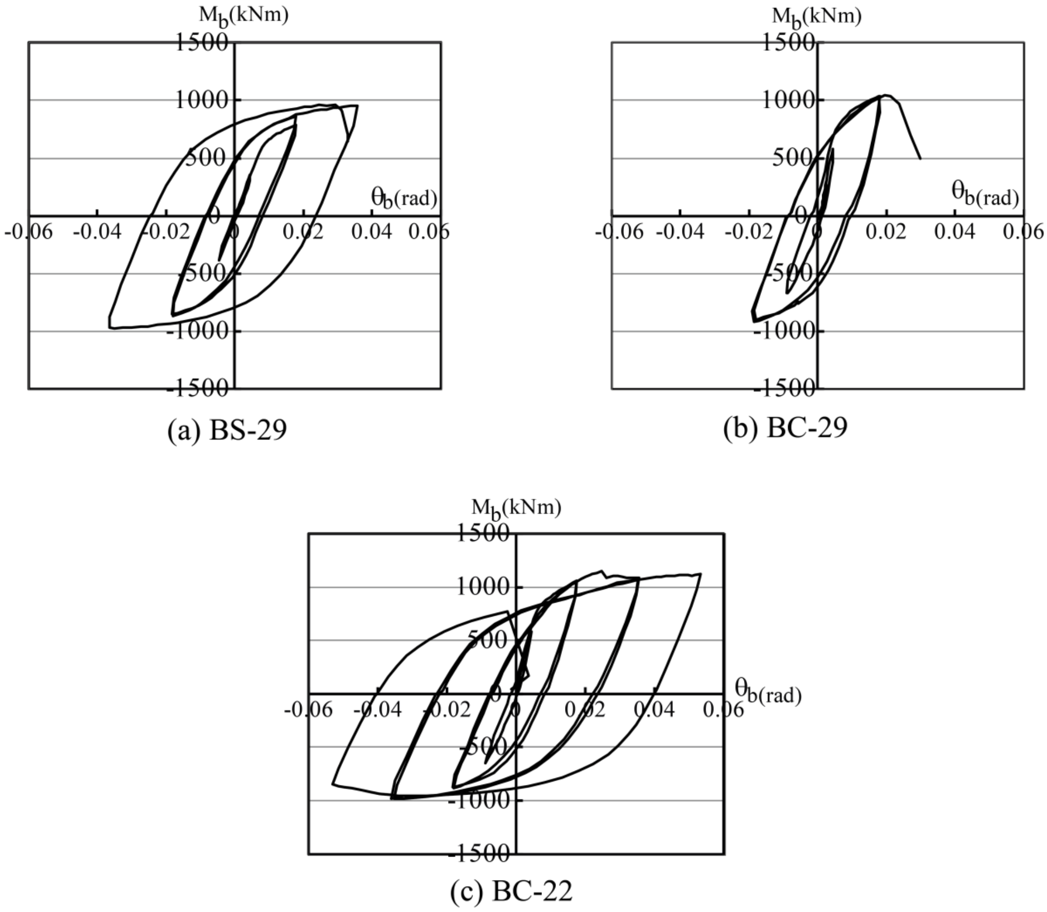

Fig. 2.9: M_b-θ_b Hysteresis graphs

2.3.2 Steel beam damage observations

2.3.2.1. Crack initiation and progress

In all specimens, regardless of width-to-thickness ratio and existence of slab, crack initiation happened at the root of weld access hole of bottom flange. But in the composite specimen with large width-to-thickness ratio of 29 (CB-29) this crack occurred in the considerable early cycle of loading, which was second cycle of +2.0 θ_p. While in the composite specimen with smaller width-to-thickness ratio of 22 (CB-22) this crack occurred in the later stage of loading, which was second cycle of +4.0 θ_p. Stage of loading which the crack initiated in the bare steel beam specimen (BS-29) was first cycle of +4.0 θ_p , which was later than CB-29 and earlier than CB-22. Crack initiation was defined when 0.2 mm crack was observed using crack scale. In Figure 2.10 typical crack initiation and progress at the root of weld access hole is shown for all specimens in the first cycle of +4.0 θ_p. Summary of first crack initiation of all specimens is illustrated in Figure 2.11. It was observed that for the composite beam specimen which was connected to the RHS column with larger width-to-thickness ratio (CB-29), speed of crack growth was higher than the specimen with smaller ratio (CB-22 specimen). However, local buckling was observed in the last cycle of loading of this specimen, shown in Figure 2.13.

2.3.2.2. Final failure mode

Final failure of all specimens was determined by progress of above mentioned crack at the root of scallop of beam lower flange, shown in Figure 2.14. These fractures reproduced the failure modes of connections in the 1995 Hyogoken-Nanbu earthquake. Final failure manner of all specimens, were determined by quite ductile manner.

(a) BS-29: Crack initiation(at+3.0θ_p) (b) CB-29:Crack progress(width:0.9mm) (c) CB-22: No crack

Fig. 2.10 Typical crack initiation and progress at the root of scallop in the first cycle of +4.0θ_p

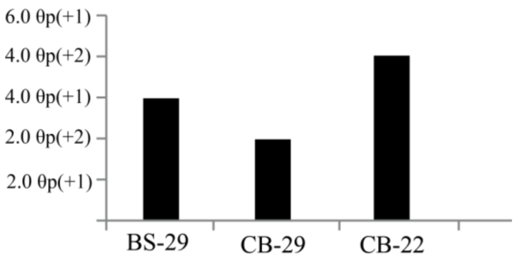

Fig. 2.11 First crack initiation during the loading test

Loading cycle	**BS-29**	**CB-29**	**CB-22**
	Root of Weld Access Hole (Scallop) of Lower Flange		
$2.0\theta_p(+2)$	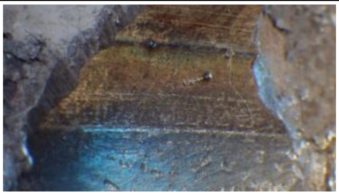 No Crack	 Initiation; Peak of cycle:0.35 mm	 No crack
$4.0\theta_p(+1)$ Cycle	 $+3.0\theta_p$ – Crack initiation: **0.2** mm	 $2.0\theta_p(+3)$ -Crack progress: 0.9 mm	 No crack
$4.0\theta_p(+1)$ Peak	 $+4.0\theta_p$ – Crack progress: 0.6 mm	 Before peak($2.4\theta_p$) Crackprogress:1.4mm	 No crack
$4.0\theta_p(+2)$	 $+3.0\theta_p$ – Crack progress: 1.2 m		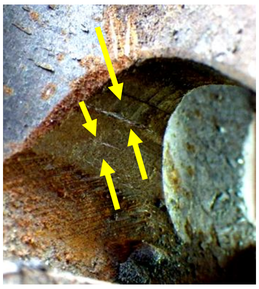 Peak of cycle- Crack initiation 0.2 mm
$6.0\theta_p(+1)$			

Fig. 2.12: Crack initiation and progress at the root of scallop during loading cycles

Lower Flange **Local Buckling**	**BS-29**	**CB-29**	**CB-22**
$2.0\theta_p(-2)$ Peak of cycle	No buckling		No buckling
$4.0\theta_p(-1)$ Peak of cycle		- - -	
$6.0\theta_p(-1)$ Peak of cycle	- - -	- - -	

Fig. 2.13 Local buckling of lower flange of specimens

Fig. 2.14 Typical final failure mode

2.3.3 Concrete slab damage observations

The concrete slabs were subjected to subsequent tensile and compressive load and the formation of cracks traced as loading progressed. In both composite specimens, three patterns of slab damage were observed during the test. “Longitudinal crack” which was parallel to the steel beam, “transverse crack” which formed perpendicular to the steel beam, and “bearing crush” which occurred due to direct compression and formed at the vicinity of column face.

In both width-to-thickness ratios of 29 and 22 specimens, comparable transverse cracks and longitudinal cracks occurred at similar cycle of loading which was first cycle -0.5θ_p and +2.0 θ_p , respectively (Figure 2.15).

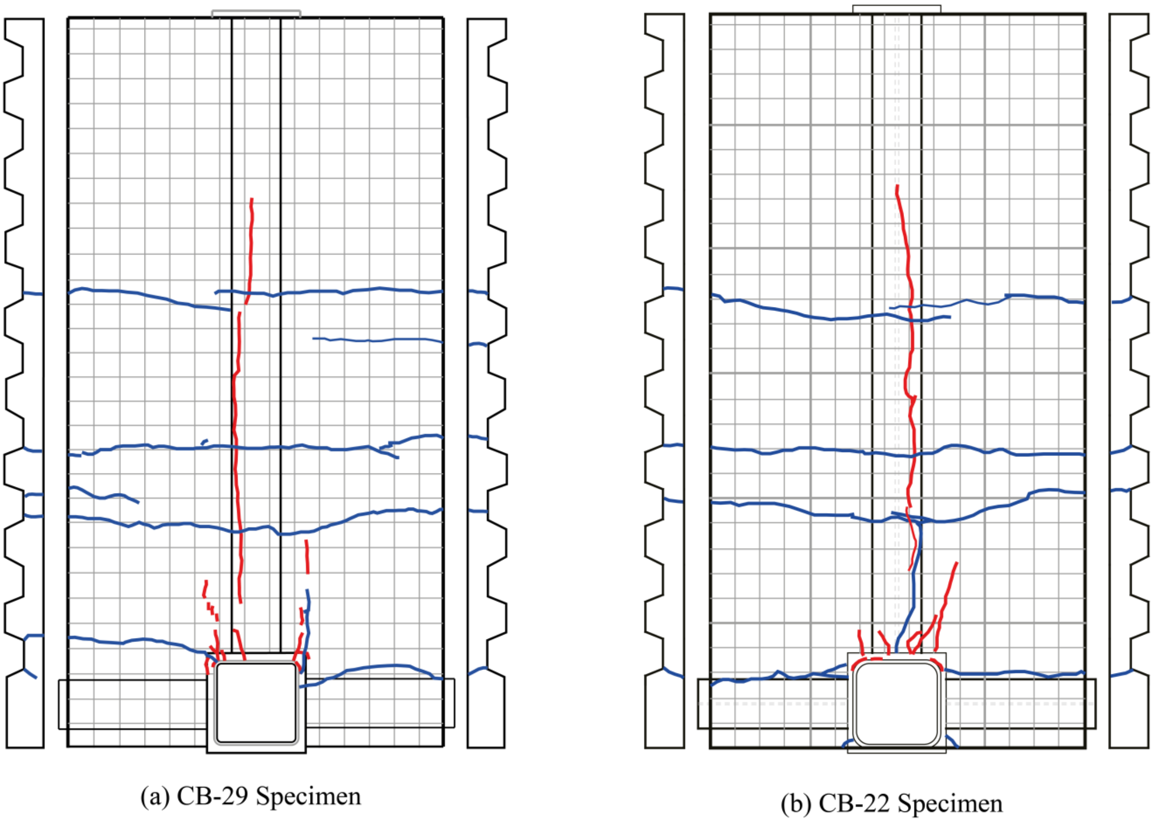

Fig. 2.15 Formation of longitudinal and transverse cracks (end of first cycle of +2.0 θ_{p})

Initiation of bearing crush at the corners of RHS column were also happened at similar cycle of loading which was first cycle of +2.0 θ_p in both composite specimens, shown in Figure 2.16(a) and (b). However, in CB-29 this crush did not progressed due to failure of specimen, while for the specimen with smaller width-to-thickness ratio (CB-22), by progress of loading cycles, sever concrete crush occurred at the vicinity of column face and over the whole slab depth during the first cycle of +4.0 θ_p , shown in figures 2.17 and 2.18. This crush resulted to the sudden strength degradation which can be seen in Figure 2.9(c) hysteresis diagram and was discussed in sec. 2.3.1.

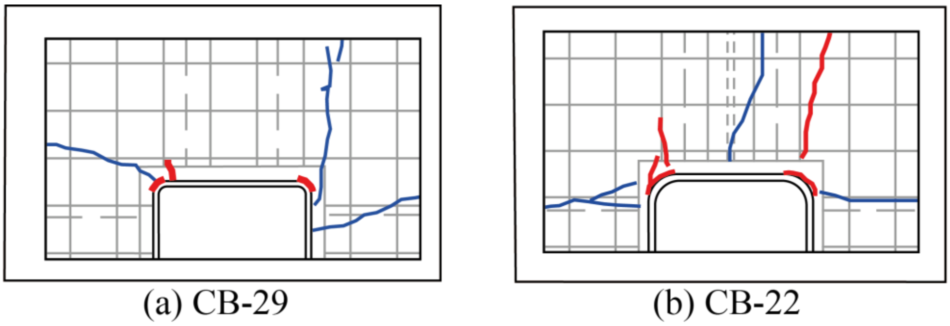

Fig. 2.16 Initiation of bearing crush at corners of RHS column in comparable loading cycle of +2.0 θ_p(+1)

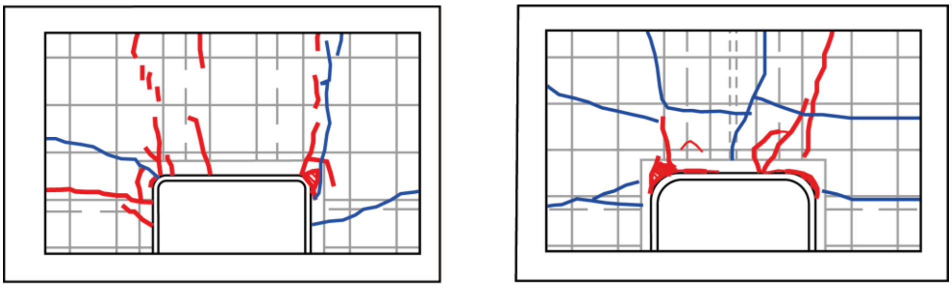

(a) CB-29 (b) CB-22

Fig. 2.17 Comparable development of bearing crush at corners of RHS column, until end of loading cycle +2.0 θ_p(+2)

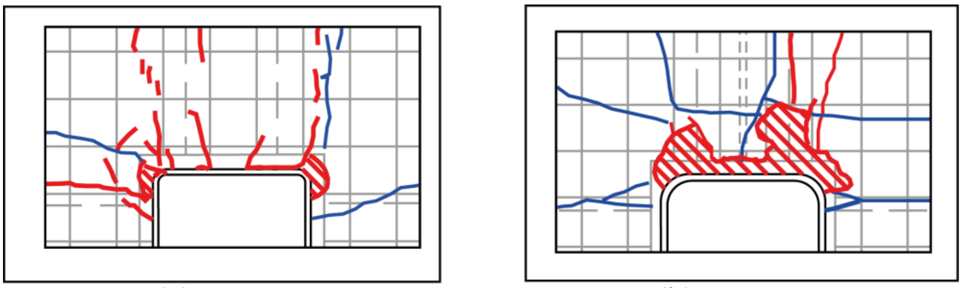

(a) CB-29 (b) CB-22

Fig. 2.18 Final condition of concrete crush adjacent to the of RHS column face

2.4 Effects of width-to-thickness ratio of RHS column

2.4.1 M_b-θ_b Skeleton curves

The skeleton curves obtained from M_b-θ_b hysteresis diagrams are plotted in Figures 2.20 (a) and (b). The method for plotting the skeleton curves, is shown in Figure 2.21 .
Figure 2.20(a) corresponds to skeleton curve obtained from positive loading, and Figure 2.20(b) corresponds to skeleton curve obtained from negative loading. In these graphs, actual plastic strength values are shown with solid circles, which are corresponding to one-sixth stiffness reduction, obtained by definition shown in Figure 2.22.
In positive flexure, regardless of difference in column width-to-thickness ratio(*B/t*), considerable increase in the elastic stiffness of composite specimens can be seen. The elastic stiffness of CB-29 and CB-22 are 1.93 and 1.83 times of bare steel beam, respectively. But in the case of negative flexure regardless of existence of slab, from the early stages of elastic region the stiffness is almost same.
Figures 2.23(a) and (b) illustrate the amount of elastic stiffness of specimens in the positive and negative flexure, respectively. In the figure, the amount of elastic stiffness in $\pm 0.5\theta_p$ and $\pm 2.0\ \theta_p$(second cycle) are shown, and the calculated stiffness is plotted with horizontal dotted line. In $+0.5\theta_p$ positive flexure, considerable increase of stiffness in both composite specimens comparing with the bare steel beam specimen (BS-29) can be seen, But by progress of loading and development of damages in the concrete slab until $+2.0\ \theta_p(+2)$, stiffness of both composite beam specimens reduced, and finally reached to the bare steel beam stiffness.
As shown in Figure 2.23(b), in the negative flexure considerable difference for reduction of stiffness was not found between specimens. It can be explained that this behavior is resulted from removal of composite action in the negative flexure.
Regarding the actual plastic strength, from Figure 2.20(a) it can be seen that in the positive flexure both composite specimens showed almost similar increase of plastic strength comparing with BS-29. The plastic strength of CB-29 and CB-22 are 1.27 and 1.31 times of bare steel beam, respectively. Also it is shown that in the bare steel beam specimen BS-29, after reaching to actual plastic strength, almost steady increase of strength can be seen until 0.05 rad. After reaching to this rotation angle, strength degradation happened due to development of crack in the root of weld access hole (scallop), which was explained in Sec. 2.3.2. In the case of composite beam specimens, it can be seen that both specimens showed similar behavior until 0.02 rad, but in CB-29 specimen degradation of strength gradually happened due to initiation and progress of

crack at the root of lower flange weld access hole (scallop). On the other hand, in CB-22 specimen increase of strength continued by progress of loading until 0.025 rad . But sudden strength degradation can be seen in the skeleton curve of this specimen which was associated with concrete bearing crush at the vicinity of RHS column, which was discussed in sec. 2.3.3, and resulted to 5% strength reduction. After this drop in the strength, constant moment transmitted until 0.05 rad.

Figure 2.20 (b) shows that in the negative flexure, actual plastic strength of all specimens were comparable to the calculated plastic moment capacity of bare steel beam, which is plotted with dotted horizontal line in the figure.

Table 2.5 summarizes the results of observed ultimate strength of each specimen. Due to composite action, 8% increase in the ultimate flexural capacity of BC-29 observed comparing with bare steel beam specimen BS-29. Reduction of RHS column width-to-thickness ratio in CB-22 resulted to 10% increase in the ultimate strength of this specimen comparing with CB-29.

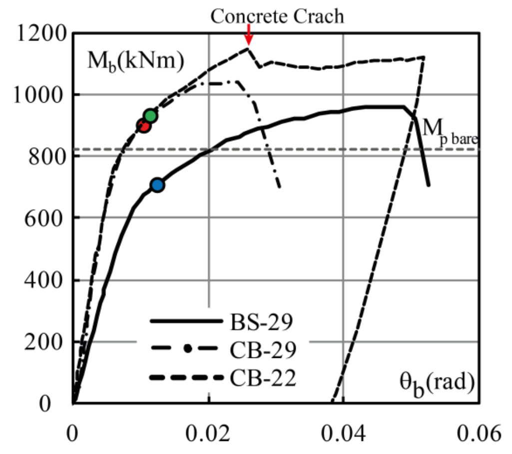

(a) Positive flexure

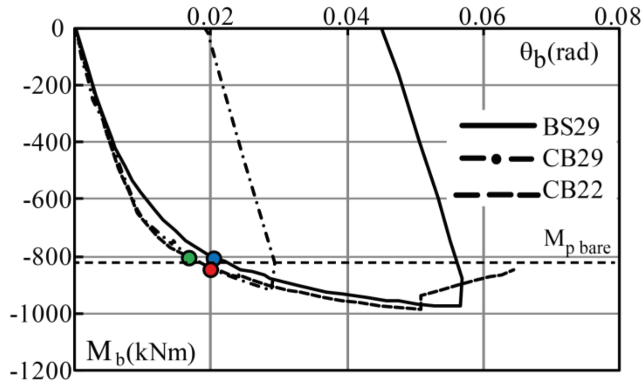

(a) Negative flexure

Fig. 2.20 M_b-θ_b Skeleton curves

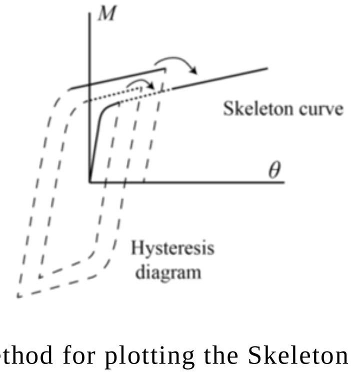

Fig. 2.21 Method for plotting the Skeleton curve

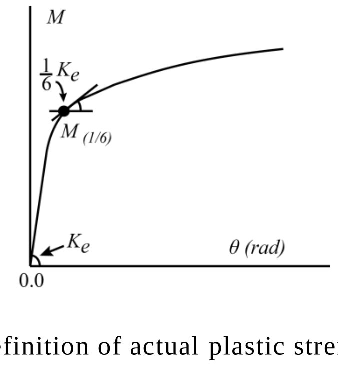

Fig. 2.22 Definition of actual plastic strength

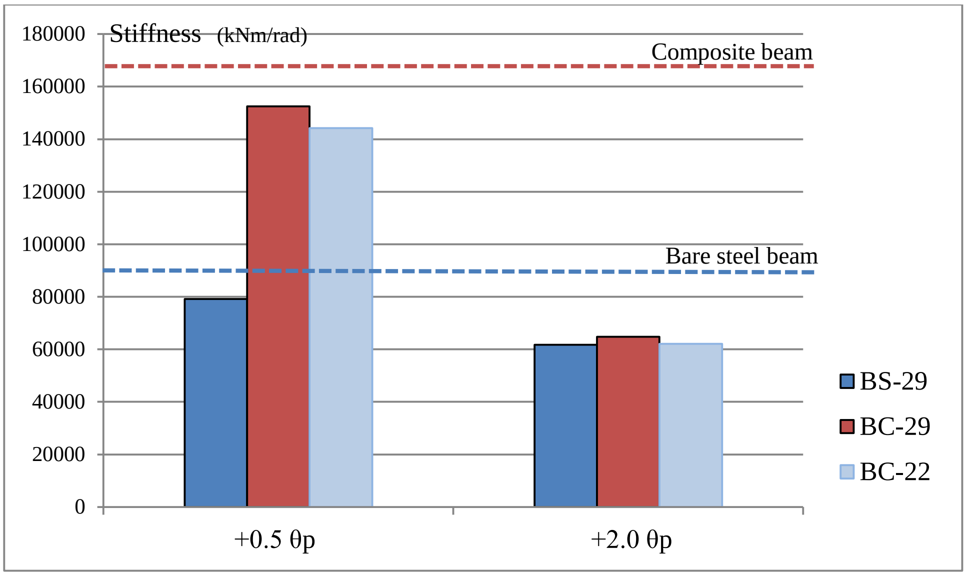

(a) Positive flexure

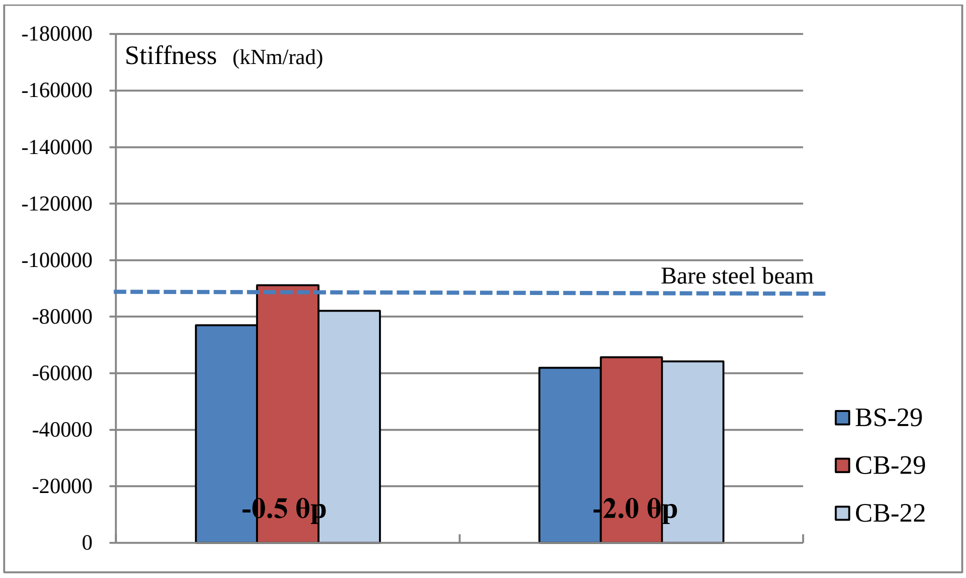

(b) Negative flexure

Fig. 2.23 Elastic stiffness of specimens

Table 2.5 Test results

Specimen	Plastic Moment (kNm)		Ultimate flexural Capacity (kNm)	
	M_{p+}	M_{p-}	M_{max+}	M_{max-}
BS-29	711	803	961	974
CB-29	903	842	1042	922
CB-22	934	801	1145	986

2.4.2 Strain behavior and rotation capacity

Figure 2.24 depicts the strain distribution across the length of beams upper and lower flange in the first cycle of +2.0 θ_p . Horizontal axis is the length and vertical axis is the amount of strain, measured by gauges attached at the 30 mm position from column face. As shown in Figure 2.25(a),(b) and (c) in each specimen, strain of flanges was measured by the strain gauges which were mounted on the steel sections. Strain gauges were attached to the inside of upper flange and both sides of lower flange.

According to Figure 2.24(a), it is found that the strain on the upper flange of both composite specimens remained almost zero, while in the bare steel beam specimen BS-29, upper flange strain amount reached to 2.7% negative strain. This behavior is resulted from existence of slab, which provides constraint condition for the upper flange of composite specimens.

Furthermore, for the lower flange it can be seen that flanges were subjected to positive strain. In both sides of lower flange of composite beam which was connected to the RHS column with large width-to-thickness ratio of 29 (CB-29 specimen), amount of strain is 2.2 times of bare steel beam specimen with same width-to-thickness ratio (BS-29). By reduction of RHS column width-to-thickness ratio in CB-22 specimen, 55% reduction of strain comparing to CB-29 can be seen in both sides of flange. The amount of strain in CB-22 is just 1.2 times more than bare steel beam BS-29.

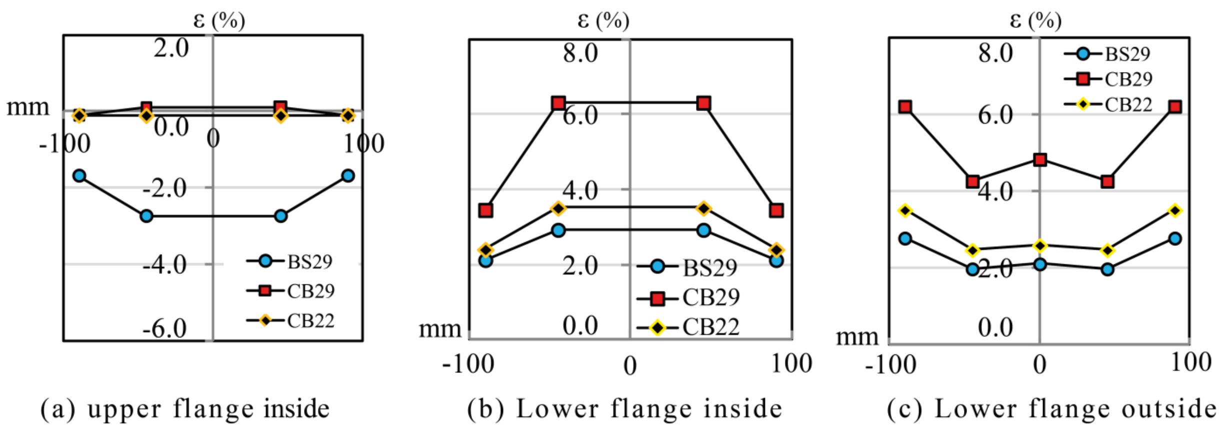

Fig. 2.24 Strain distribution across the length of beams flange in first cycle of +2.0 θ_p

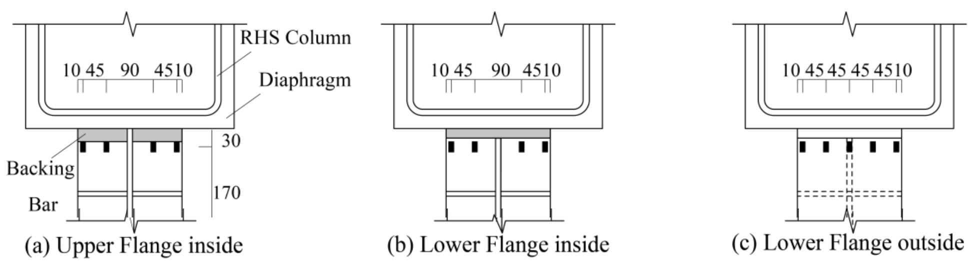

Fig. 2.25 Strain gauges arrangement on the steel section flanges

The above strain condition is associated with the specific loading cycle of +2.0 θ_p.

The strain versus beam rotation angle is illustrated in Figure 2.26. It is shown that during the entire loading steps, for all specimens regardless of existence of slab or difference of width-to-thickness ratios, by the progress of loading and increase of beam rotation angle, the amount of strain in the flanges increased. But upper flange of composite specimens sustained considerable smaller amount of strain comparing to bare steel beam specimen BS-29. On the other hand for the lower flanges, although in the bare specimen BS-29 the strain condition was comparable with its upper flange, but considerable increase of strain happened in both composite specimens BC-29 and BC-22.

It is also found that in the composite beam specimen with smaller width-to-thickness ratio CB-22, after the beam rotation angle reached to 0.025 rad and sever concrete crush occurred, sudden reduction in the slope of strain curve happened in the lower flange. At the same time, slope of strain curve in the upper flange increased. This behavior can be explained that following to sever concrete bearing crush in CB-22, reduction of upper flange constraint condition occur, and this resulted to change in the slope of strain curves of flanges.

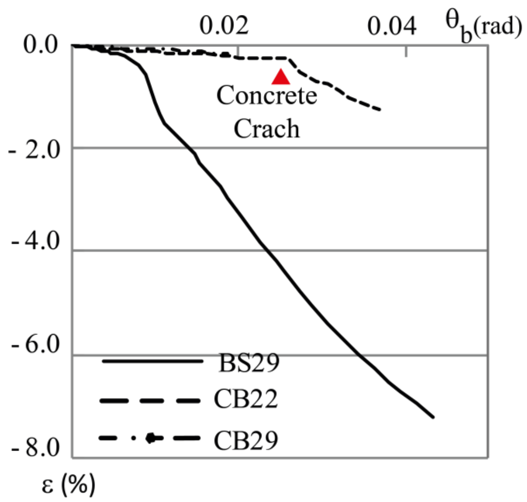

(a) Upper flange

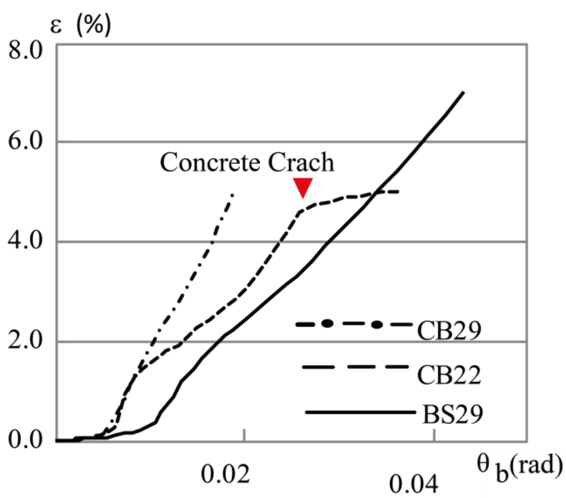

(b) Lower flange

Fig. 2.26 Strain versus beam rotation angle (θ_b)

According to strain behavior study and damage observations which were explained in sec. 2.3.2, it is found that strain condition of lower flange affected the crack growth and progress in each specimen, and finally this resulted to different rotation capacity of beams. In CB-29 specimen, higher amount of strain resulted to earlier initiation and faster progress of crack comparing to bare steel beam BS-29. In CB-22 specimen, despite the higher amount of lower flange strain comparing with BS-29, but after the occurrence of concrete bearing crush, reduction of strain in the lower flange resulted to later initiation of crack at the root of weld access hole.

Figure 2.27 depict the crack growth in each specimen. Crack growth was investigated by plotting the measured crack opening (δ_{cr}) versus beam rotation. In this figure, η is the beam cumulative plastic rotation based on the definition shown on Figure 2.28. Table 2.6 summarizes the results of cumulative rotation capacity of each specimen. Smaller amount of strain on the lower flange of CB-22 resulted to later crack initiation, slower development and finally higher beam rotation capacity.

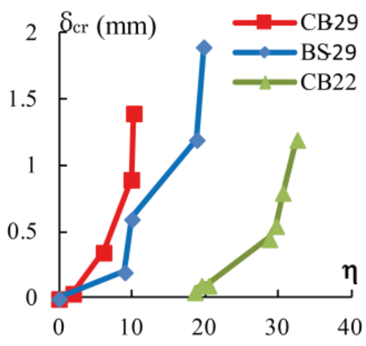

Fig. 2.27 Crack growth

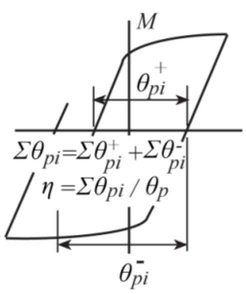

Fig. 2.28 Definition of cumulative rotation capacity

Table 2.6 Cumulative rotation capacity

Specimen	η
BS-29	20.4
CB-29	10.7
CB-22	45.3

Figure 2.29 illustrates the beam cumulative plastic rotation (η) versus connection factor (α) for this experimental test and also for specimens of Ref.(2-3) in Matsuo's experimental test results. Connection factor (α) is based on bare steel beam. In this figure, black is representing the results of specimens of this chapter and white is representing the results of Matsuo's test. Triangle is associated with bare steel beam specimens and circle is associated with composite beam specimens. Due to difference in materials between this test and Matsuo's test (SN400B), higher

cumulative rotation capacity can be seen in the specimens of Matsuo's experimental test, but it can be seen that in both tests for same Connection factor (α) cumulative rotation of composite beam is reduced to almost less than half of bare steel beam.

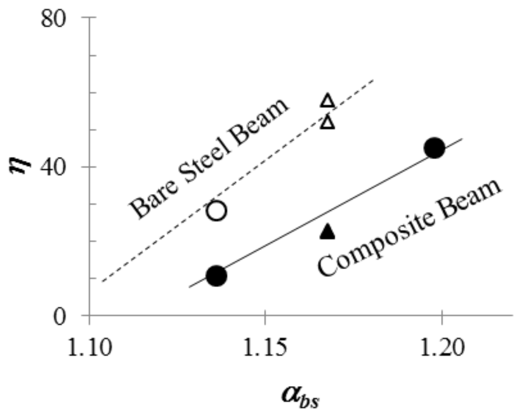

Fig. 2.29 Cumulative rotation capacity(η) versus connection factor(α) for test specimens and Matsuo's test specimens (Ref. 2-3)

2.5 Conclusions

This study was performed through the experimental test on three full scale subassemblies to investigate the elasto-plastic behavior of composite beam connected to RHS columns with different width-to-thickness ratios. The conclusions and recommendations presented in this chapter can be summarized as follows:

1- In all specimens regardless of existence of concrete slab or width-to-thickness ratio of RHS column, first crack initiation was occurred at the root of weld access hole (scallop). For the composite beam specimen CB-29 this occurred at earlier stage with higher progress, comparing with the bare steel beam connected to the RHS column with same width-to-thickness ratio (BS-29 specimen) and composite beam connected to RHS column with smaller width-to-thickness ratio (CB-22 specimen). Final failure pattern was determined by propagation of this crack.

2- In the beam connected to RHS column with width-to-thickness ratio of 29, composite action resulted to 27% increase of actual plastic strength and 92% increase of stiffness in positive flexure, comparing with bare steel beam connected to RHS column with same with-to-thickness ratio. But cumulative rotation capacity of composite beam significantly reduced comparing with bare steel beam. Strain study in the first cycle of +2.0 θ_p showed that composite action increased the strain amount of lower flange 2.2 Times of bare steel beam. This strain condition resulted to early crack initiation with higher progress, and finally reduction of rotation capacity of composite beam.

3- Reduction of RHS column width-to-thickness ratio in CB-22 specimen, did not result to considerable difference in the actual plastic strength and elastic stiffness in positive flexure comparing with CB-29, but 10% increase of beam ultimate strength observed. Also considerable improvement in the cumulative rotation capacity observed which was 4.2 times of CB-29. Experimental test results revealed another specific difference between composite specimens. It was observed that in the specimen with smaller width-to-thickness ratio severe concrete bearing crush happened at the vicinity of column face.

4- Strain behavior study in CB-22 specimen, showed that in the first cycle of +2.0 θ_p , the amount of strain in the lower flange of CB-22 specimen was 55% smaller than

CB-29 and 20% more than bare steel beam BS-29, but after the occurrence of sever crush in the concrete slab, sudden reduction in the tangent of strain in the lower flange happened. This resulted to smaller rate of strain increase, even comparing to the bare steel beam BS 29. Finally, this resulted to higher rotation capacity of CB-22 comparing with CB-29 and also BS-29.

5- Occurrence of concrete crush can be considered as the start of removal of composite effect and start of closing to the bare steel beam condition. Further investigation about the mechanism of stress and strain transfer of composite beam is needed, which is presented in the next chapter of this research.

6- It was observed that for same connection factor (α) cumulative rotation of composite beam (η) is reduced to almost less than half of bare steel beam.

.

3. Mechanism of Elasto-Plastic Behavior of Composite Beam Connected to RHS Column

3.1 Introduction

Following to observations of experimental test shown in Chapter 2, considerable difference between rotation capacity of composite beam connected to RHS column with different width-to-thickness ratios was observed. Another specific difference was also found that in the composite beam connected to RHS column with smaller width-to-thickness ratio. Occurrence of bearing crush of concrete at the vicinity of column face resulted to significant change in the condition of strain of lower flange. Further comprehensive understanding of elasto-plastic behavior of composite beam is needed to show the effect of out-of-plane deformation of RHS column on the behavior of composite beam.

This research is conducted to clarify the structural condition of web connection. In this chapter FEA study is conducted to understand the mechanical effects of composite action and out-of-plane deformation of RHS column on the elasto-plastic behavior of composite beam. Mechanism of stress transfer and strain concentration is shown by the means of FEA results.

Furthermore, investigation about the ultimate flexural capacity of web connection is conducted by the limit analysis. Correspondence between FEA and limit analysis is shown and evaluation of ultimate flexural capacity of composite beam connection is proposed.

3.2 Limit analysis of web connection

According to past researches, effect of out-of-plane deformation was mostly considered based on the concern regarding reduction of web flexural capacity. This research is conducted to clarify the structural condition of web connection, not only based on the flexural capacity considerations, but also by considering the effect of axial force subjected to the web. This investigation is helpful to understand the interaction effects of both axial force and flexural moment on the capacity of composite beam web connection simultaneously. In fact in the case of composite beam, web connection has to play two different roles: transmission of flexural capacity (same as bare steel beam) and transmission of axial force resulted from concrete slab compression force. This research is conducted to investigate the interaction of both effects. Actually it is already known that increase of RHS column width-to-thickness ratio results to movement of neutral axis (NA) toward top flange, but according to this limit analysis location of neutral axis can be shown by interaction of different width-to-thickness ratio and different axial force (N).

Evaluation of ultimate flexural strength of web connection in the bare steel beam connected to RHS column is shown in AIJ "Recommendation for Design of Steel Structures" [3-1)~3-2)]. In this section, a method for evaluating the flexural strength of composite beam web connection is presented by considerations regarding out-of-plane deformation of column flange and application of the yield line theory.[3-3)~3-4)] According to that theory, yield lines are developed at location of maximum moments. Yield lines are straight, and constant ultimate moments are developed along them. Elastic deformations within segments are negligible.

In this section, derived equations are introduced to take count in the reduction of web connection capacity of composite beam due to increase of RHS column width-to-thickness ratio and axial force.

3.2.1 Collapse mechanisms

According to past researches, in order to evaluate flexural strength of composite beam Tanaka et al. [3-7)] conducted numerical calculation with referring to the collapse mechanism shown in AIJ "Recommendation for Design of Steel Structures" [3-5)].

Adopted collapse mechanisms are shown in Figure 3.1(a) and (b). Mechanism I is same as bare steel beam collapse mechanism shown in Ref. 3-5 except the difference in the location of neutral axis (N.A). Mechanism II is adopted according to the collapse mechanism which was proposed in Ref.3-7. In this figure, "β" is the unknown parameter for the location of neutral axis of composite beam. "α_U" and "α_L" are unknown parameters for the depth of web yield region. *"s"* is the parameter regarding scallop height. "${}_jM_{wu}$" and "N_w" are the ultimate flexural strength of web connection, and axial force acting on web, respectively.

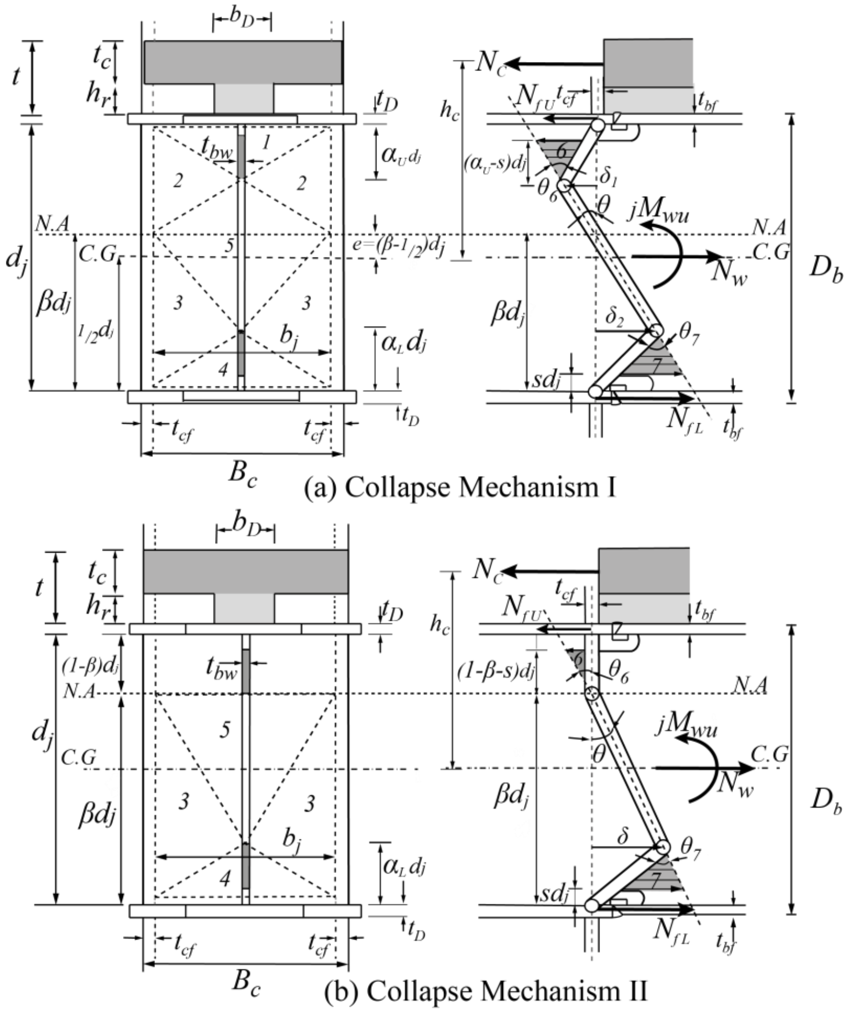

Fig. 3.1 Collapse Mechanisms

According to Figure 3.1, application of virtual work in these mechanisms is represented by equation (4.1). Right side of this equation is internal energy dissipation.

$${}_jM_{wu}\theta + N_w\left(\beta - \tfrac{1}{2}\right)d_j\theta = \sum d_i \tag{3.1}$$

Here, the acting point of ${}_jM_{wu}$ and N_w, is considered at the center of gravity of steel beam. Hereinafter, in this paper m_o and n will be considered as nondimensional ultimate flexural strength and nondimensional axial force of web respectively, which is defined as:

$$m_o = {}_jM_{wu}/M_{wp}\ , \qquad (3.2)$$

$$n = N_w/N_{wy} \qquad (3.3)$$

where:

$M_{wp} = \frac{1}{4} d_j^{\,2}\, t_{bw} \cdot {}_{bw}\sigma_y$ (3.4)

$N_{wy} = d_j t_{bw} \cdot {}_{bw}\sigma_y$ (3.5)

3.2.2 Mechanism I

According to Figure 3.1(a) dissipated energy in the yield lines of regions 1 to 7 are summarized in Table 3.1.

Table 3.1 Dissipated Energy based on Mechanism I

Region	***Rotation Angle***	***Dissipation (d_i)***
1	$\theta_1 = \left(\frac{1-\beta}{\alpha_U} - 1\right)\theta$	$2b_j\left(\frac{1-\beta}{\alpha_U} - 1\right) m_p\,\theta$
2(×2)	$\theta_2 = 2(1-\beta-\alpha_U)\frac{d_j}{b_j}\,\theta$	$8\frac{d_j^{\,2}}{b_j}(1-\beta)(1-\beta-\alpha_U)\, m_p\theta$
3(×2)	$\theta_3 = 2(\beta-\alpha_L)\frac{d_j}{b_j}\,\theta$	$8\frac{d_j^{\,2}}{b_j}\beta(\beta-\alpha_L)\, m_p\theta$
4	$\theta_4 = \left(\frac{\beta}{\alpha_L} - 1\right)\theta$	$2b_j\left(\frac{\beta}{\alpha_L} - 1\right) m_p\,\theta$
5	$\theta_5 = \theta$	$2b_j m_p\,\theta$
6	$\theta_6 = \left(\frac{1-\beta}{\alpha_U}\right)\theta$	$\frac{1}{2}\frac{(\alpha_U - s)^2}{\alpha_U}(1-\beta)d_j^{\,2}\, n_{wy}\theta$
7	$\theta_7 = \left(\frac{\beta}{\alpha_L}\right)\theta$	$\frac{1}{2}\frac{(\alpha_L - s)^2}{\alpha_L}\beta d_j^{\,2}\, n_{wy}\theta$

where $m_p = {}_c\sigma_y t_{cf}^2/4$

Differential of equation (3.1) based on collapse mechanism I over α_U, α_L and β reach to:

$$\alpha_L = \alpha_U = \frac{\sqrt{kr^3s^2+1}}{r\sqrt{kr-4}} \qquad (3.6)$$

$$\beta = \frac{1}{8}\, n\, k\, r + \frac{1}{2} \qquad (3.7)$$

where "k" and "r" in the above equations are as follows:

$k = \left(b_j/t_{cf}\right)^2 \left(t_{bw}/d_j\right)\left({}_{bw}\sigma_y/\ {}_c\sigma_y\right)$;

$r = d_j/b_j$

By substituting α_L, α_U and β in the equation (3.1), equation of m_o is obtained by:

$$m_o = \frac{4\sqrt{kr-4}}{kr^2}\sqrt{kr^3s^2+1} - \frac{2}{kr^3} + \frac{4}{kr} - 4s - \frac{1}{4}n^2kr \qquad (3.8)$$

According to equation (3.6), depth of yield region of web (α_L, α_U) are equal to the depth of bare steel beam in Reference [3.2]. Also m_o which is obtained by equation (3.8) is same to the equation of bare steel beam which is introduced in that reference, except the last term of equation.

According to Equation (3.7), location of neutral axis (N.A) is dependent on the amount of axial force (n) and may move toward upper flange. Considering the constant depth of web yield region shown by Equation (3.6), it is necessary to consider β limitation as :

$$\beta \leq 1 - \alpha_U$$

According to this limitation, in this mechanism for application of equation (3.8) the following requirement of n must be satisfied:

$$n \leq \frac{4}{k\,r}\left(1 - \frac{2\sqrt{kr^3s^2+1}}{r\sqrt{kr-4}}\right) \qquad (3.9)$$

In the case of non scallop beam, these equations are applicable by just substituting $s = 0$.

3.2.3 Mechanism II

Figure 3.1(b) illustrates the collapse mechanism after n exceeding the requirement of equation (3.9). Dissipated energy in the yield lines of regions 3 to 7 are summarized in Table 3.2.

Table 3.2 Dissipated Energy based on Mechanism II

Region	***Rotation Angle***	*Equivalent hinge Length*	***Dissipation(d_i)***
3(×2)	$\theta_3 = 2(\beta - \alpha_L)\dfrac{d_j}{b_j}\,\theta$	$2 \times 2\beta d_j$	$8\dfrac{{d_j}^2}{b_j}\beta(\beta - \alpha_L)\,m_p\theta$
4	$\theta_4 = \left(\dfrac{\beta}{\alpha_L} - 1\right)\theta$	$2b_j$	$2b_j\left(\dfrac{\beta}{\alpha_L} - 1\right)m_p\,\theta$
5	$\theta_5 = \theta$	$2b_j$	$2b_j m_p\,\theta$
6	$\theta_6 = \theta$	$(1 - \beta - s)d_j$	$\dfrac{1}{2}(1 - \beta - s)^2 {d_j}^2\, n_{wy}\theta$
7	$\theta_7 = \left(\dfrac{\beta}{\alpha_L}\right)\theta$	$(\alpha_L - s)d_j$	$\dfrac{1}{2}\dfrac{(\alpha_L - s)^2}{\alpha_L}{d_j}^2\beta\, n_{wy}\theta$

Differential of equation (1) based on collapse mechanism II over α_L and β, again reach to the same α_L given by equation (3.6), and β is defined by:

$$\beta = \frac{kr^2(n+1) - \sqrt{kr-4}\sqrt{kr^3s^2+1}}{r(kr+4)} \tag{3.10}$$

By substituting α_L and β in the equation (3.1), m_o equation for mechanism II is obtained by:

$$m_o = \frac{2}{(kr+4)}\left[(n+1)\left(\frac{2}{r}\sqrt{kr-4}\sqrt{kr^3s^2+1} + 4 - krn\right) - \frac{kr-4}{kr^3} - 2s\big(kr + 4(1-s)\big)\right] \tag{3.11}$$

According to Equation (3.10), location of neutral axis may move toward top flange, shown in Figure 3.2. So limitation for boundaries of β in the Mechanism II can be explained as:

$$\alpha_U \leq \beta \leq 1 - s$$

For application of equation (3.11) the following requirement of n must be satisfied:

$$\frac{4}{k\,r}\left(1-\frac{2\sqrt{kr^3s^2+1}}{r\sqrt{kr-4}}\right)\leq n\leq\frac{1}{kr^2}\left[r(1-s)(kr+4)+\sqrt{kr-4}\sqrt{kr^3s^2+1}\right]-1 \qquad (3.12)$$

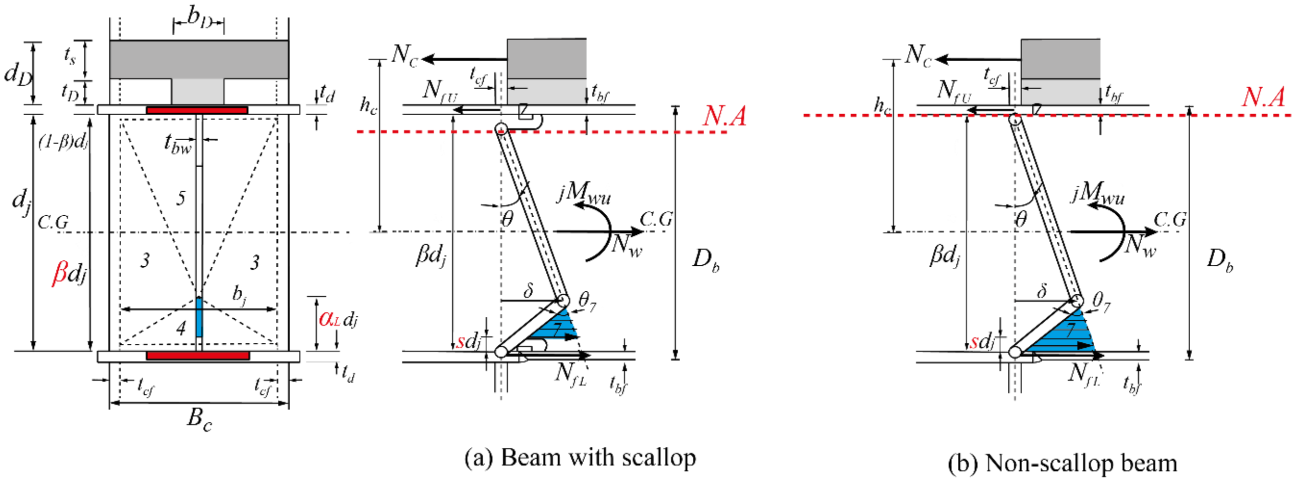

Fig. 3.2 Upper boundary of Mechanism II

Same to mechanism I, by substituting $s=0$ in the above equations result to evaluation of non scallop beam strength.

3.3 Finite element analysis study

Following to the experimental test observations of three full-scale beam-to-RHS column sub-assemblies, numerical investigation is conducted to understand the mechanism of mechanical behavior and effect of out-of-plane deformation on the elasto-plastic behavior of composite beam.

In order to study the stress and strain transfer mechanism of composite beam, finite element analysis results are explained in this section.

3.3.1 Outline of analysis and modeling

Following to experimental test results, and in order to conduct investigation regarding the effect of RHS column out-of-plane deformation on the behavior of composite beam, finite element study were carried out by general finite element analysis program ABAQUS Ver.6.5. Analysis conducted for 8 models as shown in Table 3.3. The configuration of finite element model is illustrated in Figure 3.2. In this model slab is modelled by truss element to make the analysis simple. Considering the actual geometry of steel deck, concrete is consisted of 2 parts: continues concrete slab over the ribs and concrete located in the ribs (lower part of deck). So two truss elements were prepared corresponding to these two regions of concrete slab. In the truss element corresponding to the main slab part, effective width is equal to 1.3 times of width of RHS column from the column face to the first stud, and after first stud and in the remaining part of beam, effective widths is determined according to the "Design Recommendations for Composite Constructions", (AIJ 2010) [3-5]. In the second region of concrete slab located in the ribs, width of concrete is considered 140 mm and thickness is 50 mm, which is same to the actual steel deck geometry.

Another slab is also prepared from the first stud to the centre of RHS column. From the centre of column it is connected to transverse beam by rigid constrain. This part is representing bearing stress transfer. In this model it is assumed that bearing crush will occur between the column face and first stud.

Another truss element with different length were prepared to represent stress transfer to the transverse beam.

If truss element is connected to the RHS column wall directly, concentration of load transfer might happen. To prohibit such problem, some stiffening is provided in the region that slab is attached to the RHS column face.

Studs are modelled by spring elements which are connected to the beam flange by rigid element. Half model is prepared due to symmetry and appropriate constraints have been applied on the symmetry part. The yield criterion on the basis of Von Mises and associated flow rule were employed to model plastic behavior of steel material.

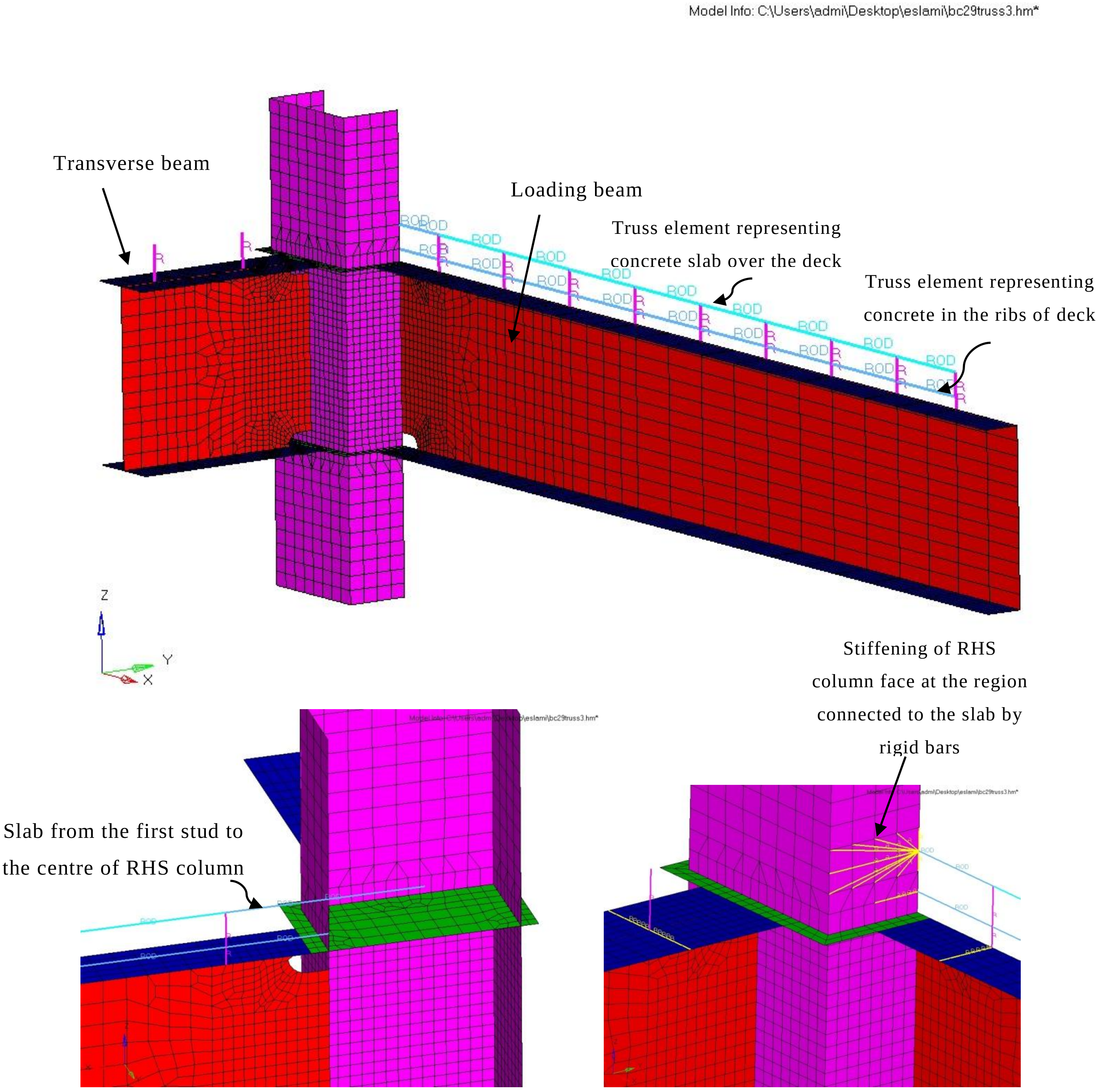

Fig. 3.2 Finite element model of composite beam

Table 3.3 FEA models specifications

Specimen	Concrete Slab	Width-to-thickness ratio of RHS column
BS00	No	0
BS16	No	16
BS22	No	22
BS29	No	29
CB00	Exist	0
CB16	Exist	16
CB22	Exist	22
CB29	Exist	29

For the steel material, yield stress and ultimate stress are taken from the laboratory test performed on the materials of tested specimens. Concrete material model is shown in Figure 3.3 which is decided based on previous research on bearing capacity of concrete, conducted by Inoue[3-6)]. Calibration of concrete model in comparison with Inoue study is shown in Figure 3.4. The strain at which maximum compressive stress occur is extended in the plateau part of curve comparing with Inoue's model. The first softening part of curve is parallel to Inoue's curve and more gradual softening is decided in the next part.

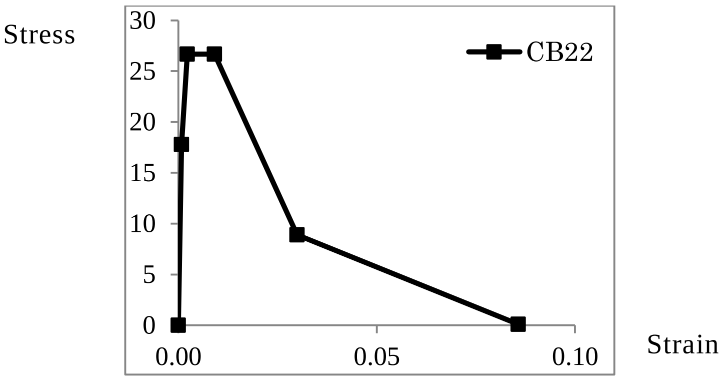

Fig. 3.3 Compressive stress-strain curve used for concrete

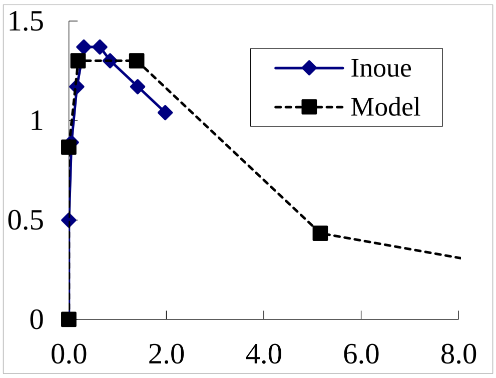

Fig. 3.4 Calibration of concrete model according to previous study conducted by Inoue

3.3.2 Correspondence of FEA and experimental test results

Results of numerical monotonic loading are compared with skeleton curves obtained from experimental cyclic loading test for beam rotation in Figure 3.5 (a). In these graphs the horizontal axis is beam rotation angel (θ_b) and the vertical axis is beam moment at the column face (M_b). Thicker solid line is associated to the FEA results and thinner solid line is associated to the experimental test result. For all specimens regardless of RHS column width-to-thickness ratio and existence of concrete slab, acceptable correspondence between numerical analysis and experimental test results can be observed. In the case of composite beam, the model is capable of taking count in the effects of concrete crush in the restraining characteristics. Considering the fact that in CB-29 actual failure was determined by progress of crack at the root of scallop, and FEA result has correspondence to the maximum strength, it can be concluded that even in CB-29 concrete was near to reach to its ultimate capacity, but premature failure prohibited reaching to this capacity.

In the case of strain behavior, the correspondence between strain versus beam rotation angle of specimens are illustrated in Figure 3.5 (b) which depicts that in the case of width-to-thickness of 29 regardless of bare or composite, some less estimation of strain by the model exist (which is more considerable for the bare steel beam) . But globally it can be seen that model estimation of strain is not significantly different with the actual strain behavior.

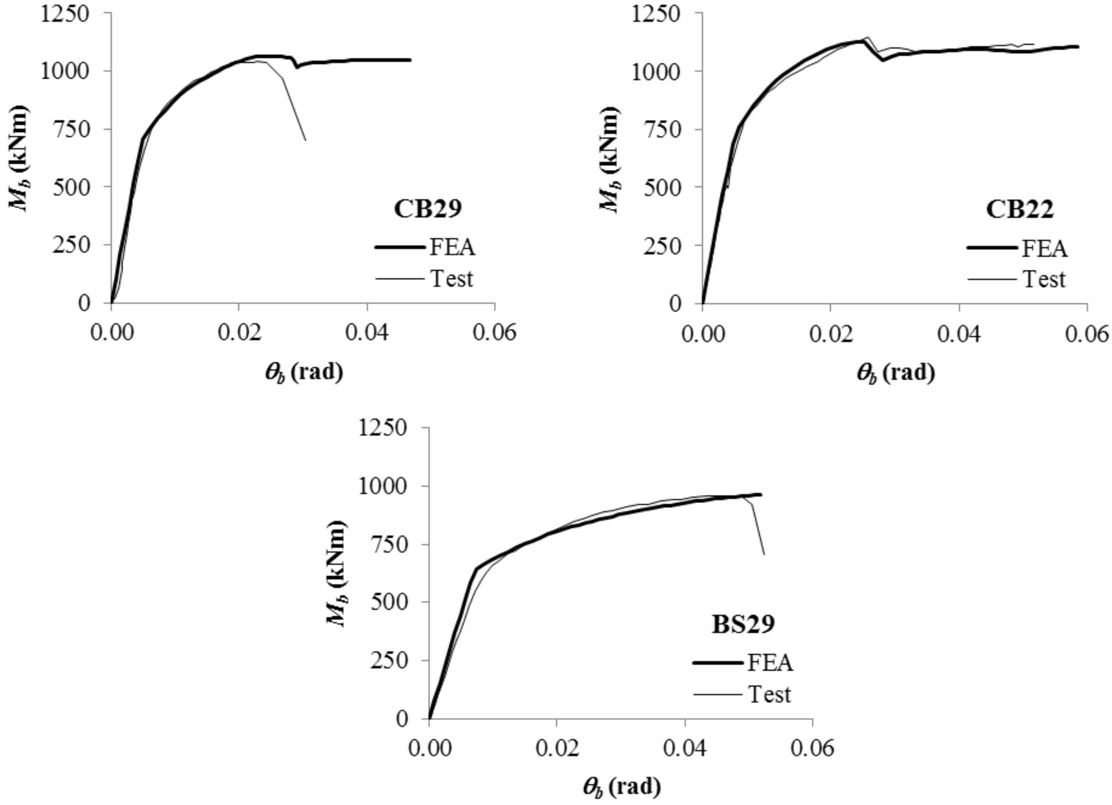

(a) M_b-θ_b curves

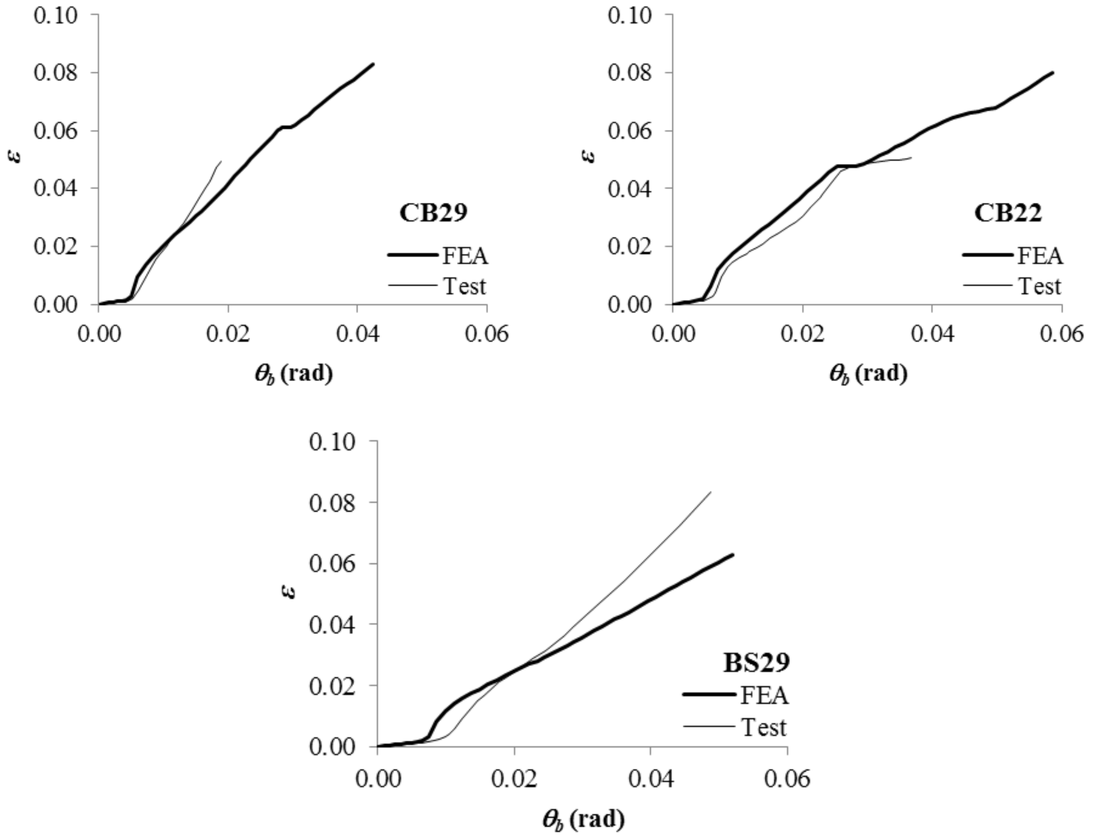

(b) Strain versus beam rotation angle (θ_b)

Fig. 3.5 Correspondence of FEA and experimental test results

3.4 Mechanism of behavior of composite beam connected to RHS column

3.4.1 Finite element analysis results

1) Global behavior

Figure 3.6 illustrates the effects of width-to-thickness ratio of RHS column in M_b-θ_b curves. Regardless of existence of concrete slab, in both bare steel beam and composite beam effect of RHS column width-to-thickness ratios can be seen.

However despite this similarity, difference in characteristics of strain hardening can be seen.

In the case of bare steel beam, for different width-to-thickness ratio premature yielding happen, but by keeping high strain hardening and after significant rotation, regardless of premature yielding finally closing to the rigid condition happen. While in the case of composite beam, strain hardening manner is different for different width-to-thickness ratios.

In the smaller width-to-thickness ratio of composite beam, by progress of rotation tendency of reaching to higher capacity exist. After that sudden strength reduction occur and keeping the constant strength after that reduction.

So, much more considerable difference in the characteristics of strain hardening can be observed in the composite beam.

According to experimental test observations of chapter 2 for CB-22 specimen, it is know that this sudden reduction of strength has correspondence with bearing crush in the concrete.

Considering the point that some difference in the moment amount at 0.06 rad between bare and composite beam exist, it is found that after concrete softening still some difference in the different *B/t* composite beams exist.

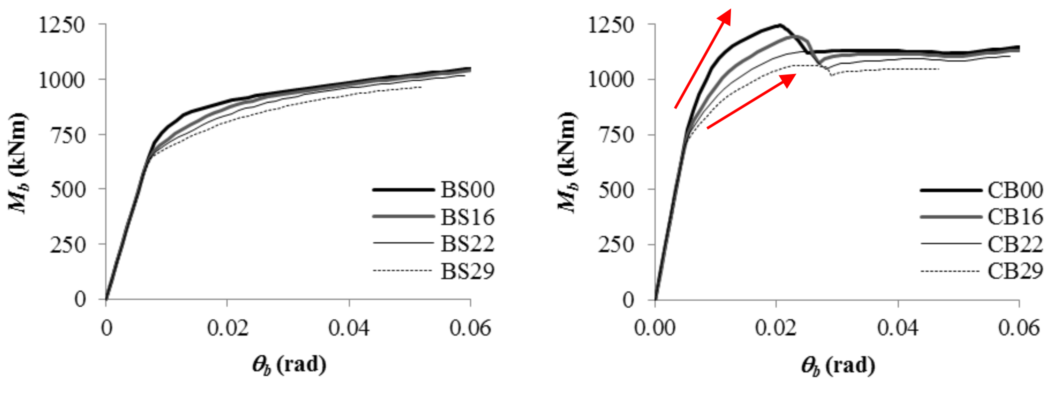

Fig. 3.6 Effects of width-to-thickness ratio of RHS column in M_b-θ_b curves

2) Web moment

According to Figure 3.7 for the web moment condition, similarity of effect of width-to-thickness ratio of RHS column can be seen in both bare steel beam and composite beam. Almost same effect can be found for different width-to-thickness ratios.
However, in the case of composite beam, increase of web moment consists of 2 stages. After reaching to a certain rotation, effect of width-to-thickness ratio is decreasing. It seems that it can be related to the rotation which maximum moment was observed in Figure 3.6. It can be seen that effect of composite action is considerably different after certain rotation. This behavior will be discussed later.

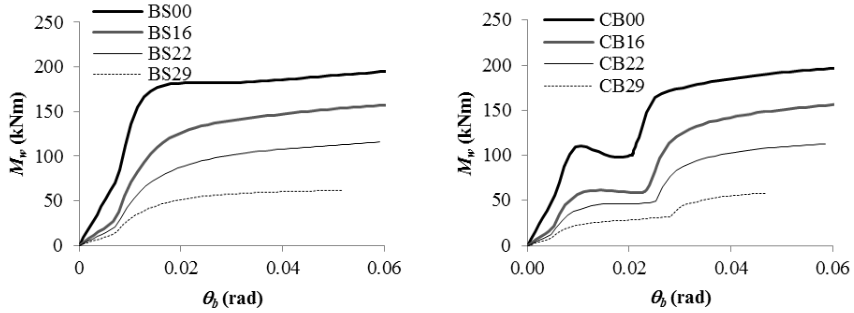

Fig 3.7 Web moment

3) Strain behavior

Effect of RHS column width-to-thickness ratio in the strain condition of both composite and bare steel beam flanges can be seen by the Figure 3.8 .According to Figure 3.6 it is already known that in the case of composite beam, around $2\theta_p$ corresponds to before start of concrete softening. So it can be seen that in this rotation angle strain of top flange is quite small, while bottom flange strain is considerably high. In the case of bare steel beam (right side Figures), strain of bottom flange is smaller comparing to composite beam.
Ratio of strain increase by increase of width-to-thickness ratio is higher in the composite beam rather than bare steel beam. Larger width-to-thickness show much higher strain compare to the bare steel beam.
Beam rotation angle $4\theta_p$ correspond to almost after concrete crush. Strain of top flange is considerably increased, but still some width-to-thickness effect can be seen.

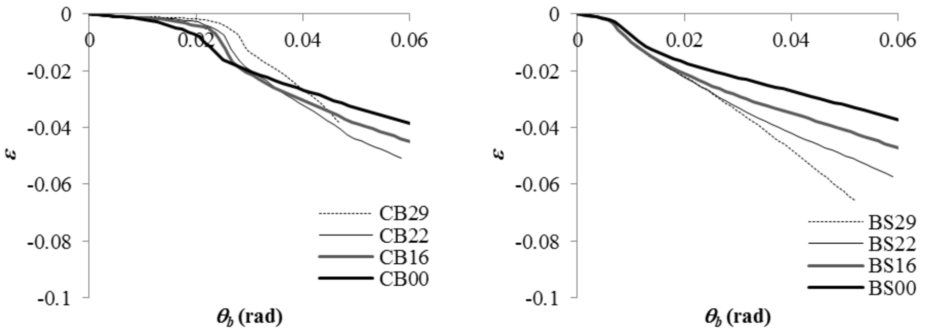

(a) Top flange

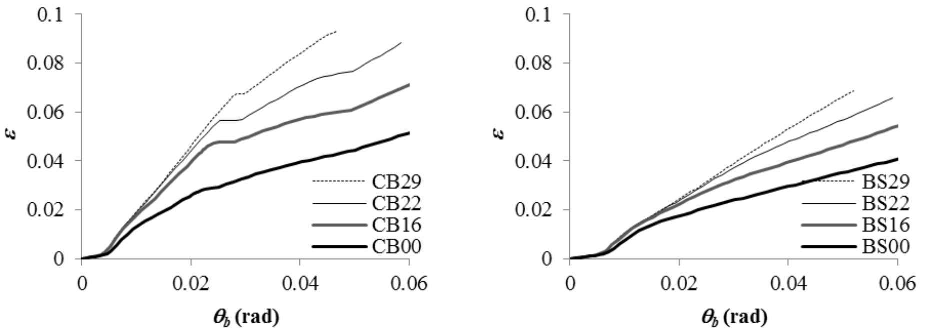

(b) Bottom flange

Fig. 3.8 Strain behavior of flanges

3.4.2 Stress transfer

1) Global behavior

Figure 3.9 illustrates flexural moment of beam at column surface. Comparison between bare steel beam and composite beam global behavior is shown. Thick black solid line represents composite beam, and thin gray line represents bare steel beam. It can be seen that effect of composite action in moment capacity is increased by reduction of width-to-thickness ratio of RHS column.

In these figures, each moment component of composite beam contributed by slab and steel beam are shown by gray thick solid line and broken line, respectively.

Slab moment component is estimated by axial force of slab elements at the vicinity of connection multiplying to the distance from center of gravity of steel beam for each slab element. Steel beam moment component is estimated by remaining of total moment excluding the slab moment component.

Steel beam moment in composite beam shows correspondence to the bare steel beam moment in the elastic region. But reduction of yield moment of composite beam can be seen because of effect of axial tensile force in steel part, generated by composite action corresponding to slab compression force. This reduction of yield moment is reduced by decreasing of width-to-thickness ratio of RHS column.

N_{slu} shown in figures represents the condition that slab axial compressive force reach to the maximum capacity which is corresponding to bearing crush of slab at the vicinity of column.

Steel beam moment component of composite beam start to increase higher rate after slab force reach to maximum. Vertical broken line shows the correspondance between ultimate condition of slab N_{slu} and change in the rate of steel component curve , shown by white triangle. Finally, after certain increase of beam rotation, steel beam component reach to almost same capacity of bare steel beam model regardless of width-to-thickness ratio of RHS column.

M_{bu} indicated in figures represents the condition that total beam flexural moment of composite beam reachs to maximum capacity. In the case of CB00 and CB16, beam rotation corresponding to N_{slu} and M_{bu} are amost same, but in the case of CB22 and CB29, beam rotation corresponding to M_{bu} is larger than the rotation corresponding to N_{slu}. Namely, maximum flexural moment capacity of composite beam occur in the certain increase of beam rotation after slab bearing capacity.

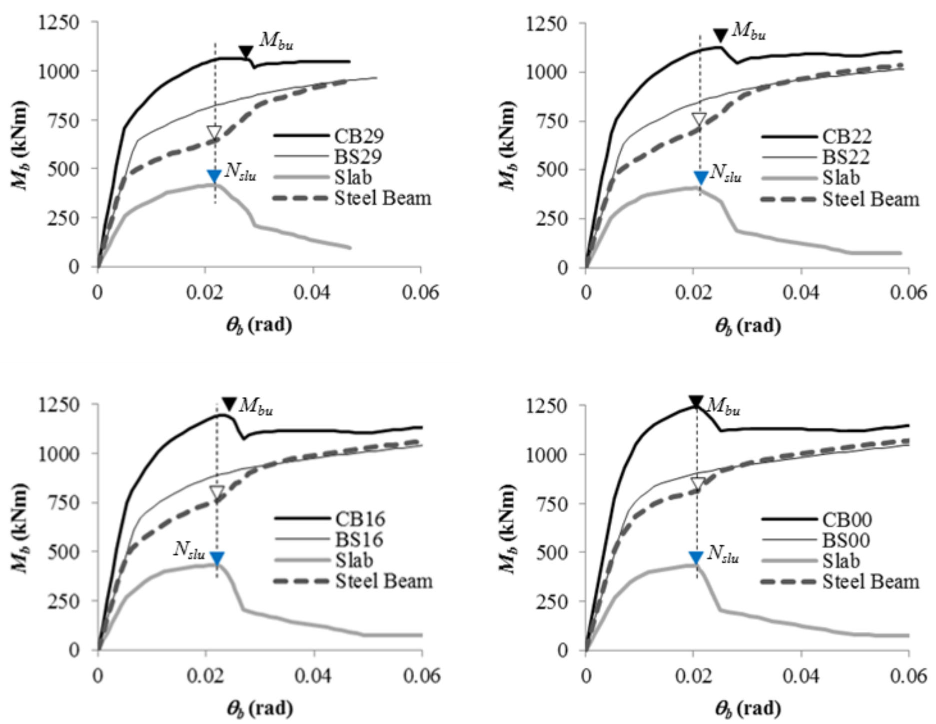

Fig. 3.9 Global bahivior of composite beam

2) Axial force of each component

Figure 3.10 shows axial force of bottom and top beam flange behavior at column face with different width-to-thickness ratio of column. Horizontal two lines in figures correspond to yield capacity, N_{fy}, and tensile capacity, N_{fu}, of beam flange.

In the case of bottom flange behavior shown in Figure 3.10(a), axial force increases with increasing of width-to-thickness ratio of column after axial force reach to yield capacity. This is resulted from effect of out-of-plane deformation of column flange at beam web connection. Finally this effect results to reduction of beam rotation, which correspond to bottom flange axial force reach to tensile capacity by increasing of width-to-thickness ratio of column. This result shows conformity to the reduction of rotation capacity by the increasing of width-to-thickness ration of column, seen in test results described in chapter 2.

On the other hand, axial force of top flange behavior shown in Figure 3.10(b) reduces with increasing of width-to-thickness ratio of column. In the case of lager width-to-thickness ratio, it can be found that considerable amount of beam rotation is required to reach to the yielding of top beam flange.

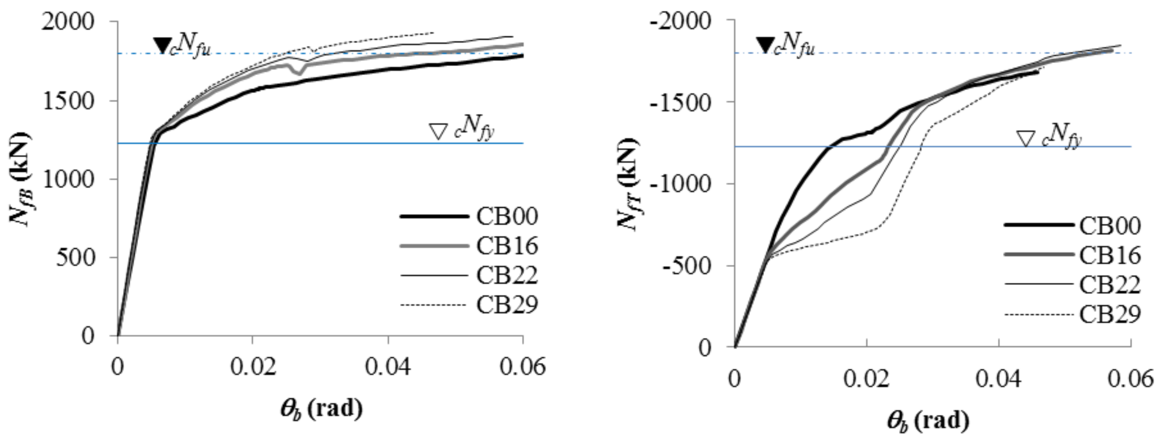

(a) Bottom beam flange (b) Top beam flange

Fig. 3.10 Beam flange axial force behavior

Figure 3.11 and 3.12 show slab axial force and beam web axial force behavior at column face respectively. In the case of slab axial force, behaviors are almost same regardless of the difference in width-to-thickness ratio of column. On the other hand, beam web axial force considerably reduces with increasing of width-to-thickness ratio.

Horizontal line shown in Figure 3.11 and 3.12 shows slab bearing capacity calculated by Equation 3.13.

$$ {}_cN_{slu} = 1.3(B_c \cdot t_e + A_d)F_c \tag{3.13} $$

Here, B_c, t_e and A_d correspond to width of column, effective thickness of slab and slab concrete section area corresponding to region of concrete filled on the top beam flange, respectively. ${}_cN_{slu}$ gives good estimation to the maximum capacity of slab axial force. Beam rotation which correspond to maximum axial force are almost 0.022 rad (2.5 θ_{bp}).

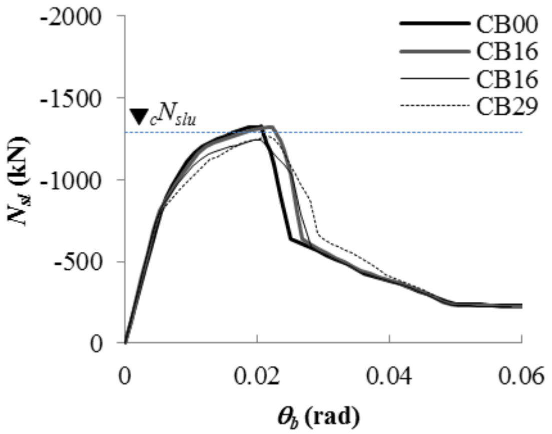

Fig. 3.11 Slab axial force behavior

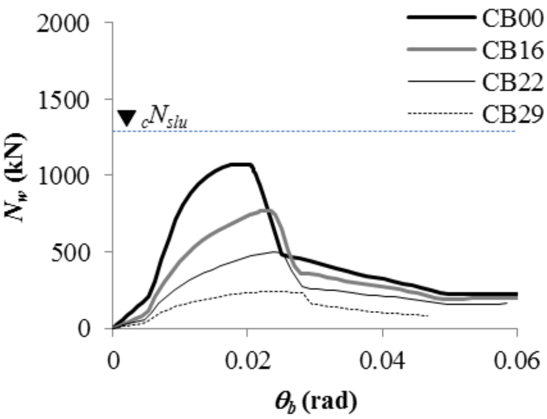

Fig. 3.12 Beam web axial force behavior

Figure 3.13 shows each component of axial force to beam rotation relationships. In each figures, N_{fB} and N_{fT} correspond to the axial force of bottom and top beam flange at column face, respectively. Also, N_{sl} and N_w correspond to the component of slab and web at the column face, respectively.

In each figures, vertical two broken line show the beam rotation when total beam flexural moment reach to the maximum capacity, M_{bu} and slab bearing force between slab and column flange reach to the maximum capacity, N_{slu} .

As described in global behavior in this section, beam rotation corresponding to M_{bu} is larger than the rotation corresponding to N_{slu} in the case of lager width-to-thickness ratio of RHS column. Except CB00, discontinues of slope in N_{fB} behavior can be seen when beam rotation reach to M_{bu} condition. In this point, axial stress at bottom flange behavior reach to unloading condition and again loading condition instantaneously.

In the case of CB00, difference between axial force of top and bottom flanges is not considerable, and difference between axial force of slab and web is not also considerable too. In fact, difference of axial force of top and bottom flanges must be equal to the difference of slab axial and beam web due to force equilibrium requirement to the axial direction. Namely, steel beam section is subjected to tensile axial force corresponding to slab compressive axial force introduced by composite action. Since steel beam web connection in the case of CB00 has sufficient rigidity and strength, so beam web can transmit most of amount of tensile axial force subjected to steel beam section. This sufficient capacity of web connection results to less difference of top and bottom flange axial force. On the other hand, considerable reduction of web axial force can be seen in CB29. Eventually this reduction of axial capacity of web connection result to considerable reduction of top flange axial force.

After slab axial behavior reach to softening condition, increase of slope in top flange axial force behavior can be seen except CB00 and especially in the case of lager width-to-thickness ratio of column. This increase of the slope in lager width-to-thickness ratio of column result to total flexural moment increase even after slab axial force behavior reach to softening condition until beam rotation corresponding to M_{bu}. Hollow circle shown in figures represent that top flange axial force reaches to yield capacity. It can be said beam rotation corresponding to total flexural maximum capacity, M_{bu}, is determined by the yielding of top flange except CB00. Also decreasing of web axial force is determined by the yielding of top flange, except CB00. In the case of CB00, yielding of top flange can be seen prior to the beam rotation corresponding to N_{slu}.

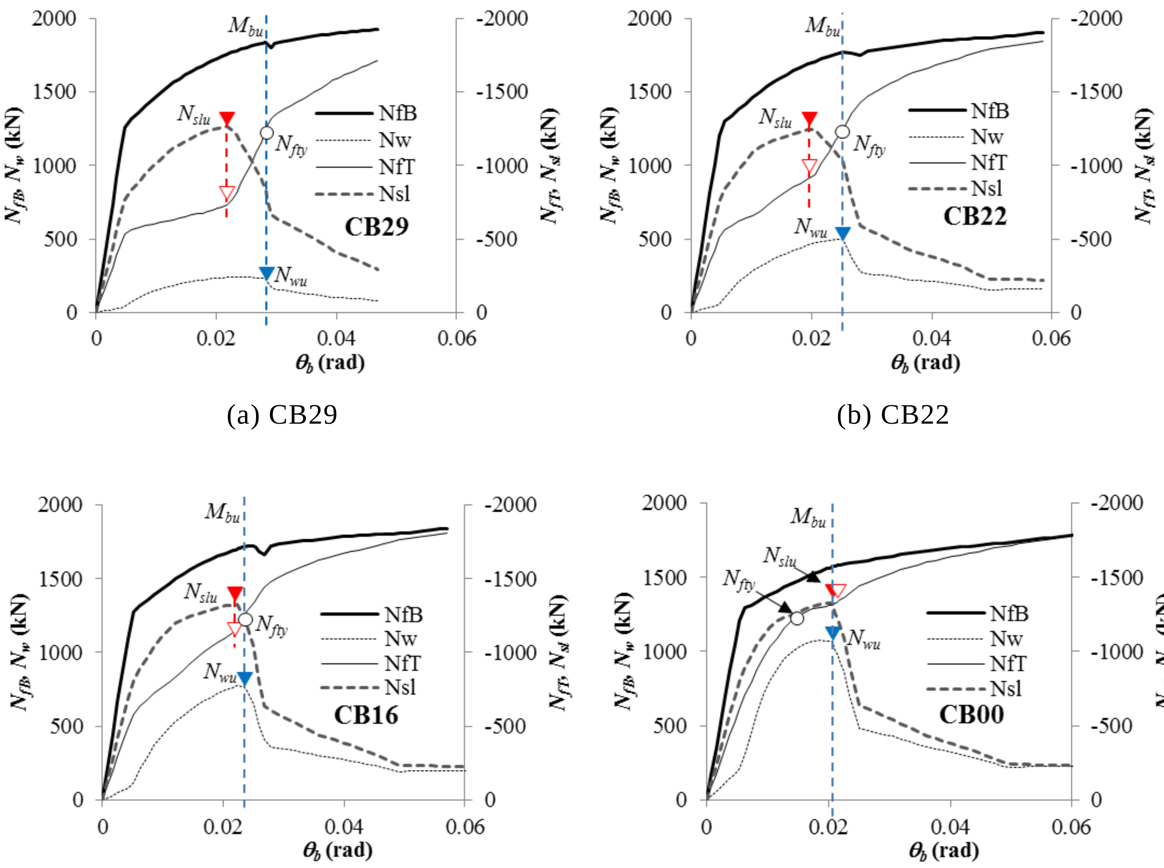

(a) CB29 (b) CB22

(c) CB16 (d) CB00

Fig. 3.13 Axial force component of each part

3) Web connection behavior

Figure 3.14 show beam web flexural moment versus beam rotation. In here web flexural moment, M_w, is estimated at the face of column. In this figure, web flexural moment of bare steel beam model and composite beam model are compared, and also web axial force, N_w, is shown by broken line. Scale of N_w is shown vertical axis of right side.

In early stage of beam rotation, behavior of bare steel beam model and composite beam model are almost same. But, web flexural moment of composite beam model is reduced compared to bare steel beam model because of the existence of axial force of beam web. As mentioned formerly in axial force component behavior in this section, when total flexural moment reach to maximum capacity, which is determined by yielding of top flange in the case of larger width-to-thickness ratio of column, web axial force N_w start to reduce. Web flexural moment start to increase with reduction of web axial force, Nw, and finally, web flexural moment behavior of composite beam model is closing to behavior of bare steel beam model.

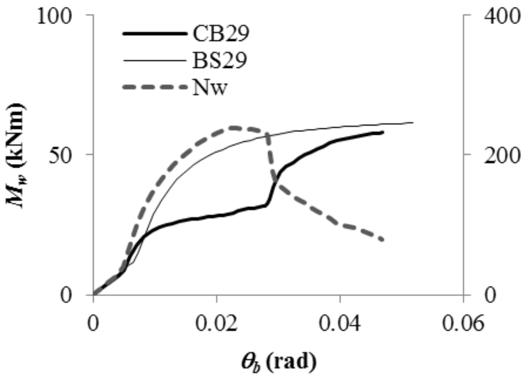

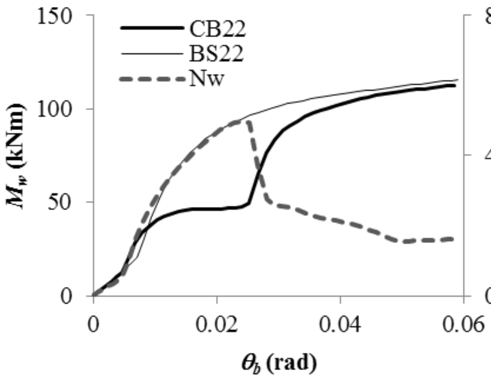

(a)

(a) CB29 (b) CB22

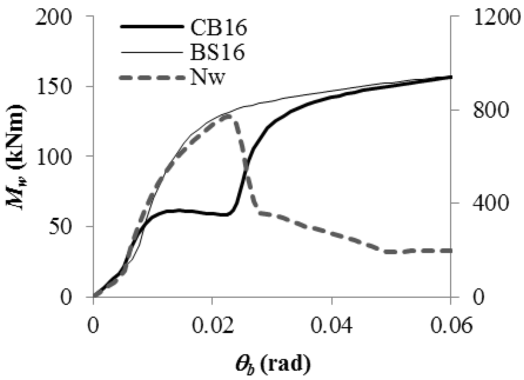

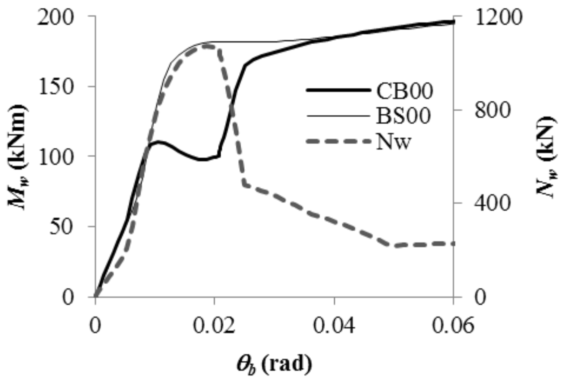

(c) CB16 (d) CB00

Fig. 3.14 Axial force component of each part

Figure 3.15 shows M-N interaction of web connection obtained from results of FEA and also limit analysis. M-N interaction which is indicated by “Rectangular Section” corresponds to the interaction of web effective section considering the effect of lack of section by existence of scallop.

It can be seen that results of limit analysis give good estimation to results of FEA. In the case of large width-to-thickness ratios web connection capacity due to axial force and flexural moment is considerably reduced. However, in the case of CB16 it can be considered as close to CB00.

According to FEA results shown in Figure 3.15, in the early stages of beam rotation angle, steady progress of M and N can be seen. After a certain rotation angle, change in the rate of increase of N happen, but in this stage N increase is not accompanied by reduction of M. It means that in this condition, connection is not in the plastic condition and it corresponds to initiation of yielding and development of plastification in the connection. This stage is corresponding to plateau part of M curve which was shown in Figure 3.14.

By progress of beam rotation angle, increases of N continue until web reach to almost full plastic condition. After this condition reduction of N due to concrete crush happen and at the same time increase of M can be seen.

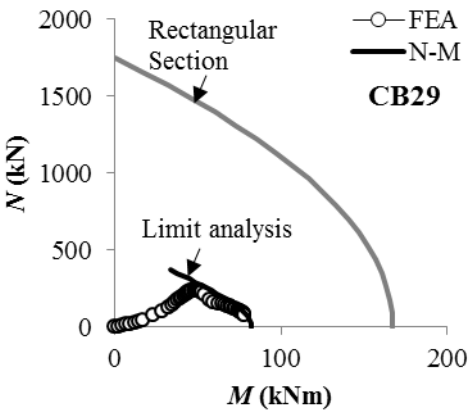

(a) CB29

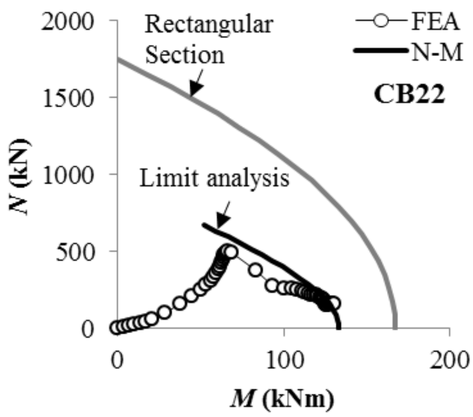

(b) CB22

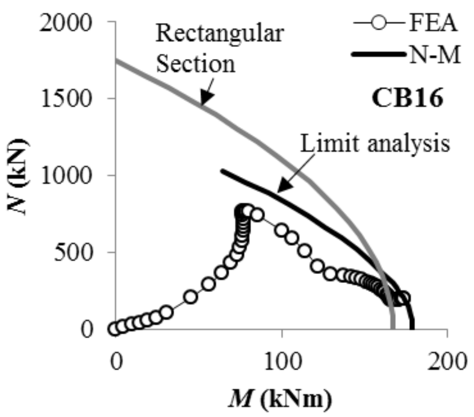

(c) CB16

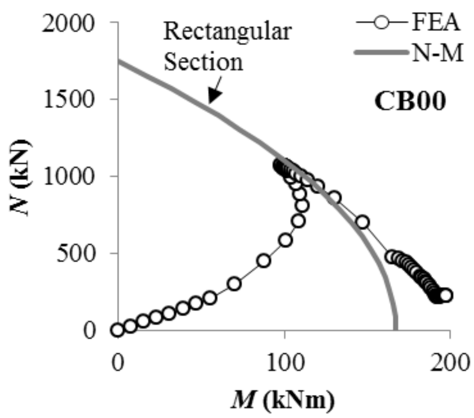

(d) CB00

Fig.3.15 M-N interaction curves

4) Longitudinal distribution of axial force component

Longitudinal distribution of top and bottom flange axial force, at certain loading condition of $2\theta_p$ and $4\theta_p$ are shown in Figure 3.16 (a) and (b). Beam rotation angle $2\theta_p$ is corresponding to the condition that concrete almost reach to its maximum capacity (almost final condition before concrete start softening behavior), and $4\theta_p$ is representing almost final stage of concrete softening.

In Figure 3.16 (a) and (b) horizontal axis is beam length (x) and the vertical axis is positive tensile and negative compression force of bottom and top flanges, respectively. Black circles represent bottom flange and white circles represent top flange force .

According to the Figure 3.16 (a), it can be seen that by reduction of RHS column width-to-thickness ratio, the diferrenc between bottom and top flanges reduces. Relation between slop of distribution of top and bottom falnge is also depond on the width-to-thickness ratio. In large width-to-thickness ratio of 29 both flanges are almost parallel while in the CB00 are not parallel and diferenc of slop at the vicinity of connection is reducing. This Figure is also helpful to undrestand level of stress of top flange and length of yeild region in the bottom flange.

However, after the occurrence of concrete crush, both flange forces become comparable at the vicinity of connection, as it is shown in 3.16 (b). But it can be seen that in CB29 still difference of flange forces exist, indicating that some width-to-thickness ratio effect still exist after concrete crush (but considerably reduced comparing with 2 θ_p). This behavior can be explained that in larger width-to-thickness ratio, concrete softening and reduction of axial force should significantly increase top flange stress, as previously described in the part 2 of this sec. by Figures 3.10(b) and 3.13.

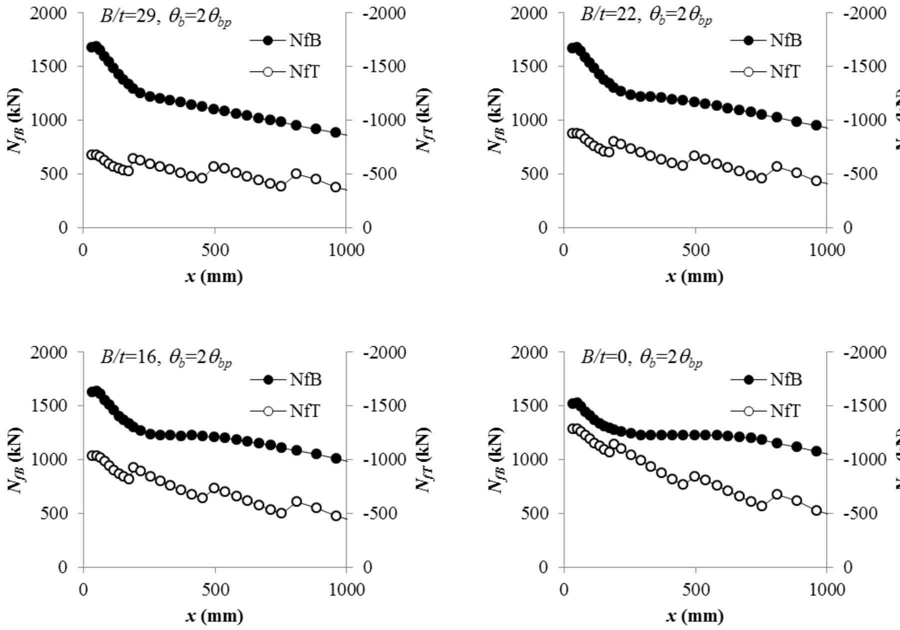

(a) Distribution of flange axial force at beam rotation angle of $2\theta_p$

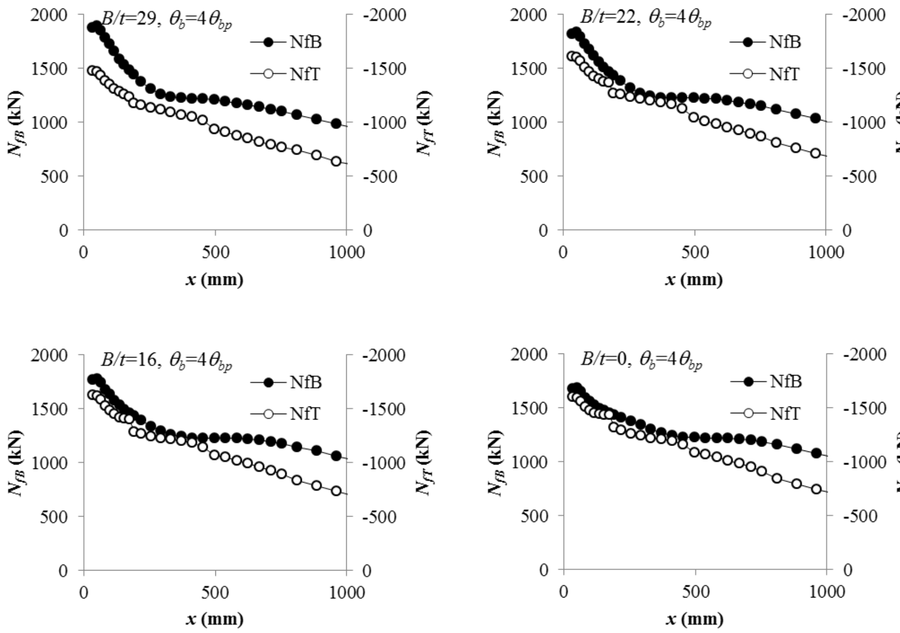

(b) Distribution of flange axial force at beam rotation angle of $4\theta_p$

Fig. 3.16 Longitudinal distribution of top and bottom flange axial force

Longitudinal distribution of axial force in the web and concrete slab in $2\theta_p$ and $4\theta_p$ are shown in Figure 3.17 (a) and (b). Horizontal axis is beam length (x) and the vertical axis is positive tensile and negative compression force of web and slab, respectively. Black circles represent web and white circles represent slab force.

According to Figure 3.17 (a), It can be seen that slab force is less affected by width-to-thickness rarios and almost comparable condition of slab force can be seen in CB29 to CB00. This was already pointed out in Sec. 3.4.2 (Part2) and Figure 3.11. However, considrable effect of width-to-thickness ratio is obsereved in the web axial force. Significant amount of web axial force is obtained in the small CB00.

Eeffect of width-to-thickness also can be seen in the difference of amount of web and slab forces. For large width-to-thickness ratio this difference is considrable, while for small width-to-thickness ratio this difference is not significant.

Since axial force subjected to the composite beam is proportional with the amount of concrete slab force, so the ratio between black and white circle correspond to ratio of axial force which is transmitted by web connection. The portion of force which is not transmitted by web is transmitted by differnce of flanges stress levels. It can be seen that in CB00 at the vicinity of column face almost all the axial force is transmitted by web connection. So the distance between salb and web in Figure 3.17 (a) is comparable with the distance between flanges shown in Figure 3.16 (a).

Following to the occurrence of concrete crush, reduction in the amount of axial force of concrete slab and web occurred, which is more considerable for the slab and shown in Figure 3.17 (b). It can be observed that despite concrete crush and considerable reduction of slab force, but still some slab axial force exist, which is almost constant and comparable for all different width-to-thickness ratio specimens. It also can be seen that in $4\theta_p$ away from the column face, some minor increase happened in the slab compression force. It can be explained that following to concrete crush, studs located away from the vicinity of column face transmit more shear force resulted from the compression force in the slab. This behavior of slab in $4\theta_p$ is vice versa of slab behavior in $2\theta_p$ which showed reduction of slab force along the beam length.

Removal of slab constraint at the column face resulted to this change of behavior in the slab compression force. By the way, in CB00 in around *x=500 mm* away from the column face, almost all axial force is transmitted by the web, which indicates that effect of connection capacity is appeared in around less than 500 mm away from the column face.

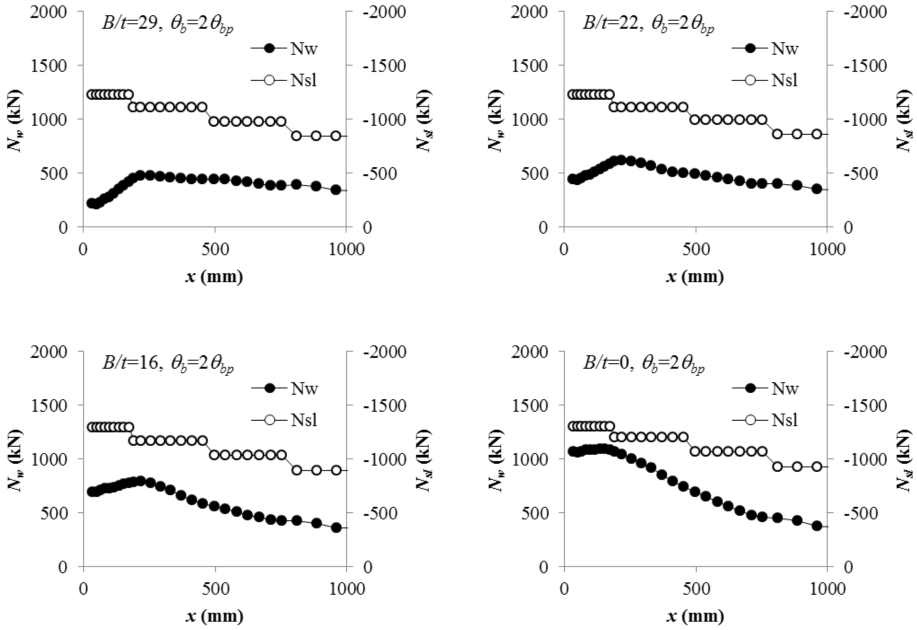

(a) Distribution of web and slab axial force at beam rotation angle of $2\theta_p$

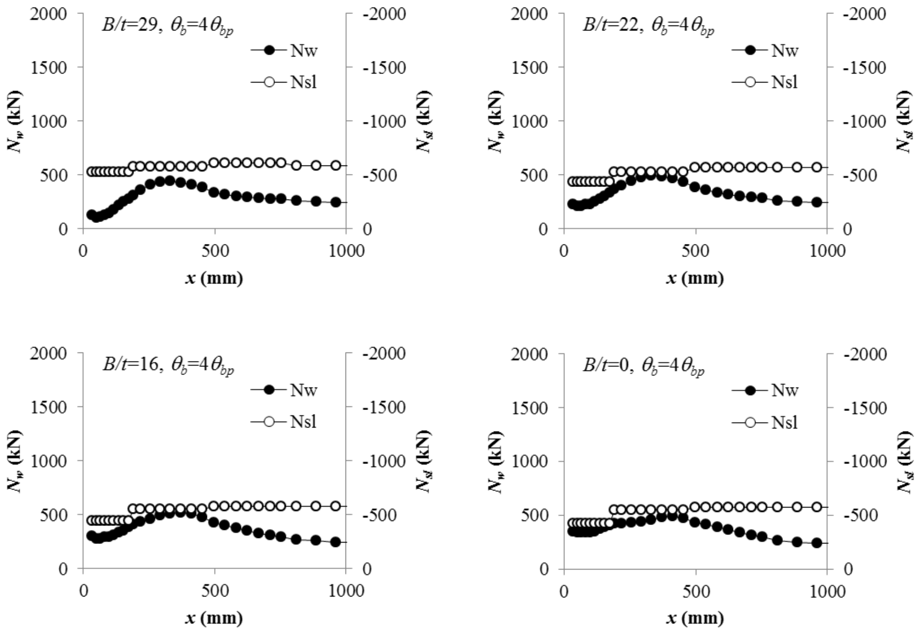

(b) Distribution of web and slab axial force at beam rotation angle of $4\theta_p$

Fig. 3.17 Longitudinal distribution of axial force in the web and concrete slab

5) Evaluation of total ultimate flexural moment capacity of connection

According to Figure 3.1, consideration of moment equilibrium condition for the connection reaches to the total flexural strength of connection ${}_jM_u$, defined as:

$$ {}_jM_u = N_c h_c + N_{fT} \frac{d_b}{2} + N_{fB} \frac{d_b}{2} + {}_jM_{wu} \tag{3.13} $$

For calculation of ${}_jM_{wu}$ in the above equation, estimation of "web axial force" is needed which is derived according to force equilibrium condition of Figure 3.1, and represented by:

$$N_w = N_c + N_{f\,T} - N_{f\,B} \qquad (3.14)$$

In equation (3.14), N_{fT}, N_{fB} and N_c are top flange compression force, bottom flange tensile force and concrete slab compression force, respectively. According to finite element study shown in Sec. 3.4.2 (part 2) , condition of flanges forces shows that composite beam top flange stress level is hardly to assume as tensile strength(σ_u). So in this report, N_{fT} and N_{fB} are assumed as:

$$N_{f\,B} = \sigma_u .\ A_{bf} \qquad (3.15)$$

$$N_{f\,T} = \sigma_y .\ A_{bf} \qquad (3.16)$$

Where, σ_y is yield stress and A_f is section area of beam flange.

For calculation of N_c , equation (3.17) is conventionally used as an empirical formula.

$$N_c = 1.3\, f_c(t_c\, B_c) \qquad (3.17)$$

This model is prepared for the conditions which the neutral axis remain in the beam web.

After the neutral axis exceed the boundary of Mechanism II and enter the upper flange, modification in the stress condition of upper flange is needed, which is explained as:

$$N_{fU} = \sigma_y\, A_{bf} - (N_c - N_{w\,(boundary\ Mech.II)}) \qquad (3.18)$$

In this condition, according to modification of upper flange stress, total flexural strength of connection ${}_jM_u$ which is defined in equation (3.13) can be can be shown by Figure 3.18.

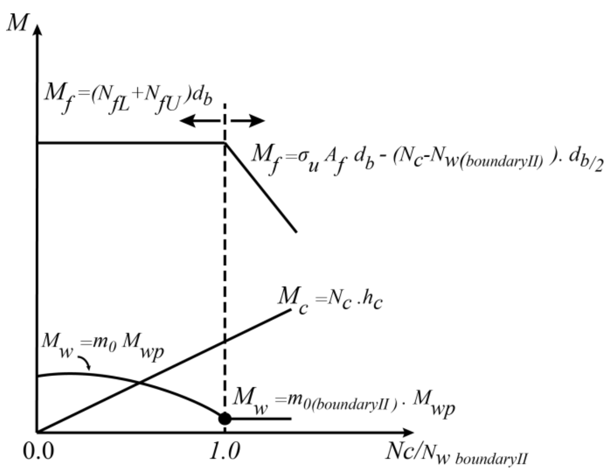

Fig 3.18 Evaluation of total moment after reaching to the boundary of Mechanism II

For the specimens which were mentioned in chapter 2 and Ref.3-7 to 3-10, total strength are evaluated based on proposed model. Figure 3.19 illustrates the M-N interaction curve for the web connection of these specimens.

According to equation (3.3), for CB-22 specimen $n=0.251$ and corresponding m_o in Mechanism II will be 0.372. For CB-29 the nondimentional axial force of web exceed the boundary of Mechanism II, so the m_o corresponding to the boundary is selected, which equals to 0.146 .

Table 3.3 summarizes the calculated $_jM_u$ and ratio between test results and the model. According to Figure 3.20, despite the differences in width-to-thickness ratios, acceptable agreement between the model and experimental test results can be observed for specimens which the web axial force did not exceed the boundary of Mechanism II.

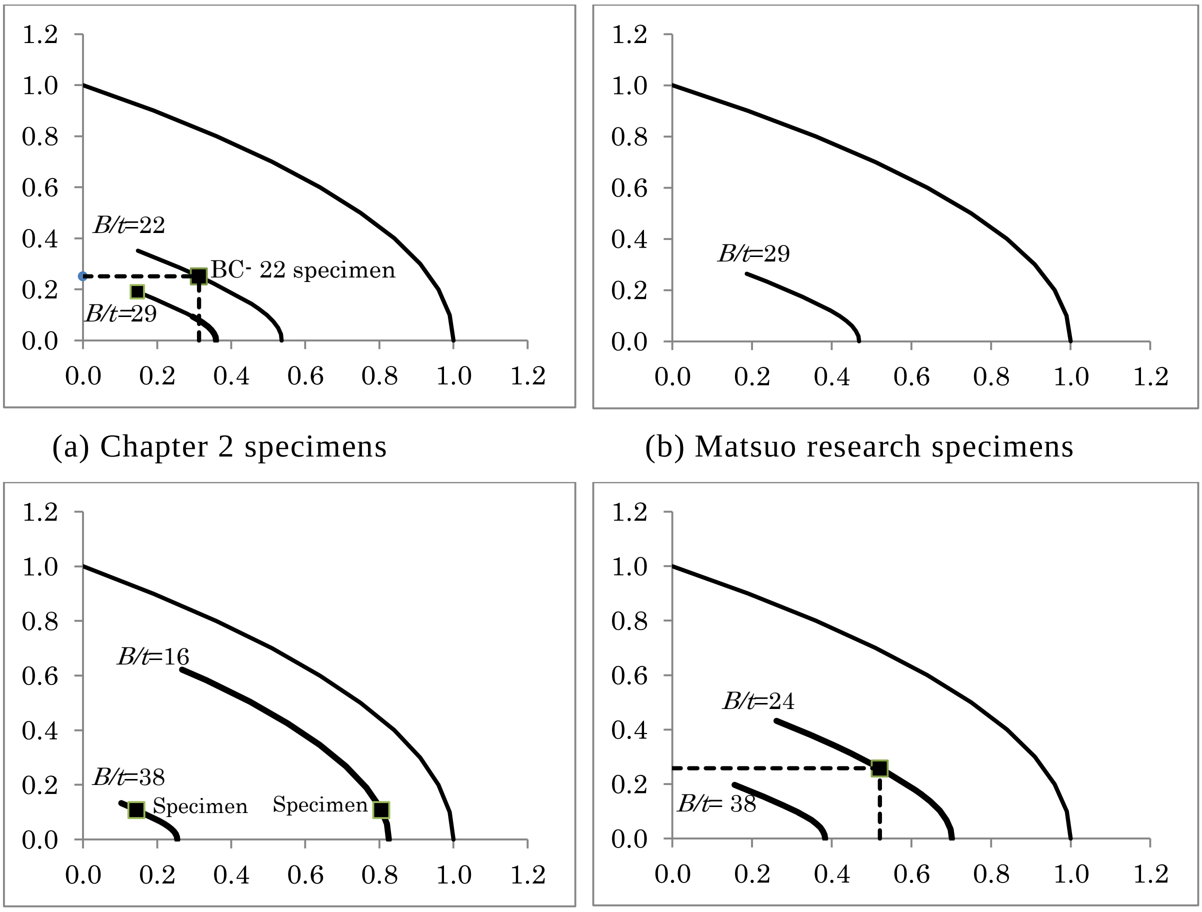

(a) Chapter 2 specimens (b) Matsuo research specimens

(c) Tanaka research specimens (d) Okada(2003) research specimens

Fig. 3.19 Web connection M-N interaction curve for reference specimens

Table 3.3 Evaluation of total strength of reference specimens

Test Reference	*Specimen*	*B/t*	n	m_o	${}_jM_{wu}$ (kN.m)	${}_jM_u$ (kN.m)	M_{+max} (test)	Ratio (M_{+max}/ ${}_jM_u$)
Chapter 2	CB-22	22	0.251	0.312	72.3	1145	1145	1.00
Chapter 2	CB-29	29	0.251*	0.146	33.7	1108	1042	0.97
Matsuo	AN-1	29	0.263*	0.186	34.7	994.7	904	0.91
Matsuo	AN-2	29	0.263*	0.186	34.7	994.7	926.6	0.93
Tanaka	CSCS-3.0	16	0.108	0.805	175	1156.7	1102.6	0.95
Tanaka	CSCW-3.0	38	0.108	0.144	31.4	1013	1021.2	1.01
Okada	3	24	0.258	0.521	174.3	1581.3	1650	1.04
Okada	4	38	0.196*	0.156	52.2	1244.5	1430	1.14

* : n=boundary of mechanism II

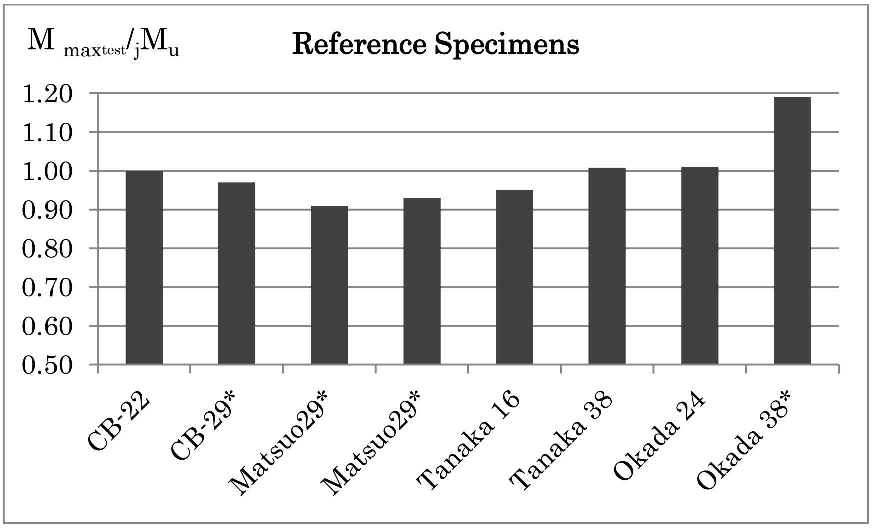

`

Fig. 3.20 Correspondence between ultimate strength evaluation by proposed method and test results

3.4.3 Strain behavior

1) Global behavior

Comparison between strain condition of bottom flange versus rotation angle in the bare steel beam and composite beam is illustrated in Figure 3.21 for different width-to-thickness ratios. Average of strain of beam lower flange at the face of RHS column is shown in this Figure. Effect of composite action on the strain condition can be seen by comparison between bare steel beam and composite beam in each specimen. It can be seen that effect of composite action is highly depend on with-to-thickness ratio. It is observed that by increase of rotation angle, difference between bare and composite beam strain is considerable in large width-to-thickness ratio specimen CB29, while reduction of difference can be seen in CB00.

It is found that in the composite beam, strain behavior consists of two stages, and by progress of beam rotation to a certain angle, sudden change in the rate of strain happens, while in the bare steel beam continues increase of strain exist. From the figure it can be seen that in the composite beam, rotation angle which change in the behavior of strain occur is not corresponding with slab maximum capacity N_{slu} (shown by red triangle). Steady effect of composite action continue, even after N_{slu} until M_{bu} sever effect of composite action has continued and after that effect of composite action to the strain is reduced (shown by black triangle).In small width-to-thickness ratio 29, concrete maximum capacity N_{slu} is considerably prior to this change of strain behavior. However, in CB00 both phenomenal of N_{slu} and M_{bu} happen at almost same time.

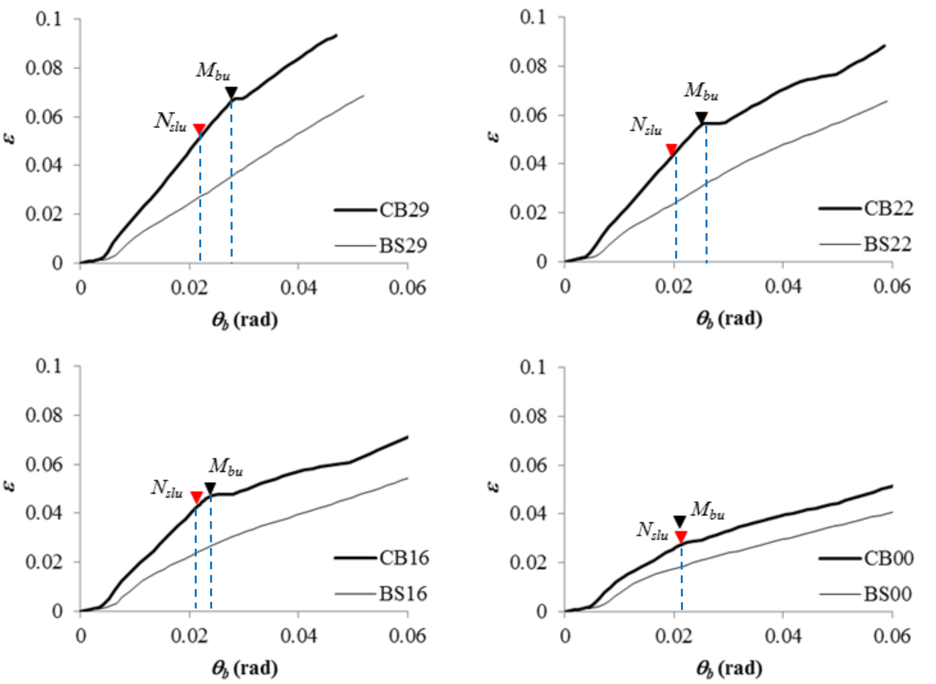

Fig. 3.21 Comparison between strain behavior of bare steel beam and composite beam

2) Longitudinal distribution of strain

In Figure 3.22, distribution of strain over the beam length is shown at beam rotation angle of $2\theta_p$ and $4\theta_p$ for different width-to-thickness ratios in the bare steel beam and composite beam. Bottom flange subjected to tensile strain is plotted on the positive side of vertical axis and top flange subjected to compression strain is plotted on the negative side of vertical axis. Horizontal axis is corresponding to the beam length.

It can be seen that in the bare steel beam regardless of width-to-thickness ratio both flanges are subjected to comparable increase of strain condition at the vicinity of column face. However, in the case of composite beam before the concrete crush at $2\theta_p$, considerable difference in the amount of strain can be found between top and bottom flanges.

Increases of width-to-thickness ratio for the bare steel beam does not result to considerable increase of strain in the flanges, while this results to significant increase of bottom flange strain in the composite beam.

By increase of beam rotation angle to $4\theta_p$ comparable increase of strain in both flanges of bare steel beam happen. While in the composite beam this rotation angle is corresponding to almost end of concrete crush and removal of constraint of top flange, increase of strain appear in both flanges. But still bottom flange is encountered with higher amount of strain and effect of width-to-thickness ratio can be found more in the condition of this flange.

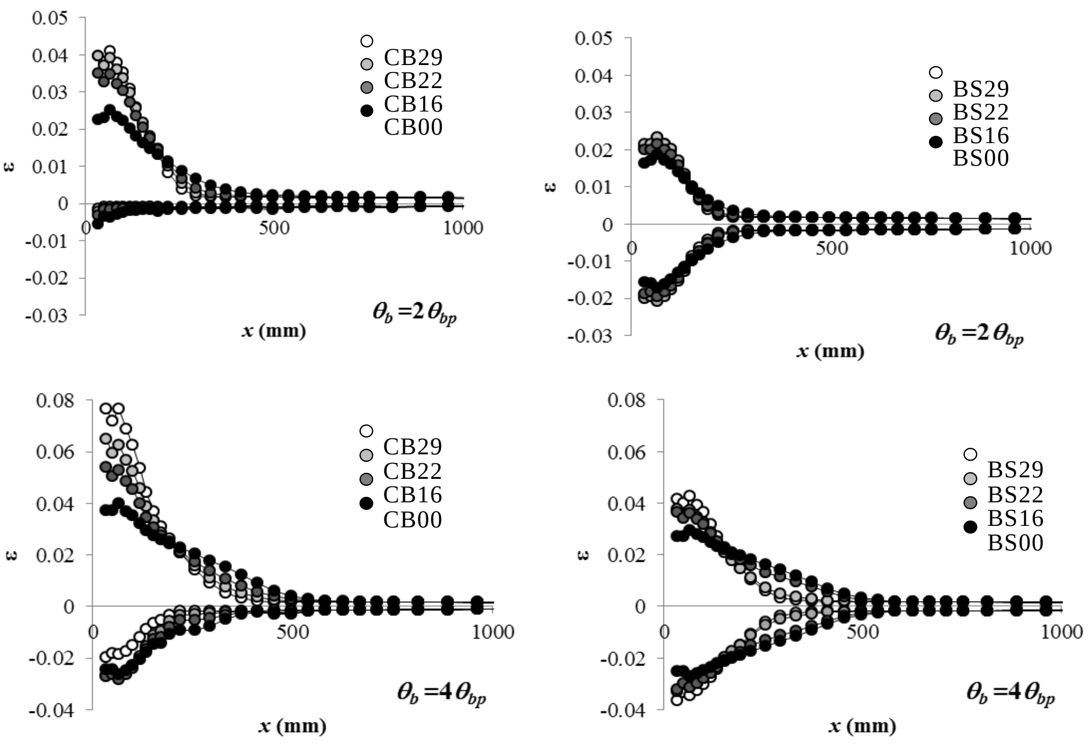

Fig. 3.22 Distribution of strain over the beam length

Figure 3.23 illustrate the difference between strain condition of bottom flange of bare steel beam and composite beam. It can be seen that effect of composite action is highly depending on the width-to-thickness ratio. At the vicinity of column face, significant difference in CB29 exist, while for CB00 the difference is smaller.

Difference of bare and composite disappear in the x almost 250 for CB29, while this difference disappear in longer length of beam for small width-to-thickness ratio.

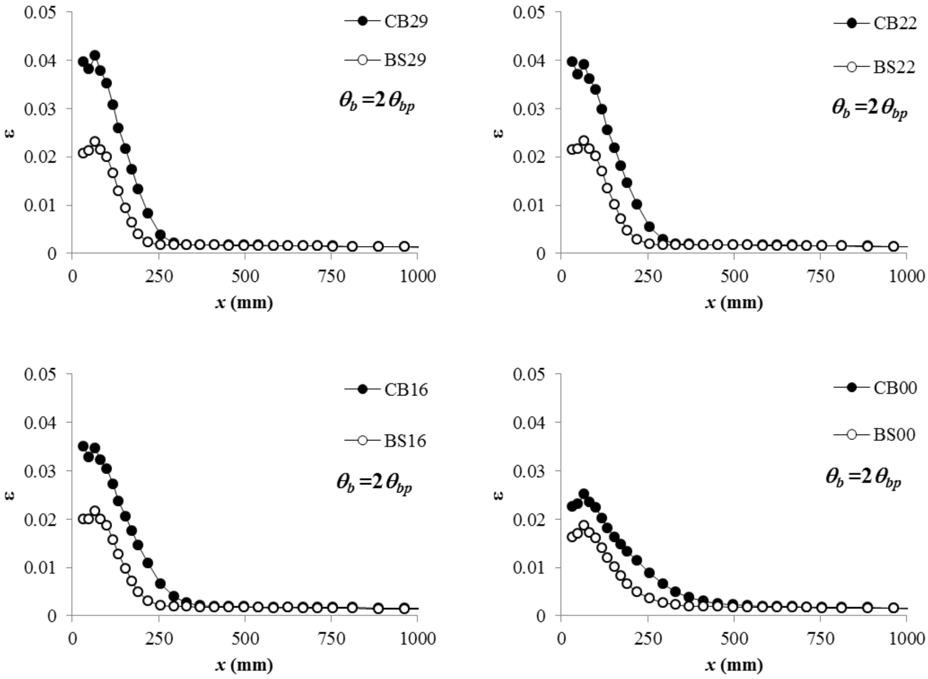

Fig. 3.23 Comparison between strain condition of bare steel beam and composite

3) Effect of reduction of web flexural capacity

Web flexural moment distribution along the beam length is illustrated in Figure 3.24 for different width-to-thickness ratios of bare steel beam and composite beam.

Effect of existance of concrete slab on the web flexural moment can be seen by comparision between the bare steel beam and composite beam.

It can be seen that web flexural capacity of composite beam is reduced to almost half due to existance of axial force (N) resulted form concrete compresion force.

However, according to this Figure it can be explianed that reduction of web flexural capacity based on the axial force (N) does not result to further strain concentration on the lower flange. Because this reduction is almost comparable with the amount of reduction in the bare steel beam. So this does not result to aditional moment which flange must transmite.

To summarize, reduction of flexural capacity due to existance of concrete slab, does not introduce further additional strain concentration and it can be considered as almost comparable to the bare steel beam.

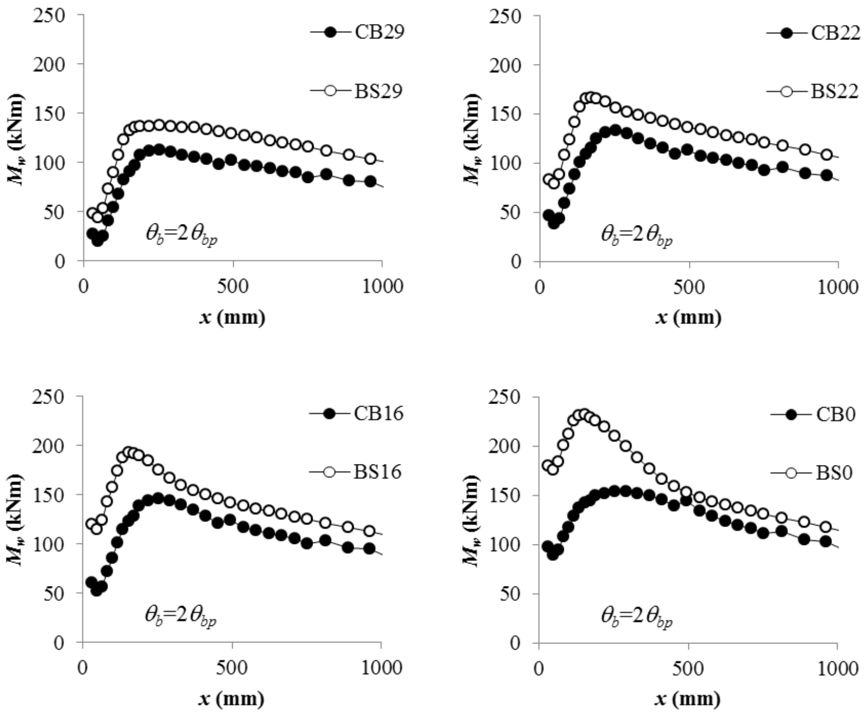

Figure 3.24 Web flexural moment distribution along the beam length

Figure 3.25 illustrates curvature distribution along the length in the bare steel beam and compoite beam for different width-to-thickness ratios.

It can be seen that difference between curvature of composite and bare at the vicinity of connection is quite small. This result is confiming the previouse discussion, and describe that reduction of web flexural capacity does not result to additional stress concentration on the bottom flange.

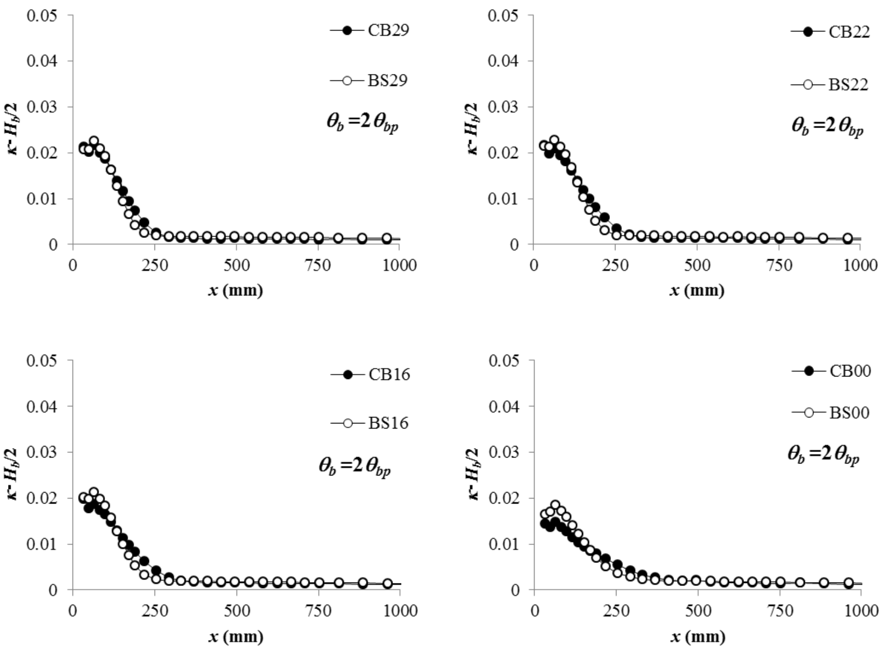

Fig. 3.25 Curveture distribution alonge the beam length

4) Effect of movement of neutral axis (NA)

Figure 3.26 depicts location of nutral axis (NA) from the center of gravity at certain loading condition of $2\theta_p$. Beam rotation angle $2\theta_p$ is corresponding to the condition that concrete almost reach to its maximum capacity (almost final condition before concrete start softening behavior). In this figure effect of composite action on the movement of neutral axis is shown and it can be seen that just vicinity of connection location of nutral axis is quite high and in other parts is almost constant.

Effect of composite action to the movement of neutral axis is deponding on the width-to-thickness ratio. In the case of CB00 also location of nutral axis is high, but for larger width-to-thickness ratios much higher location of nutral axis can be seen in CB29.

Figure 3.27 illustrates curvature versus beam rotation angle for different width-to-thickness ratios in the bare steel beam and composite beam. Although it was shown that in the same beam rotation angle curvature is not affected by composite action (especially in the case of $2\theta_p$), but it can be seen that curvature is affected by width-to-thickness ratio.

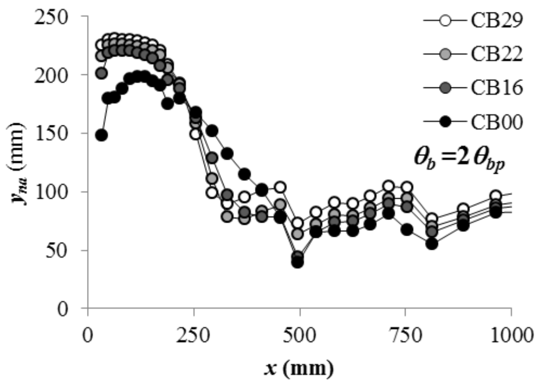

Fig. 3.26 Location of nutral axis (NA) in the rotation angle $2\theta_p$

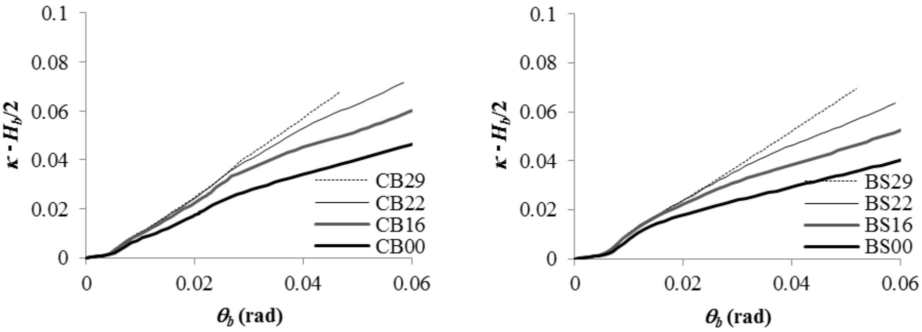

Fig. 3.27 Curvature versus beam rotation angle

Axial strain can be calculated by multiplying curvature to the location of nutral axis, which can be explained by Figure 3.28 and Equation 3.20.

Axial strain distribution along the length of composite beam is shown in Figure 3.29 . It can be seen that at the vicinity of connection, axial strain is affected by width-to-thickness ratio. Higher amount of axial strain can be seen for the large width-to-thickness ratio specimen CB29 comparing with CB00.

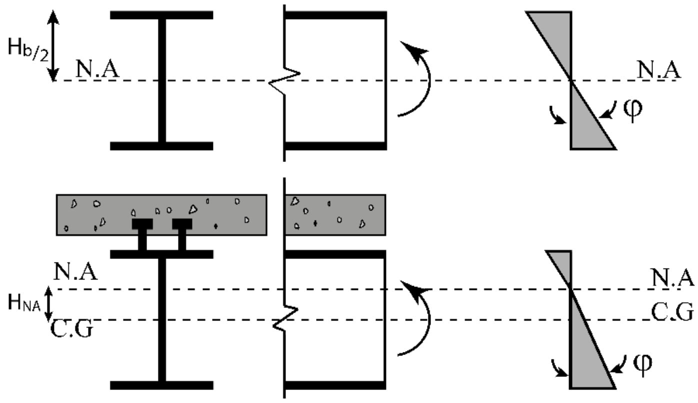

Fig. 3.28 Effect of movement of neutral axis of composite beam to the curvature

$$\varepsilon_{bare} = \varphi(\frac{H_b}{2}) \qquad (3.19)$$

$$\varepsilon_{composite} = \varphi.\frac{H_b}{2}(1+\frac{2H_{NA}}{H_b}) \qquad (3.20)$$

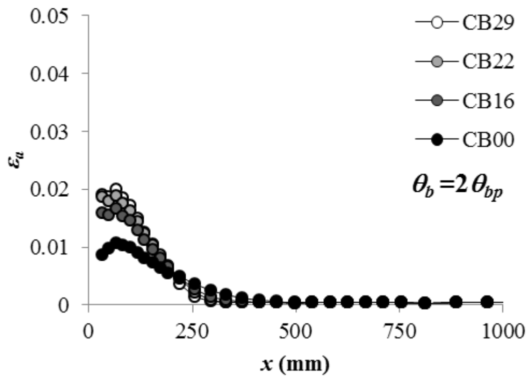

Fig. 3.29 Axial strain distribution along the length of composite beam

Strain resulted from reduction of web flexural capacity, and axial strain due to movement of neutral axis for each width-to-thickness ratio is shown simultaneously in Figure 3.30.

It can be seen that in the bare steel beam and composite beam difference between strain corresponding to reduction of web flexural capacity is small. However, this Figure can describe that difference between strain condition of bare steel beam and composite beam is determined by the axial strain.

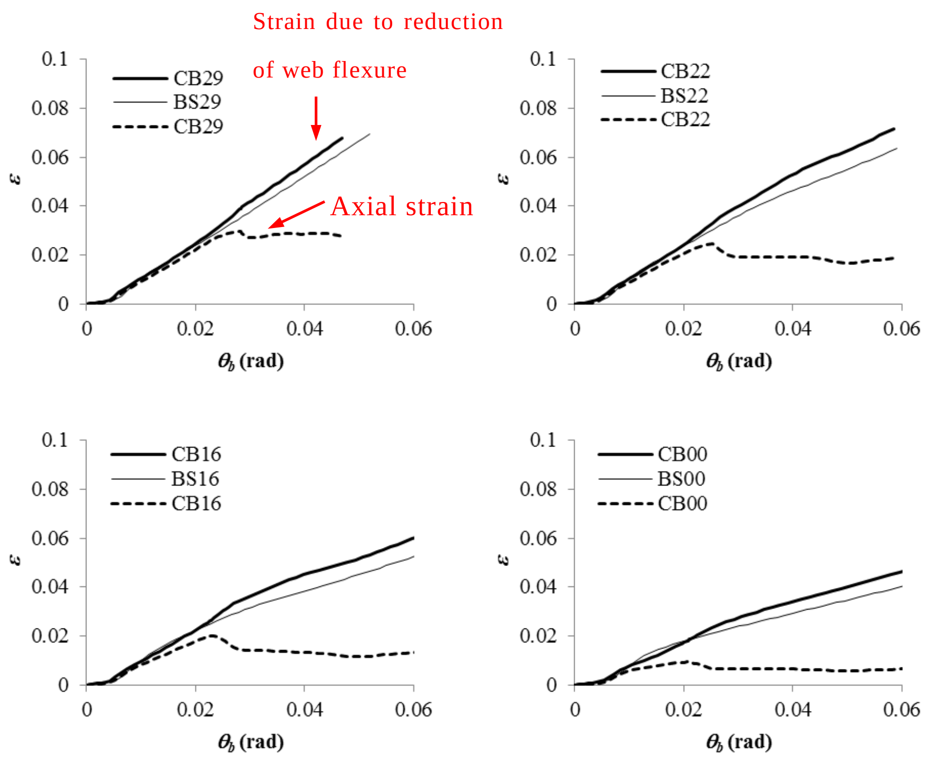

Fig. 3.30 Strain resulted from reduction of web flexural capacity and axial strain

Following to concrete crush and removal of composite action effect, neutral axis moves toward center of gravity, and this result to reduction of axial strain, shown in Figures 3.31 and 3.32, respectively.

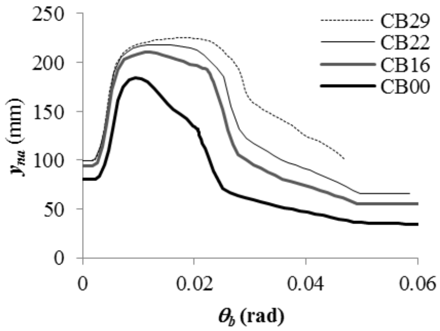

Fig. 3.31 Curvature versus beam rotation angle

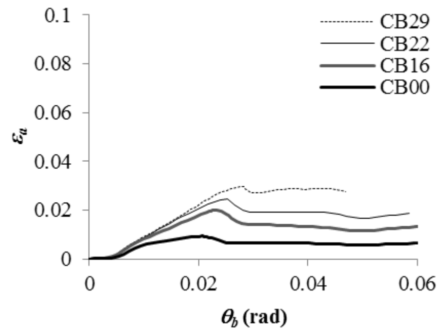

Fig. 3.32 Axial strain versus beam rotation angle

3.7 Conclusion

Following to experimental test observations, in this chapter effect of out-of-plane deformation was studied based on the approach to clarify the structural condition of web connection. Limit analysis and finite element analysis were carried out and the following conclusions are made:

1- Derived equations obtained from limit analysis could show both effects of RHS column width-to-thickness ratio and axial force on reduction of composite beam web connection flexural strength, simultaneously.

2- Adopted finite element model could show acceptable correspondence with test results. Finite element study showed that in both bare steel beam and composite beam effect of RHS column width-to-thickness ratios is considerable in the global behavior. But despite this similarity, different behavior in characteristics of strain hardening of composite beam can be seen. In the smaller width-to-thickness ratio of composite beam, by progress of rotation tendency of reaching to higher capacity exist. After that sudden strength reduction occur and beam keep the constant strength after that reduction.

3- In both bare steel beam and composite beam considerable effect of width-to-thickness ratio was shown in the strain behavior of flanges and web moment capacity. Finite element study showed that in the case of composite beam, effect of width-to-thickness is significant in the axial force subjected to the web connection, but slab force is less affected by width-to-thickness ratio.

4- Mechanism of stress transfer is shown. It was found that start of concrete bearing crush is corresponding to the start of stress increase of top flange. It was also found that maximum web axial force is not always happen at same time with start of softening of slab. In fact, in large width-to-thickness ratio reduction of axial force is first treated by flange. Top flange yield can be considered as a bench mark in the change of behavior. Sudden reduction in the total strength of M_b-θ_b curve corresponds to top flange yield.

5- Mechanism of strain concentration is explained. It is shown that in the bare steel beam and composite beam difference between strain corresponding to reduction of web flexural capacity is small. However, this difference between strain condition of bare steel beam and composite beam is determined by the axial strain. It is shown that reduction of web flexural capacity does not result to further additional strain concentration, comparing to the bare steel beam. While axial strain due to movement of neutral axis result to more sever condition of strain in the composite beam.

6- It is shown that effect of composite action to the curvature in not considerable. While effect of width-to-thickness ratio to the curvature and movement of neutral axis is considerable. So, the additional axial strain in the composite beam is depending on the width-to-thickness ratio of RHS column.

7- By application of above findings a method proposed for evaluation of ultimate flexural strength of composite beam connection. This method is prepared for the conditions which the neutral axis remain in the beam web. After the neutral axis exceeds the boundary of Mechanism II and enters the upper flange, modification in the stress condition of upper flange is needed. Accuracy of the model is verified by correspondence between the test results and model. Good agreement was observed for specimens which the web axial force did not exceed the boundary of Mechanism II.

4. Improvement of Seismic Behavior of Composite Beam Connected to RHS Column with *B/t*=29

4.1 Introduction

According to past experimental investigations [4-1] and test results shown in Chapter 2, considerable reduction happen in the rotation capacity of composite beam connected to RHS column with large width-to-thickness ratio of 29. In order to prevent excessive reduction of beam rotation capacity, in this study "slit" is provided between concrete slab and column face, which was proposed by Tagawa et al., (2003) [4-2], shown in Figure 4.1. According to that proposal, slit may reduce the composite action effects, but the question arise that if application of slit results to removal of composite action or still some partial composite action remain due to contribution of studs? Actually, comprehensive investigations regarding contribution of studs which are located on transverse beam and loading beam in the composite action has not been carried out yet.

In this research, the results of behavior of composite beam with slit is compared with the behaviour of bare steel beam and conventional type of composite beam through a series of experimental test study and finite element analysis. Post-earthquake provisions are applied in the design of specimens and sever loading protocol is used. Differences in rotation capacity of beams are discussed through the study on the steel beam damages and concrete slab damages. Also strain studies were carried out to investigate the effects of slit and stud layout on the strain condition of lower flange. Finally the discussion regarding the rotation capacity of beam is presented.

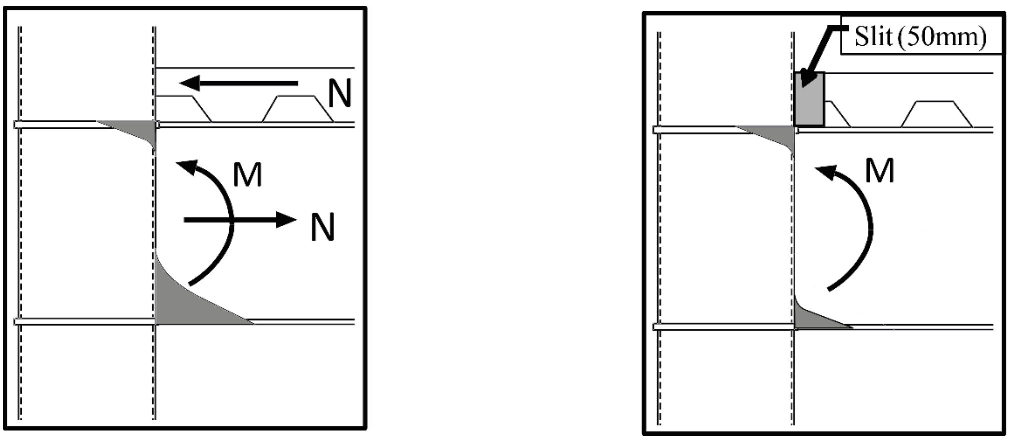

Fig. 4.1 Effect of application of slit on the strain condition in the composite beam

4.2 Experimental test specification

4.2.1 Test specimens

Cyclic loading test using T-shaped subassembly were conducted on four subassemblies of H-Beam(500×200×10×16) connected to RHS column with the width-to-thickness ratio of 29 (□-350×350×12). As shown in Table 4.1, one bare steel beam specimen and three composite beam specimens were prepared.

In order to conduct investigations about improvement of composite beam plastic behavior, in two of composite beam specimens 50mm "slit" between concrete slab and column face was provided. The difference between two slit specimens is the layout of studs at the vicinity of connection. Figure 4.2 illustrates the configuration of specimens and test setups

Table 4.1 Specimens specification

Specimen	Concrete Slab	Slit
BS-29	Not	-
CB-29	Existed	Not
CBS-29	Existed	50 mm
CBS-29M	Existed	50 mm
Beam: H-500×200×10×16	Column: □-350×350×12	

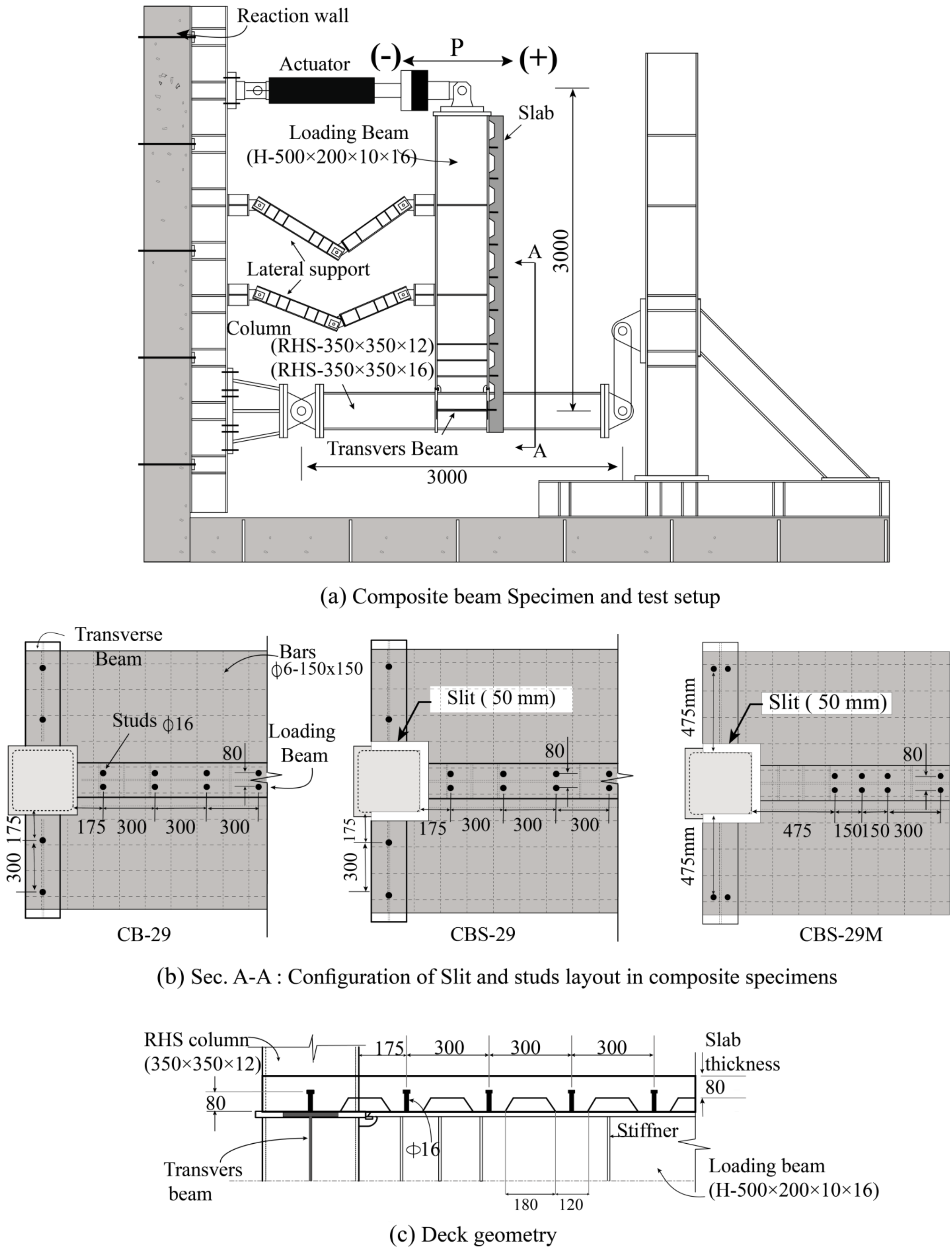

Fig. 4.2 Configuration of specimens and test setups of composite specimens

As shown in Figure 4.2, concrete slab with width of 1500 mm and thickness of 80 mm were used for composite beam specimens. In these specimens, deck plate type QL 99-50-12 applied and two stud bolts of ϕ16 were welded to the beam flange with pitch distance of 300 mm. Transverse distance between studs were considered as 80 mm. The number of shear studs is common to all specimens.

4.2.2 Weld joint details

Weld Joint detail for beam-to-RHS column connection is illustrated in Figure 4.3. Beam flanges are connected to the column by "through diaphragm" to achieve smooth stress transfer from beam flange to the column, and preventing local deformation of RHS column wall. Beam web is connected to the wall of RHS column directly, and fillet welds were applied in both sides of the beam. This detail is widely used in Japan and it is recommended in JASS 6 2007 as an effective method. In all specimens shop welded joint type used by complete joint penetration (CJP) groove welds. CO_2 gas shielded metal arc welding method (GMAW) using YGW11 electrodes was conducted. Ceramic run of tabs were used and backing bars left in place. The weld access hole which is known as "scallop", was consisted of two arcs with radiuses of 35 and 10 millimetres, which is corresponded to post Hyogo ken-Nanbu earthquake scallop geometry type.

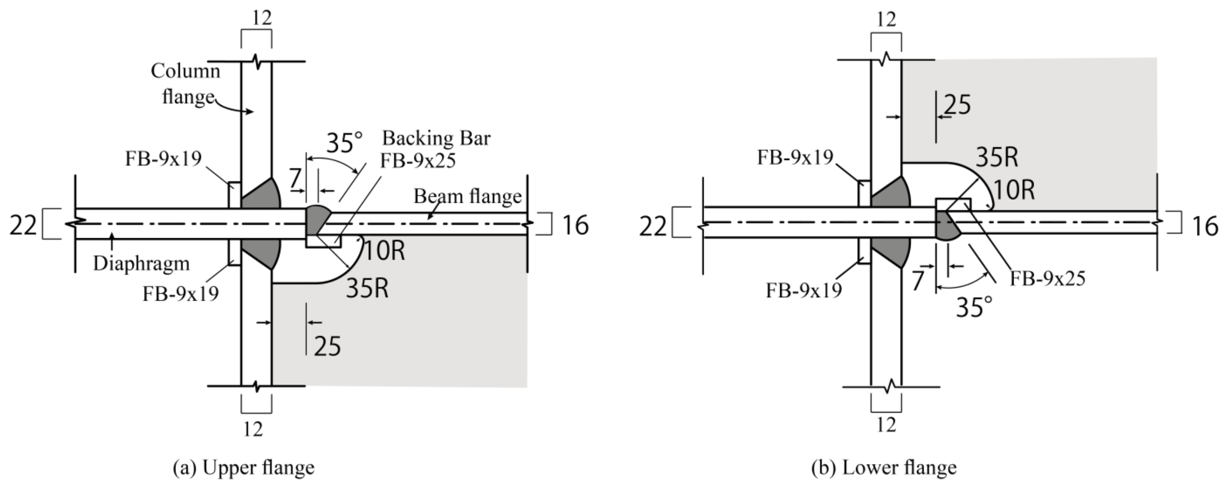

Fig. 4.3 Weld Joint detail

4.2.3 Material properties

The material utilized for the specimens were hot rolled sections with steel grade of SM490A and cold formed BCR295 for beams and columns, respectively. Diaphragm plates material were used with steel grade SN490B. Actual material properties obtained by tensile coupon tests are reported in Table 4.2.

Regarding the beam material toughness, Figure 4.4 plots the values of material Charpy V-Notch (CVN) impact test results associated with “fillet” area, which obtained from coupon tests. Fillet area is defined as the meeting point between the web and the flange which is illustrated in Figure 4.4(a). Studs material were used with steel grade JIS B1198-1995, and push-out tests were also carried out for the purpose of evaluating the shear strength and elastic stiffness of shear studs, summarized in Table 4.3.

The design strength of concrete used for composite beam specimens was 21.0 N/mm^2. The average concrete strength from cylinder tests was 28.4 N/mm^2 .

Table 4.2 Material Properties

Member		Material Grade	σ_y (N/mm^2)	σ_u (N/mm^2)	YR= σ_y/σ_u	EL (%)
Beam	Flange	SM490A	383	551	69.5	40.6
	Web		422	541	78.1	36.6
RHS Column		BCR295	328	425	77.0	48.9
Diaphragm		SM490A	370	531	69.7	49.9
Weld Metal		YGW11	420	536	78.3	31.4

Table 4.3 Shear stud push out test results

Elastic Stiffness (kN/mm)	Shear Strength q_y (kN)	Ultimate Shear Strength q_{max} *(KN)*	δ_{max} *(mm)*
346.92	65.56	88.90	2.36

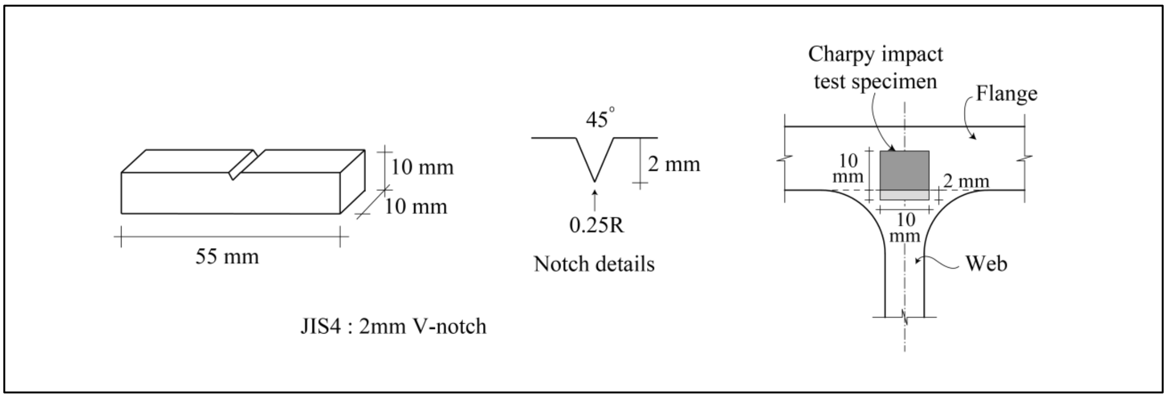

(c) Location of charpy impact test specimen

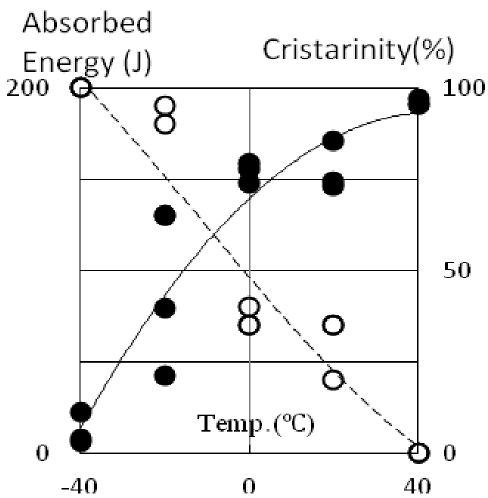

(d) CVN test results

Fig. 4.4 Charpy impact test results for “k” area of beam sections

4.2.4 Test procedure

As shown in Figure 4.5, specimens were simply supported at both ends of column and the lateral load was applied at the top of beam. θ_b is beam rotation angle based on definition presented in Figure 4.6 and Equation 4.1. The cyclic loading program was applied, so the drift of the tip of beam increases as the loading cycle advances. The test protocol for this cyclic reverse loading is shown in Figure 4.7 which is consisted of 2 cycles in each ±2.0 θ_p , ±4.0 θ_p and other cycles in ±6.0 θ_p until the failure. θ_p is the rotation corresponding to plastic moment capacity of bare steel beam (M_p), which is obtained by dividing beam's plastic moment by its initial stiffness. Failure was defined as the fracture occurrence or 10% degradation from actual maximum strength obtained during the loading test.

$$\theta_b = \frac{\delta}{h'} = \frac{v_1 - \theta_c.h' - v_c}{h'} \quad [rad] \qquad (4.1)$$

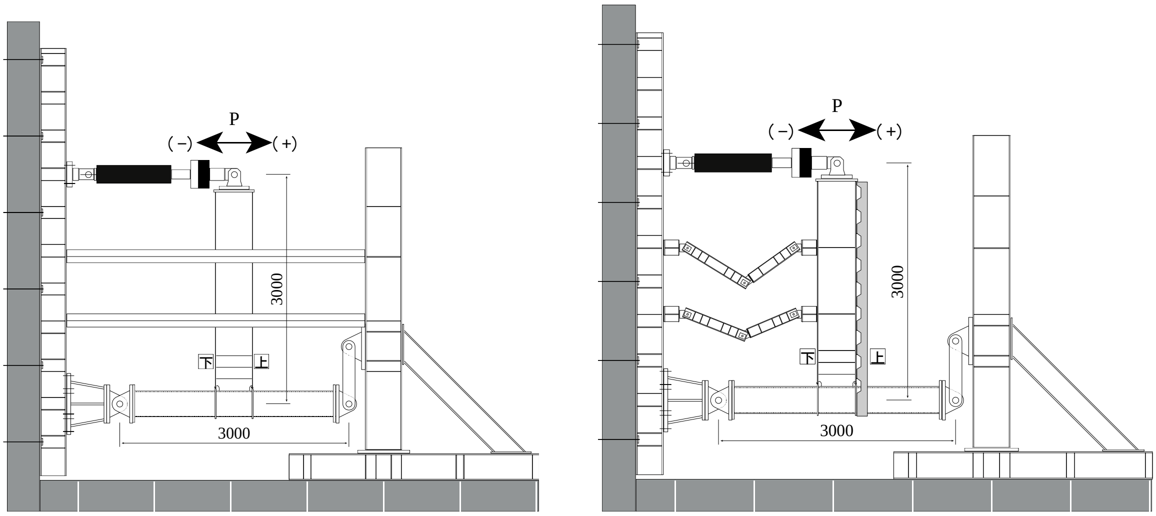

(a) Bare Steel beam specimen (b) Composite beam specimens

Fig. 4.5 Bare steel beam and composite beam test setup

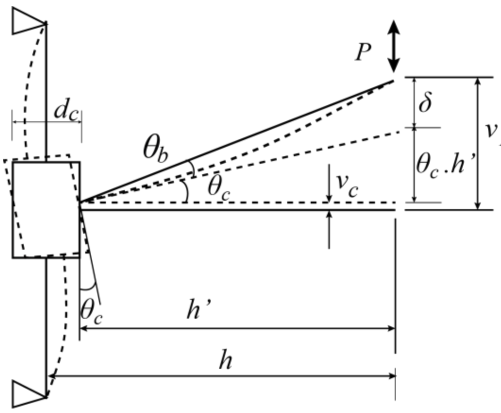

Fig. 4.6 Definition of beam rotation

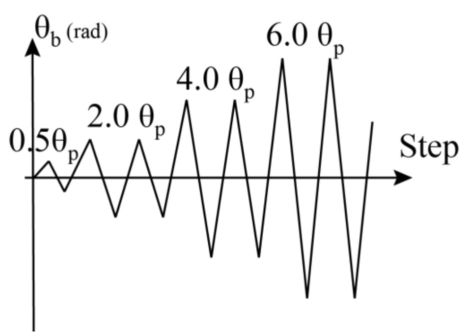

Fig. 4.7 Cyclic loading protocol

4.3 Test results

4.3.1. M_b- θ_b Hysteresis diagrams

M_b-θ_b hysteresis graphs are shown in Figure 4.9. In these graphs M_b represents beam moment at column face and θ_b is beam rotation angle. From the Figure it can be observed that in all specimens by increase of beam rotation angle, increase of strength happened. Larger amount of beam deformation was observed in the bare steel beam BS-29 comparing with conventional composite beam CB-29 and composite beam with slit CBS-29 specimen. But in the CBS-29M specimen that in addition of slit application, modification of stud layout was performed, considerable improvement of beam rotation capacity was observed.

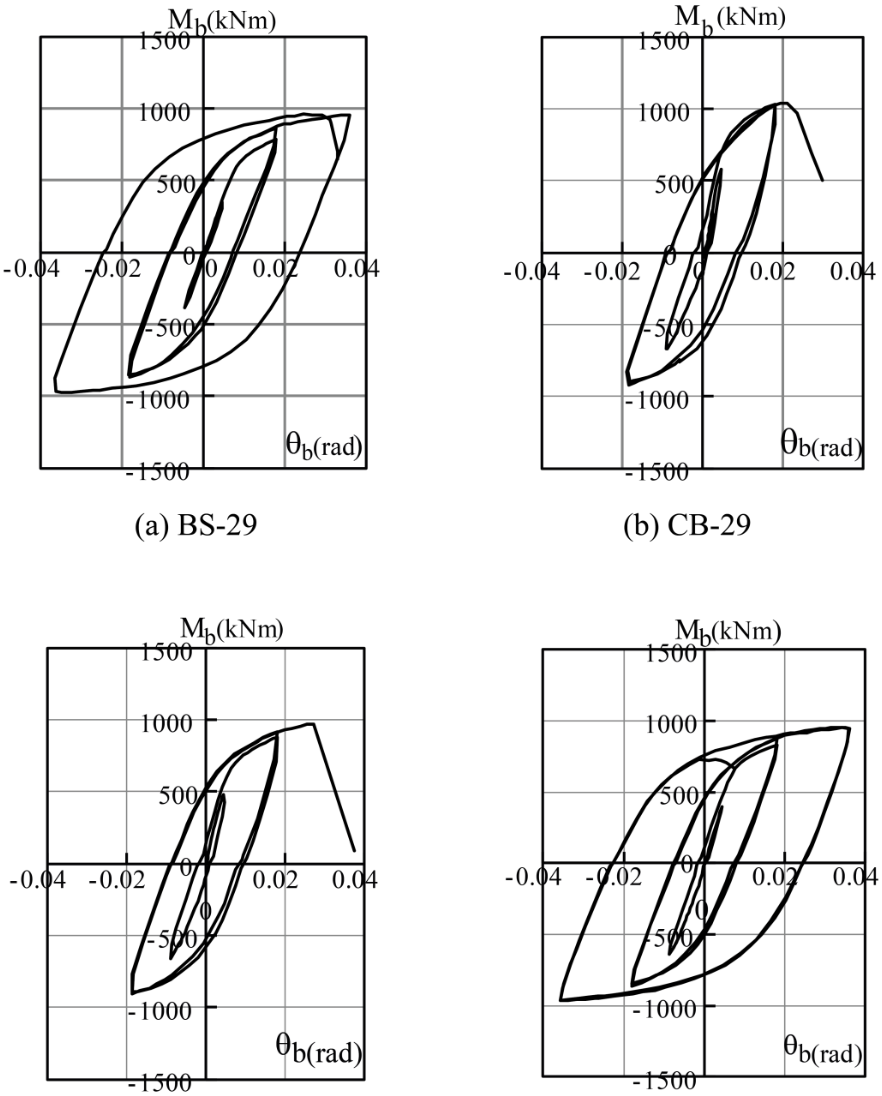

(a) BS-29 (b) CB-29

(c) CBS-29 (d) CBS-29M

Fig. 4.9 M_b-θ_b Hysteresis graphs

4.3.2 Steel beam damage observations

3.3.2.1 Crack Initiation and progress

According to experimental test results, crack initiation in all specimens, regardless of bare steel or composite beam, happened at the root of scallop of beam lower flange.

In bare steel beam specimen and both composite beam with slit specimens, crack initiation happened at almost similar cycle of loading, which was first cycle of +4.0 θ_p. But in the case of conventional composite beam specimen (CB-29), crack initiation occurred in much earlier cycle of loading (+2.0 θ_p). Also speed of crack opening was higher in this specimen. Typical condition of crack at the root of weld access hole in the first cycle of +4.0θ_p is shown in Figure 4.10. Summary of first crack initiation of all specimens is illustrated in Figure 4.11.

3.3.2.2 Final Failure Mode

Final failure of all specimens was determined by progress of above mentioned crack at the root of scallop of beam lower flange. Final failure manner of bare steel specimen, conventional composite beam specimen and slit specimen which had stud removal at the vicinity of connection, were determined by quite ductile manner. On the other hand, in the other slit specimen with no stud modification (CBS-29), final fracture manner was determined by brittle fracture, shown in Figure 4.12(a) and (b). This difference of behavior might be the result of error in the specimen. End of backing bar weld close to the scallop might be the reason of this brittle fracture.

(a) BS-29: Crack initiation(at+3.0θ_p)

(b) CB-29:Crack progress(width:0.9mm)

(c) CBS-29: Crack initiation

(d) CBS-29M : Crack initiation(at+3.0θ_p)

Fig. 4.10 Typical crack initiation and progress at the root of weld access in the first cycle of +4.0θ_p

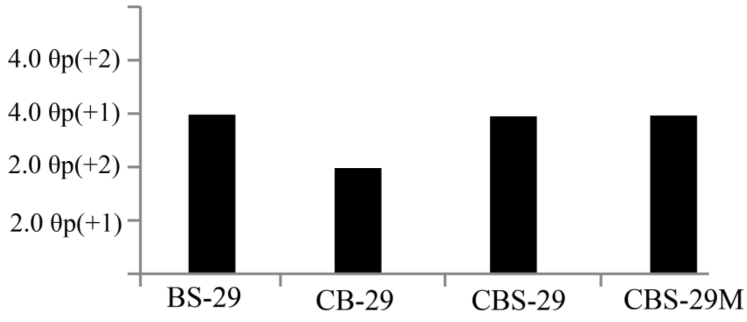

Fig. 4.11 First crack initiation during loading test

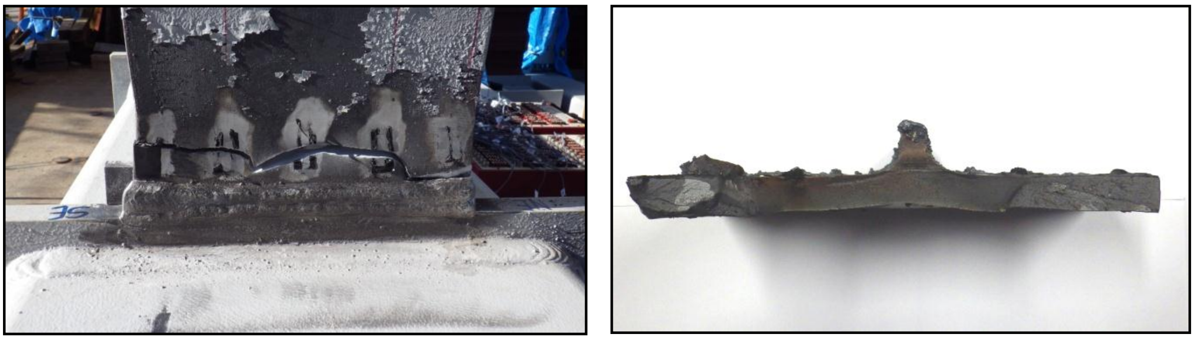

(a) Ductile fracture

(b) Brittle fracture

Fig. 4.12 Typical final failure mode of specimens

4.3.3 Concrete slab damage observations

The concrete slabs were subjected to subsequent tensile and compressive load and the formation of cracks traced as loading progressed. Figure 4.15 illustrates the condition of slab damages in each specimen. In all specimens, cracks corresponding to compression are shown in red solid line, and cracks corresponding to tension are shown with blue solid line.

It can be seen that regardless of existence of slit, comparable condition of tensile cracks were observed in all specimens. However, considerable developments of cracks corresponding to compression force were just occurred in the specimen with conventional composite beam CB-29. In this specimen compression crack developed parallel to the loading beam. While In both composite beam specimens with slit, CBS-29 and CBS-29M, limited cracks corresponding to compression force appeared, which remained almost around the transverse beam.

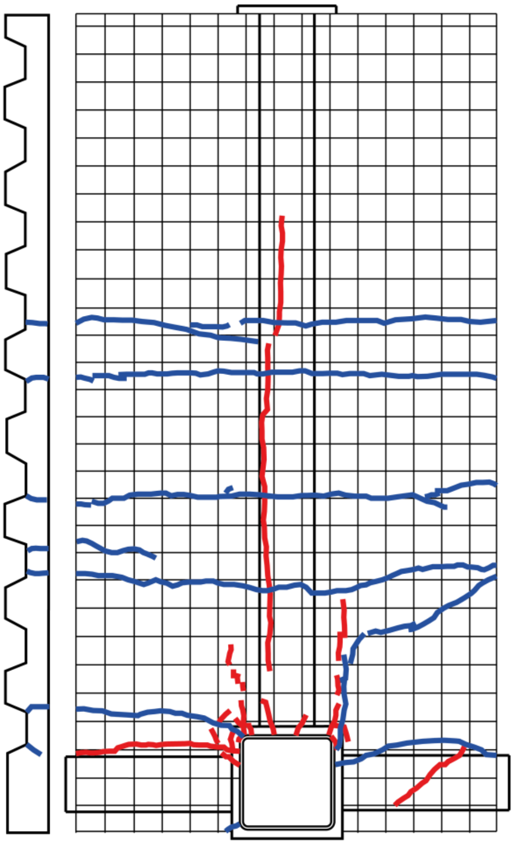

(b) CB-29 Specimen

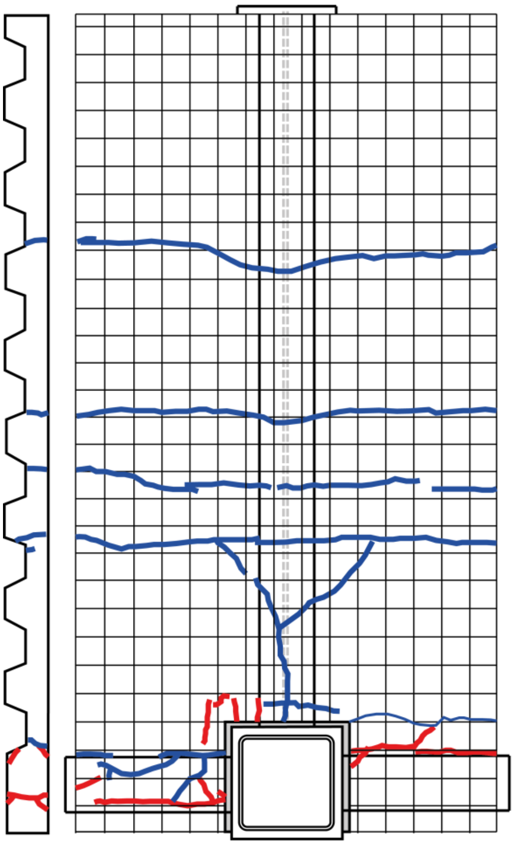

(b) CBS-29 Specimen

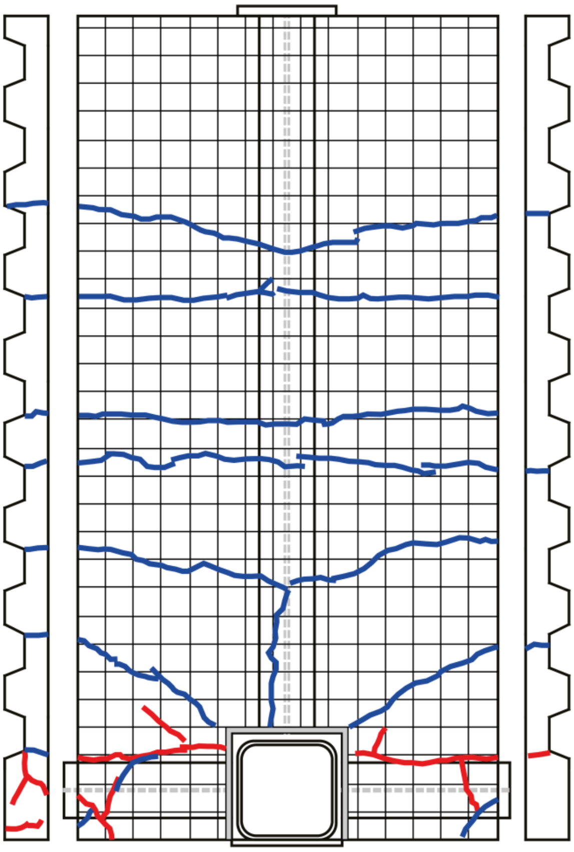

(c) CBS-29M Specimen

Fig. 4.15 Final condition of slab damages

4.4 Effects of slit and stud layout on the behavior of composite beam

4.4.1 M_b-θ_b Skeleton curves

The skeleton curves correspond to positive and negative loading are plotted in Figures 4.16 (a) and (b), respectively. In these graphs, actual plastic strength values are shown with solid circles, which are corresponding to one-sixth stiffness reduction, obtained by definition which was shown in Figure 2.22.

In positive flexure, comparing with bare steel beam specimen BS-29, considerable increase in the elastic stiffness of conventional composite specimens CB-29 can be seen, while slit resulted to reduction of composite beam elastic stiffness.

According to Figure 4.17, it can be seen that in +0.05 θ_p , elastic stiffness of CB-22 is 1.93 times of bare steel beam, while CBS-29 and CBS-29M are 1.56 and 1.21 times of bare steel beam. It can be explained that application of slit resulted to reduction of composite beam stiffness in positive flexure. But in the case of negative flexure regardless of existence of slab and slit, from the early stages of elastic region the stiffness is almost same.

Regarding the actual plastic strength, from figure 4.16(a) it can be seen that in the positive flexure both slit composite specimens did not show considerable increase of plastic strength comparing with BS-29. The plastic strength of CBS-29 and CBS-29M are just 1.06 and 1.05 times of bare steel beam, respectively. While conventional composite beam actual plastic strength was 1.31 times of bare steel beam.

In all specimens regardless of existence of slab and slit, after reaching to actual plastic strength, almost steady increase of strength can be seen until the ultimate strength. After that, strength degradation happened in all specimens due to development of crack at the root of weld access hole (scallop). Just in CBS-29 brittle propagation of this crack occurred and other specimen's failure were determined by ductile progress of this crack, which was explained in Sec. 3.3.2.

Figure 4.16 (b) shows that in the negative flexure, actual plastic strength of all specimens were comparable to the calculated plastic moment capacity of bare steel beam. Table 4.4 summarizes the results of observed ultimate strength of each specimen. Application of slit in CBS-29 and CBS-29M resulted to comparable ultimate strength condition comparing with bare steel beam BS-29. While 8% increase in the ultimate flexural capacity of BC-29 observed comparing with bare steel beam specimen BS-29.

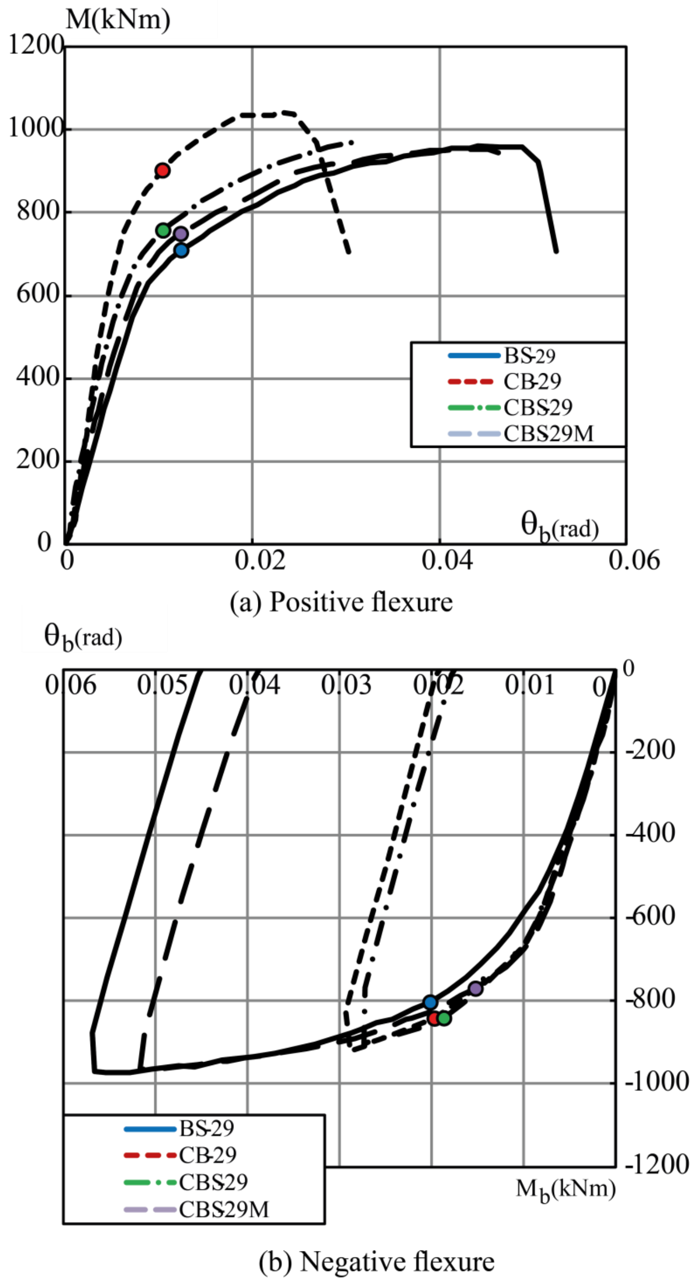

Fig. 4.16 M_b-θ_b Skeleton curves

Table 4.4 Test results

Specimen	Plastic Moment (kNm)		Ultimate Flexural Capacity (kNm)		Final Failure Pattern
	Mp+	*Mp-*	*Mp+*	*Mp-*	
BS-29	711	803	961	974	Ductile
CB-29	903	842	1042	922	Ductile
CBS-29	758	841	972	903	Brittle
CBS-29M	750	769	954	965	Ductile

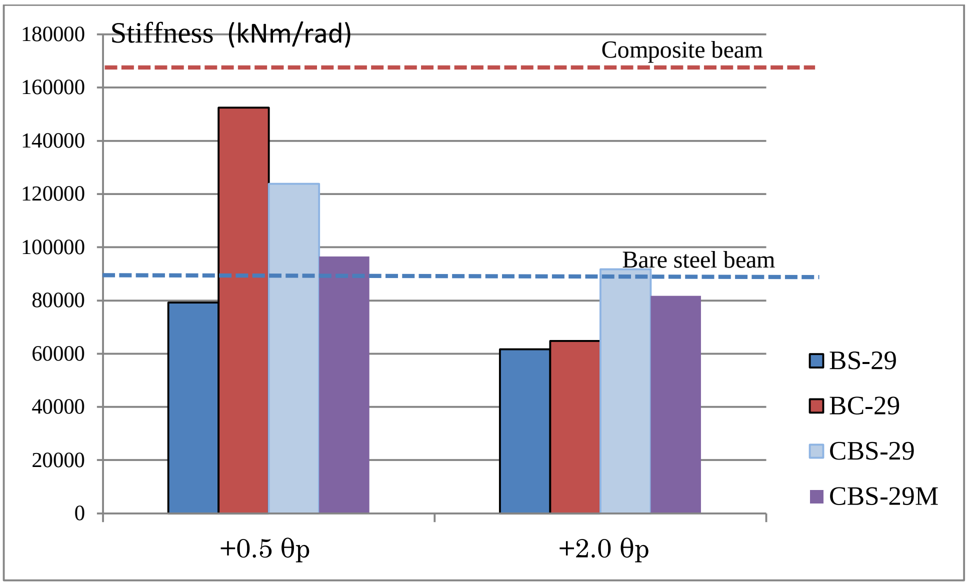

(a) Positive flexure

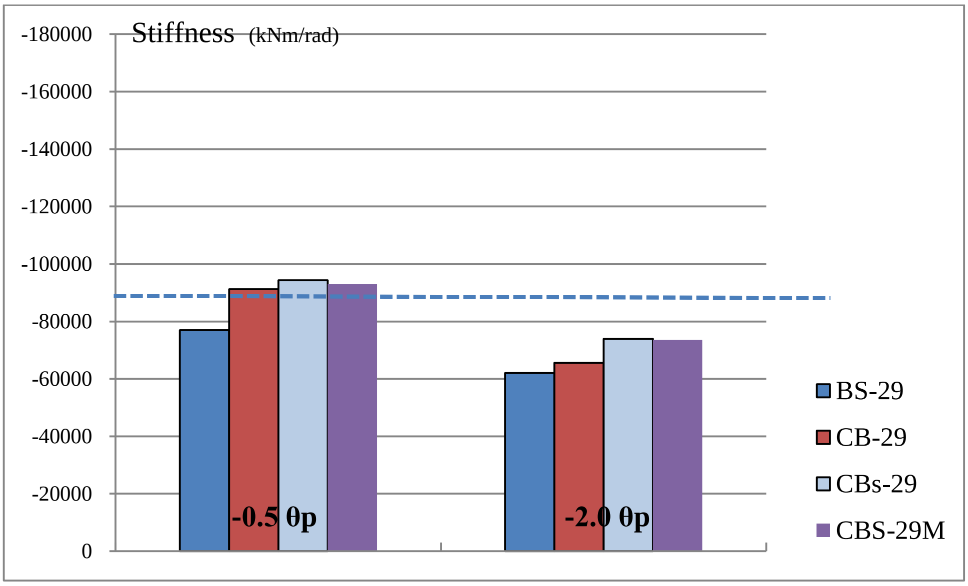

(b) Negative flexure

Fig. 4.17 Elastic stiffness of specimens

4.4.2 Strain behavior

Figure 4.18 depicts the amount of strain in the beam flanges across the beam length, measured in the first cycle of +2.0 θ_p . Horizontal axis is the beam length from the column face and vertical axis is the amount of strain, measured by gauges attached at the 30, 200, 350 and 500 mm position from column face, shown in Figure 4.19 (a) and (b).

According to Figure 4.18(a), it is found that the strain on the upper flange of conventional composite specimen remained almost zero, while in both slit specimens CBS-29 and CBS-29M, upper flange reached to 1.7% and 1.9% of negative strain, respectively. This behavior is resulted from existence of slit, which resulted to considerable reduction of constraint condition for the upper flange of composite specimens. It can be seen that the amount of strain in the upper flange of bare steel beam is 2.7 % negative strain.

Furthermore, for the lower flange it can be seen that flanges were subjected to positive strain. At the vicinity of column face, in the lower flange of both composite beams with slit, amount of strain is almost comparable to the bare steel beam specimen, while in conventional composite beam CB-29 specimen, the amount of strain is 2.5 times more than bare steel beam. At 200 mm distance from the column face, amount of strain in CBS-29M reached to BS-29, while the amount of strain in CBS-29 is higher.

It can be explained that strain condition of bottom flange, resulted to similar crack initiation behavior in the bare steel beam specimen and both composite beam with slit specimens, which was discussed in Sec. 3.3.2.

Strain condition of all specimens is comparable at the 500 mm distance away from the column face.

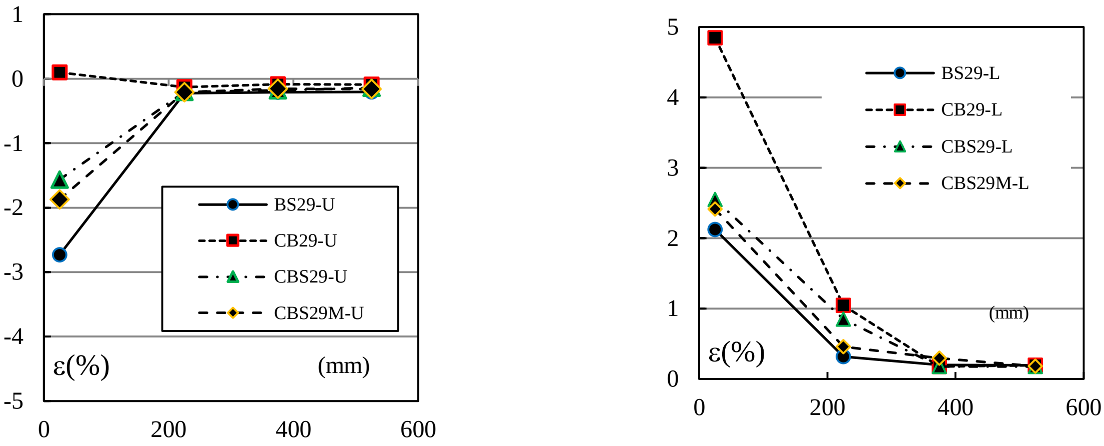

(a) Upper flange (b) Lower flange

Fig. 4.18 Strain condition of upper and lower flange

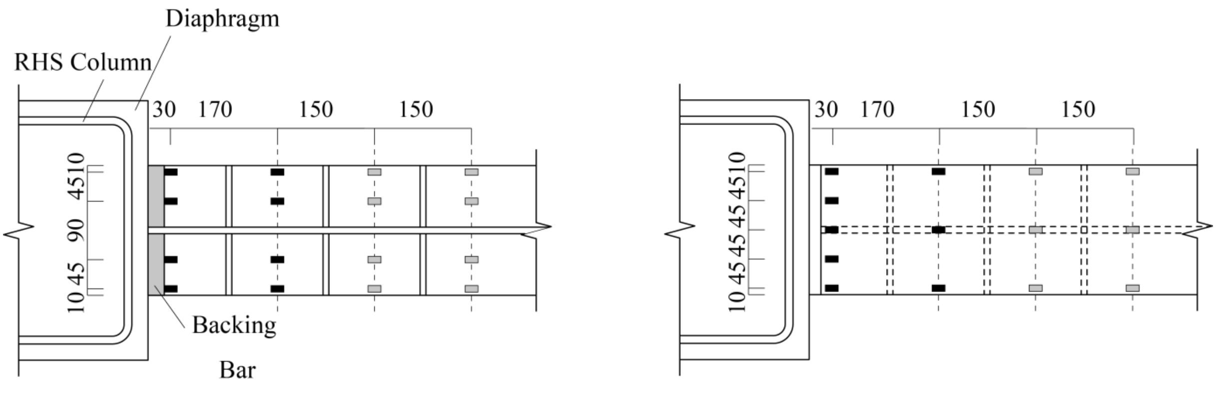

(a) Upper Flange (inside) (b) Lower Flange (outside)

Fig. 4.19 Strain gauges arrangement on the steel beam flanges

Similar test result regarding the difference of strain amount between conventional composite beam CB-29 and slit composite beam CBS-29M was obtained by Tagawa *et al.*, research (2003). But comparison of test results and finite element analysis shows that although reduction of stain on the beam lower flange could be obtained by application of slit in CBS-29, but better performance of CBS-29M specimen was the result of more reduction of strain due to removal of studs of transverse beam at the vicinity of connection. Further study about the mechanism of stress transfer is needed which will be investigated by finite element study in the next section of this chapter.

4.4.3 Finite element study on effects of slit and stud layout

According to experimental test results, different behaviors in two slit specimens were observed. The difference of these specimens was the layout of studs at the vicinity of connection.

In order to conduct investigation regarding the contribution of stud layout in the composite action and strain behavior, finite element study were carried out by general finite element analysis program ABAQUS Ver.6.5. Analysis conducted for 5 models as shown in Table 4.5. The finite element model is illustrated in Figure 4.20. Slab is modelled by shell element and studs are modelled by spring elements which are connected to the beam flange by rigid element. Half model is prepared due to symmetry and appropriate constraints have been applied on the symmetry part. The monotonic loading applied upward. The yield criterion on the basis of Von Mises and associated flow rule were employed to model plastic behavior. The Drucker-Prager criterion was adopted[3-3)] for concrete.

Table 4.5 FEA models specifications

Specimen	Slit	Removal of Stud	
		Loading Beam	*Transverse Beam*
BS-29	-	-	-
CB-29	No	No	No
CBS-29	Yes	No	No
CBS-29L1	Yes	Yes (1 stud)	No
CBS-29T1	Yes	No	Yes (1 stud)

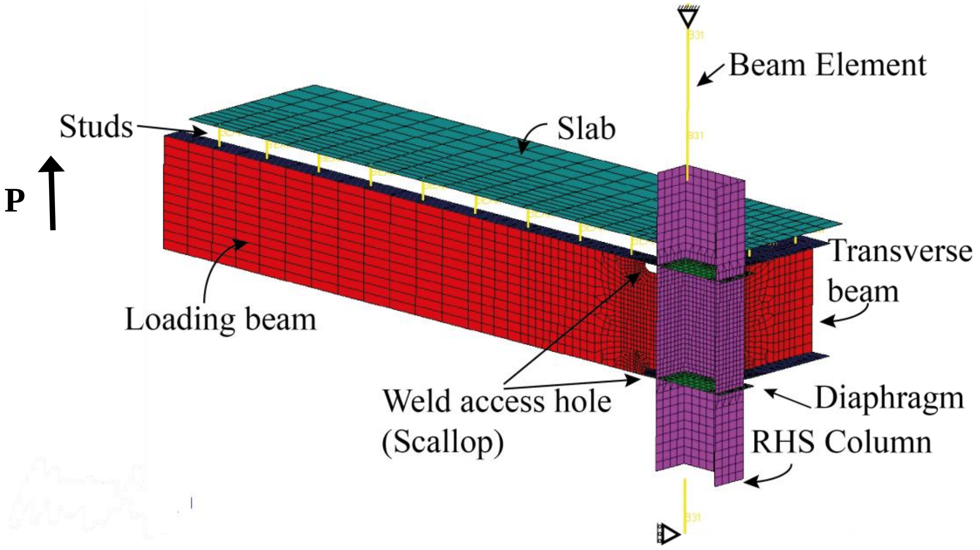

Fig. 4.20 Finite element model

In Figure 4.21, results of numerical monotonic loading are compared with skeleton curves obtained from experimental cyclic loading test for beam rotation. Acceptable correspondence between numerical analysis and experimental test results can be observed.

In a composite beam , horizontal shear force at the interface between steel and concrete surface exist [3-4)]. Figure 4.22 illustrates cumulative shear force in the studs of loading beam. According to the equilibrium requirements, in the conventional composite beam, bearing force is equivalent to the cumulative shear force of studs. It is shown that application of slit resulted to considerable reduction of shear force in the loading beam studs(CBS-29). While removal of first stud of loading beam did not make considerable change in this condition, removal of studs on transverse beam, resulted to more reduction of shear force.

Figure 4.23 plot strain condition versus beam rotation at the tip of scallop of beam lower flange. It can be seen that by application of “slit”, considerable reduction of strain obtained in CBS-29 specimen comparing to conventional composite beam CB-29. It is shown that removal of stud on loading beam of CBS-29L1 specimen did not result to more reduction of strain, while removal of studs of transverse beam in CBS-29T2 resulted to more reduction of strain, which became comparable to bare beam condition.

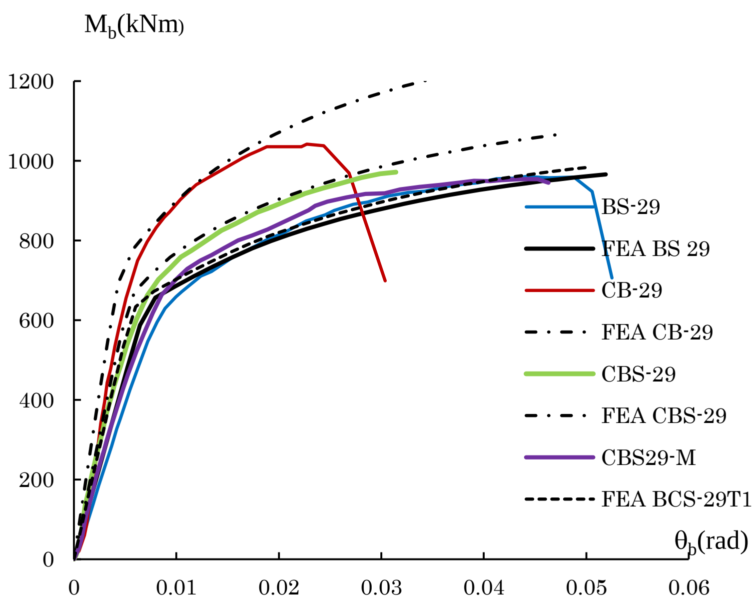

Fig. 4.21 M_b-θ_b curves

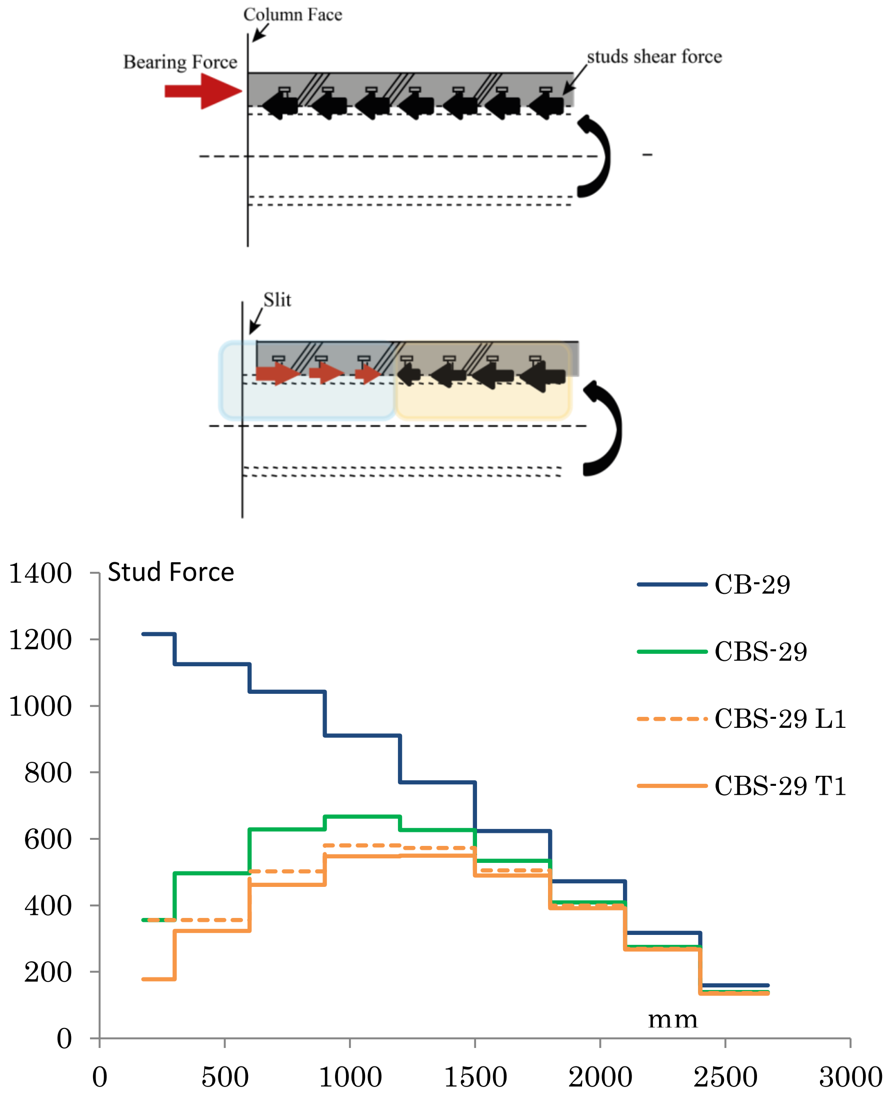

Fig. 4.22 Cumulative shear force in studs of loading beam

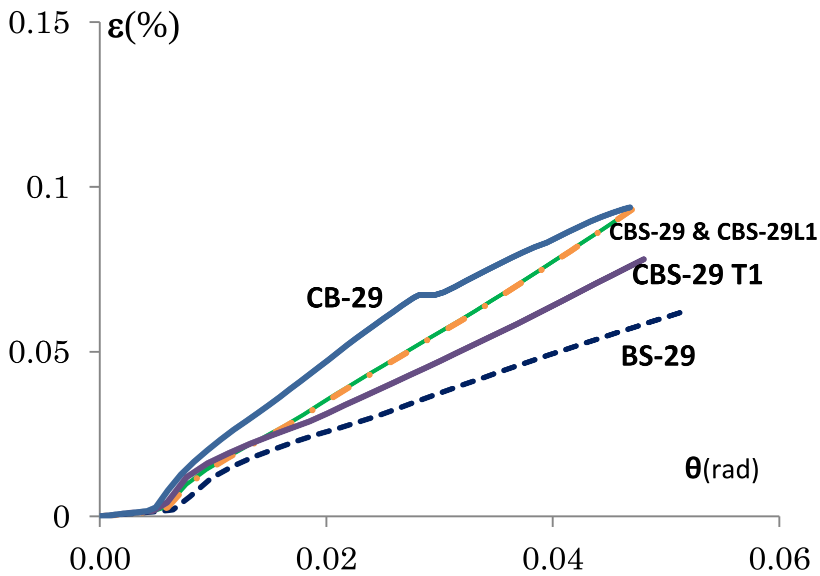

Fig. 4.23 Lower flange strain

According to investigations of chapter 3 it was found that in the case of large width-to-thickness ratio effect of axial force to the out-of-plane deformation is significant. Figure 4.24 shows that application of slit result to considerable reduction of axial force. But in large width-to-thickness ratio of 29 despite the existence of slit, still web is subjected to axial force. Removal of stud on the loading beam does not result to reduction of axial force, but removal of stud on the transverse beam resulted to reduction to almost half.

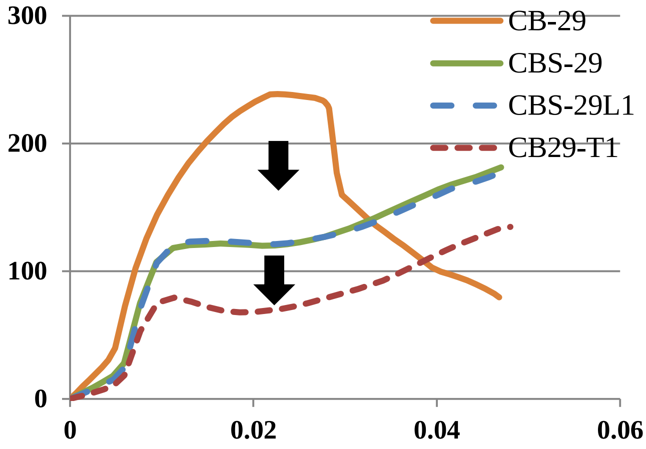

Fig. 4.24 Web axial force

It can be explained that in the case of conventional composite beam, concrete compression force is transmitted by bearing resistance of column and studs of transvers beam, shown in Figure 4.25(a). But in the case of slit specimen, constraint provided by the studs of transvers beam result to contribution to the composite action, shown in Figure 4.25(b). So just providing the slit is not enough to obtain the removal of axial force.

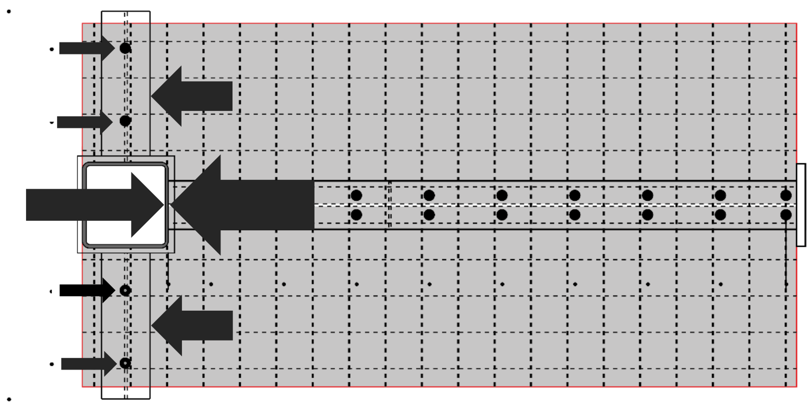

(a) Conventional composite beam

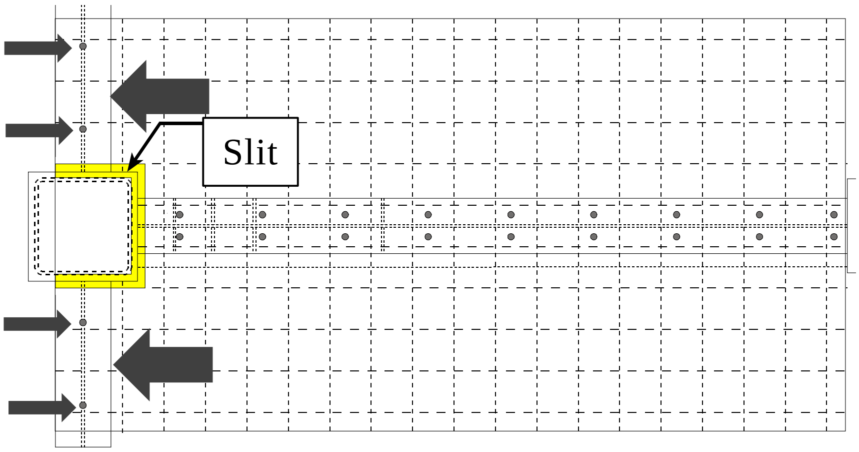

(b) Composite beam with application of slit

Fig. 4.25 Contribution of studs of transvers beam in the composite action

Contribution of studs of transvers beam depends on the location of stud. Due to torsional behavior of transvers beam shown in Figure 4.26, second stud shear is almost 40% of first stud, shown in the Figures 4.27.

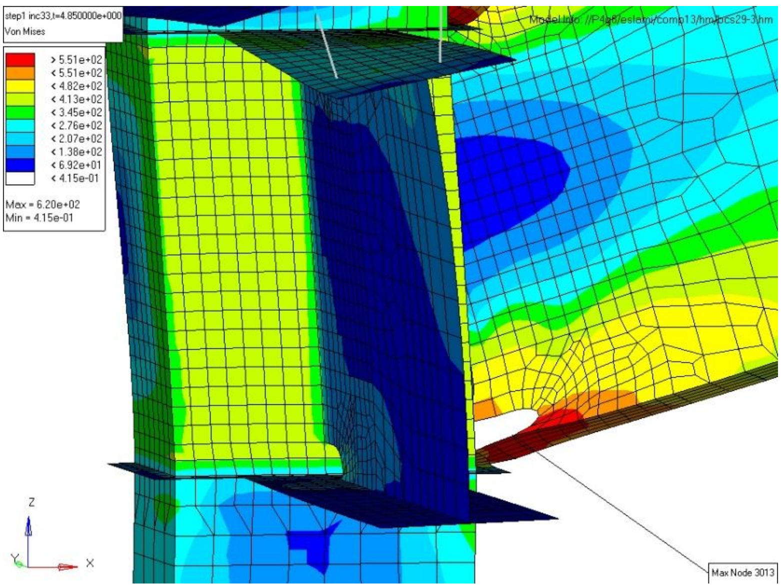

Fig. 4.26 Torsion of transvers beam

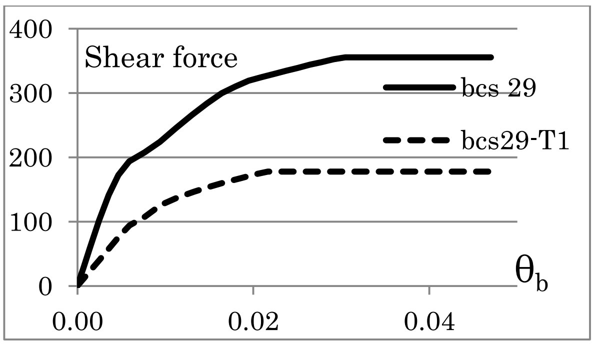

Fig. 4.27 Shear force in the first stud of transvers beam

Considering the fact that in the actual seismic condition, structural roll of transverse beam might be changed, so number of studs can be kept according to calculations, and just movement of first stud away from the column face is recommended, shown in Figure 4.28. Based on this approach to consider actual seismic loading, removal of studs at the vicinity of connection on both loading and transverse beam is recommended.

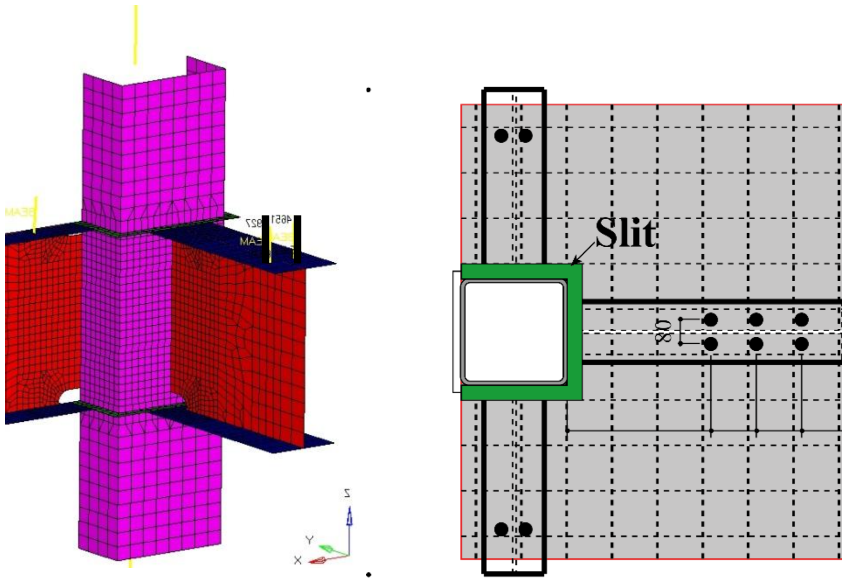

Fig. 4.28 Movement of first stud of transvers beam away from the column face

4.4.4 Rotation capacity

Figure 4.29 depicts the crack growth in each specimen. Crack growth was investigated by plotting the measured crack opening (δ_{cr}) versus beam rotation. In this figure, η is the beam cumulative plastic rotation based on the definition shown on Figure 2.28.

According to strain behavior study and damage observations which were explained in Sec. 4.4.2 and 4.3.2, it is found that strain condition of lower flange affected the crack growth and progress in each specimen, and finally this resulted to different rotation capacity of beams.

In conventional composite CB-29 specimen, higher amount of strain resulted to earlier initiation and faster progress of crack comparing to bare steel beam BS-29 and other composite specimens with application of slit.

Figure 4.30 illustrates beam moment versus cumulative plastic rotation. Table 4.6 summarizes the test results regarding cumulative rotation capacity of each specimen. Due to composite action in CB-29 the cumulative rotation capacity was almost half of bare steel beam BS-29.

Improvement of beam rotation capacity did not obtained by just application of slit in

CBS-29, while modification of studs layout in CBS-29M resulted to considerable improvement of cumulative rotation capacity, which is comparable with bare steel beam.

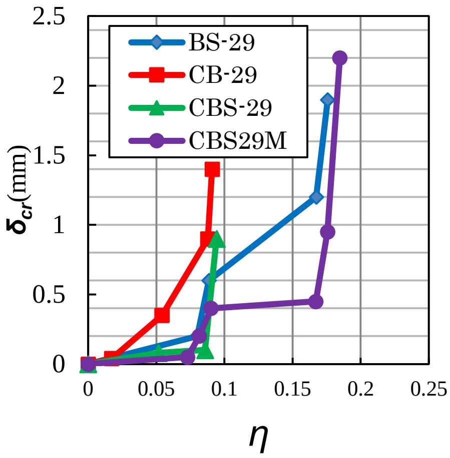

Fig. 4.29 Crack growth

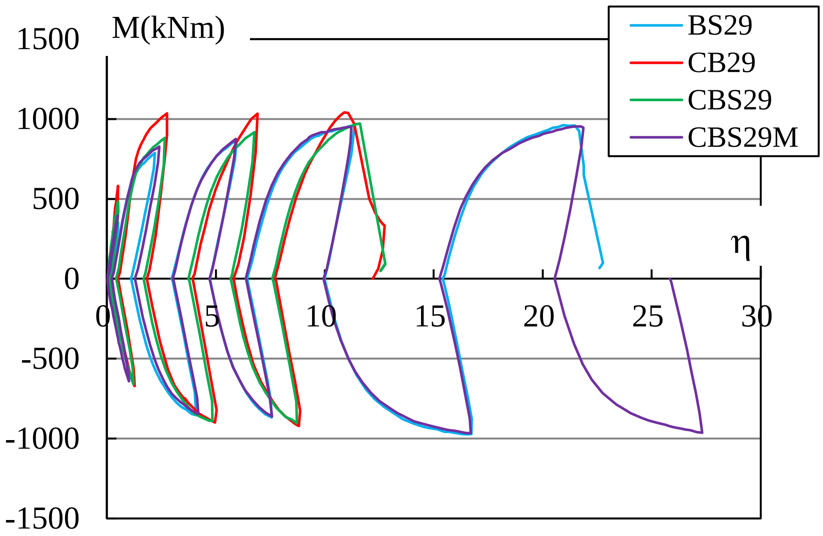

Fig. 4.30 Beam moment versus cumulative plastic rotation

Table 4.6 Cumulative rotation capacity

Specimen	**η**
BS-29	20.44
CB-29	10.70
CBS-29	10.85
CBS-29M	20.50

4.5. Conclusion and recommendations

According to this research investigation, conclusion can be summarized as follows:

1- Experimental test results showed that existence of slit could reduce the strain on the lower flange. But improvement of behavior regarding rotation capacity could be obtained by the removal of studs at the vicinity of connection.

2- Crack initiation in all specimens, regardless of bare steel or composite beam, happened at the root of scallop of beam lower flange. In bare steel beam specimen and both composite beam with slit specimens, crack initiation happened at almost similar cycle of loading, which was first cycle of +4.0 θ_p. But in the case of conventional composite beam specimen (CB-29), crack initiation occurred in much earlier cycle of loading (+2.0 θ_p). Also speed of crack opening was higher in this specimen.

3- Regarding the rack pattern of concrete slab, considerable developments of cracks corresponding to compression force were just occurred in the specimen with conventional composite beam CB-29. In this specimen compression crack developed parallel to the loading beam. While In both composite beam specimens with slit, CBS-29 and CBS-29M, limited cracks corresponding to compression force appeared, which remained almost around the transverse beam.

4- Finite element study showed that application of slit result to considerable reduction of axial force. But in large width-to-thickness ratio of 29 despite the existence of slit, still web is subjected to axial force. Removal of stud on the loading beam does not result to reduction of axial force, but removal of stud on the transverse beam resulted to the reduction to almost half.

5- Studs of transverse beam contribute in the composite action. It could be explained that these studs provide constraint condition for the slab and it may be the reason of contribution in the composite action. It is shown that roll of studs of transverse beam are similar to bearing stress transfer between slab and column face.

6- Contribution of studs of transvers beam depends on location of stud. Due to torsional behavior of transvers beam, second stud shear is considerably smaller than the first stud. So number of studs can be kept according to calculations, and just movement of first stud away from the column face is recommended.

7- Considering the actual seismic loading, removal of studs at the vicinity of connection on both loading and transverse beam is recommended.

5. Modeling of Composite Beam connected to RHS column

5.1 Introduction

Following to experimental test observations and findings of mechanical behavior investigated by FEA, in this chapter a model is proposed to represent the restraining characteristics of composite beam connected to RHS column.

5.2 Modeling specification

Model for the composite beam connected to RHS column is shown in Figure 5.1. In this model in order to consider the characteristics of out-of-plane deformation of web connection, the beam element is used and the web section is partially reduced at the vicinity of column face (just limited web section reduced near the connection). Plastic region of web can be obtained according to the result of limit analysis, presented in Chapter 3. Based on that result, the effective web section is decided.

Distribution of lack of section plays an important role. Past investigations proposed linear reduction of web section from the distance of column face. In this model almost half of beam height is reduced linearly.

Beam element is located in the center of steel beam. Concrete element prepared at center of concrete slab, corresponding to slab thickness. Concrete part modeled using truss element. Connection between steel beam and slab are connected by stiff beam element. Edge of stiff beam elements and concrete slab nodes are connected to shear springs, corresponding to stud restraining characteristics.

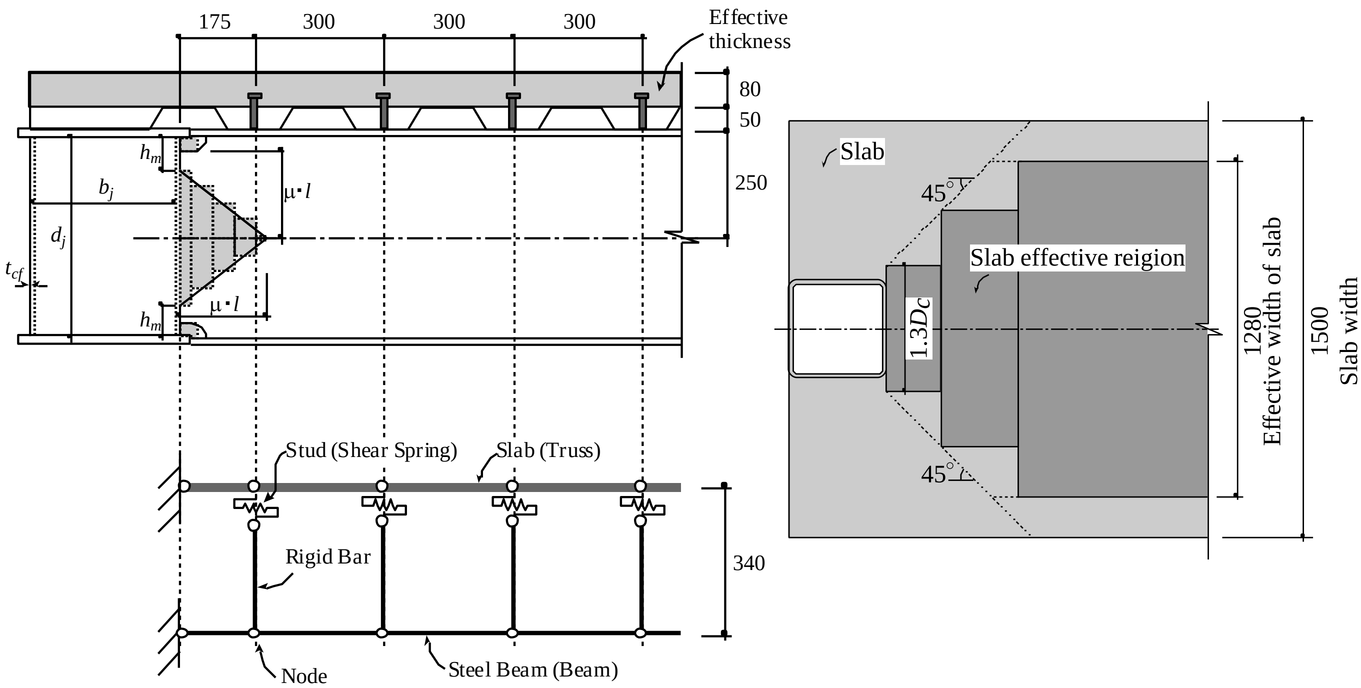

Fig. 5.1 Model for composite beam connected to RHS column

Material for steel, concrete and stud in the model is shown in Figure 5.2(a), (b) and (c) respectively. Concrete Material is selected as no-tension material. After reaching to f_c , linear softening happen, and concrete capacity is lost at 4% strain.

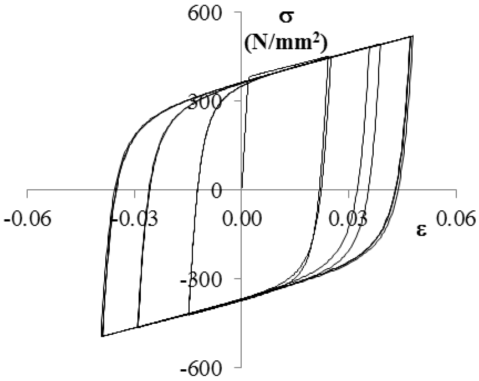

(a) Steel Material Model
(Menegotto-Pinto Model)

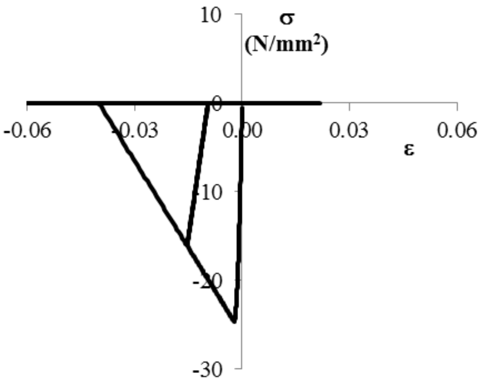

(b) Concrete Material Model
(Kent-Scott-Park + Karsan-Jirsa Model)

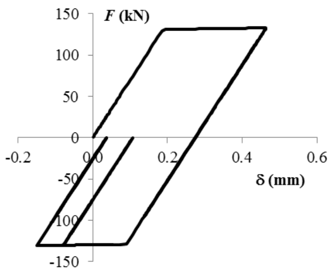

(c) Stud Shear Spring Model
(bi-Linear based on push out Test)

Fig. 5.2 Material model

5.3 Correspondence of model and test results

M_b-θ_b Hysteresis graphs are shown in Figure 5.3, which corresponds to column face moment and beam rotation. Two lines are used, which thicker solid line is corresponding to analysis and thinner red solid line is corresponding to the test result.

In all specimens acceptable good correspondence obtained from conducted analysis. Especially in BS29 quiet good correspondence can be observed. In the case of CB-22 effect of concrete bearing crush also simulated by the model analysis.

In the case of analysis quite simple behavior obtained comparing with actual test results, but acceptable correspondence can be found. In the small range of deformation some over estimation exist in the model.

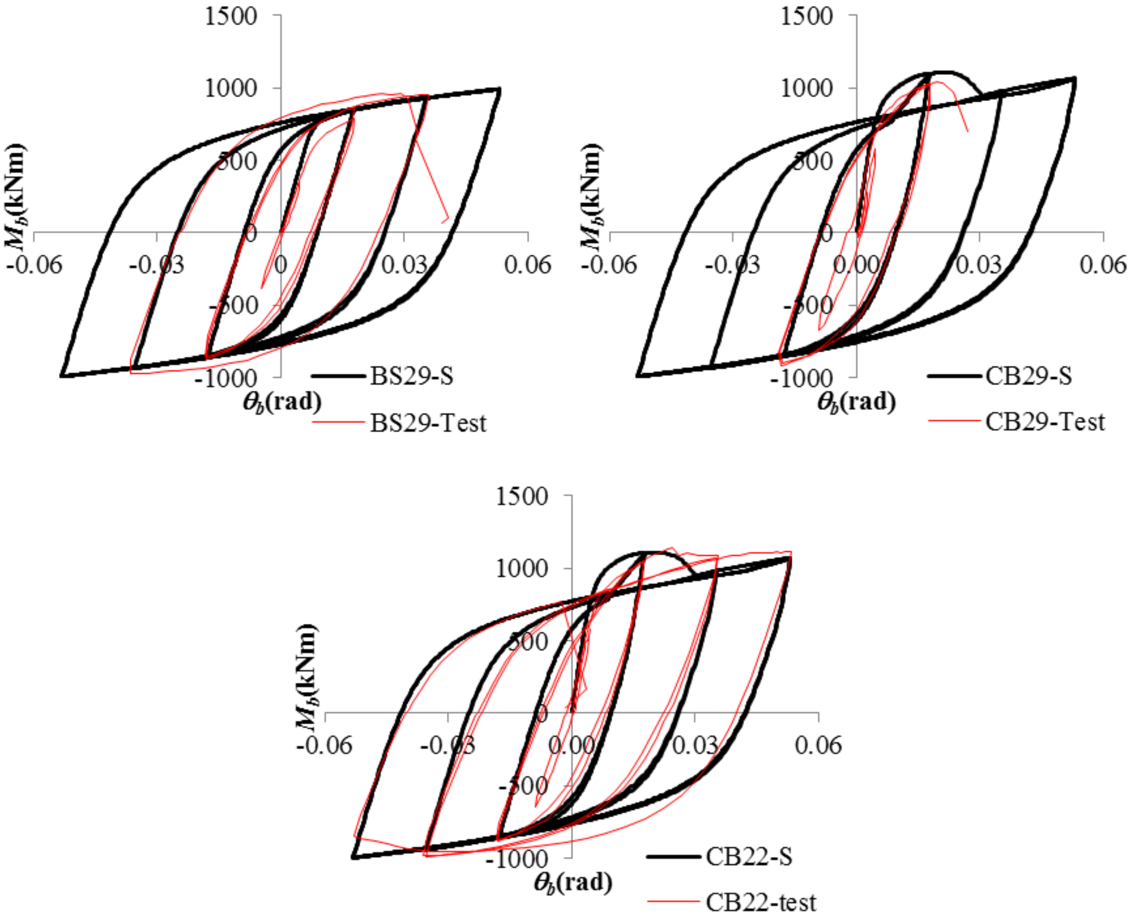

Fig. 5.3 M_b-θ_b Hysteresis diagrams

5.4 Total moment of each component

Moment components are shown in graphs of Figure 5.4. Black solid line corresponds to actual composite beam moment. Thin solid line corresponds to component of flange and thin dotted gray line corresponds to web component. Gray bold line corresponds to slab moment. Left figure is width-to-thickness ratio of zero, and right side figure is width-to-thickness ratio of 29 .Both specimens are scallop type of composite beam.

From the graphs it can be seen that model could show when concrete reach to its maximum capacity. The model could show that when concrete reach to its full capacity, beam total behavior continue strain hardening .

Model could determine relation between “slop of flange and web” versus “slab part”. Regardless of concrete reduction, still higher strength increase appear in the flange. So, still strain hardening is observed in the total behavior.

Maximum strength is appeared in the slop of between slab and steel beam part become in a comparable condition. After that strength reduction appeared. After around 3.0 θ_p , concrete reduction is finished and it keep zero, so again strain hardening is appeared.

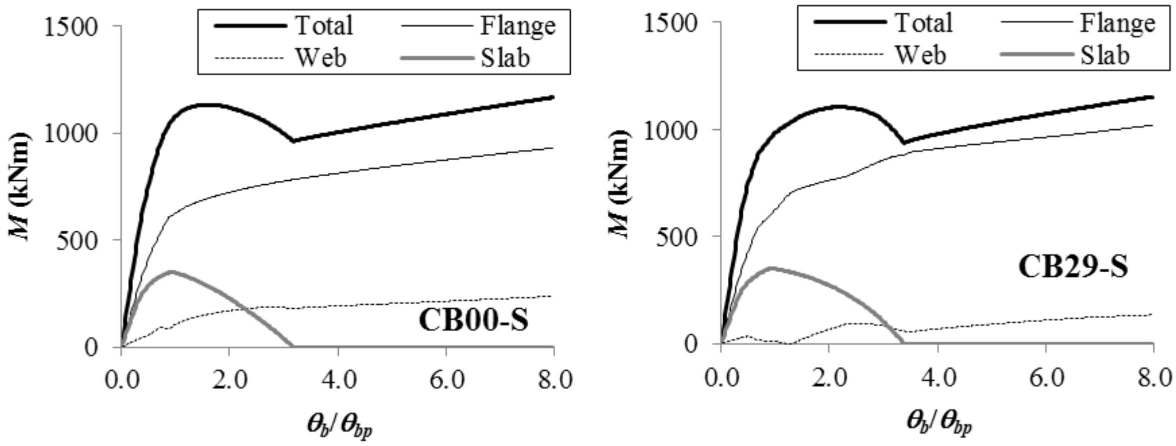

Fig. 5.4 Moment of each component

Figure 5.5 shows the effect of width-to-thickness ratio in each component. By comparison of each specimen web in the middle graph, moment reduction of web can be discussed. It can be seen that model could estimated that in CB29 the moment of web is quite small, while in CB00 considerable amount of web moment is obtained. It can be seen that effect of width-to-thickness ratio is more observed in the web moment component, rather than flange and slab component.

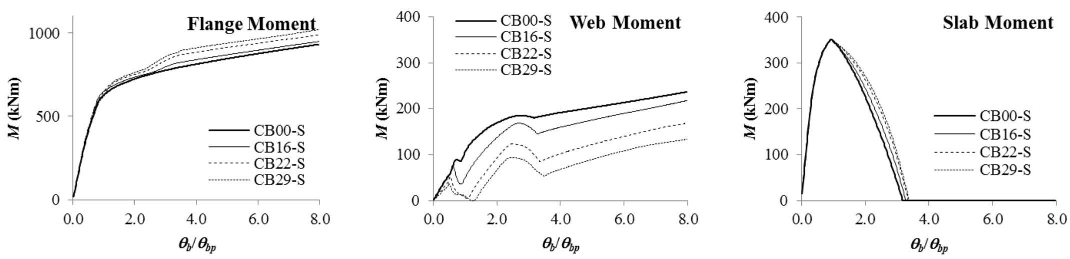

Fig. 5.5 Effect of width-to-thickness ratio in each component moment

5.5 Curvature and strain behaivior

Figure 5.6 illustrates curvature distribution along the beam length. Regardless of composite or bare steel beam it can be seen that quite comparable curvature distribution exist.

This is in confirmity with the findings of FEA study in chapter 3 (Sec.3.4.3), which was explained that curvature in not so different for bare steel beam and composite beam.

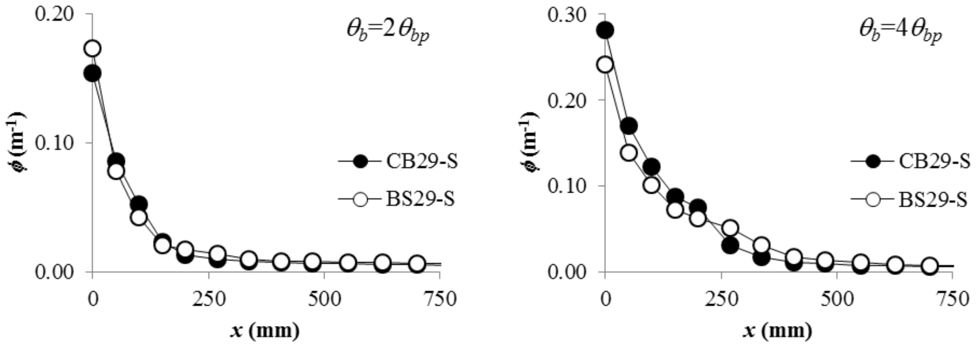

Fig. 5.6 Curvature distribution along the length of bare and composite beam

Figure 5.7 illustrates curvature in the column face for different width-to-thickness ratio for non-scallop bare steel beam and composite beam specimens. Curvature is defined as lower flange strain minus upper flange strain multiplying beam depth.

It can be seen that effect of width-to-thickness ratio is considerable in curvature in composite and bare steel beam. This is also in confirmity with the findings of FEA study in chapter 3 (Sec. 3.4.3), which was explained that curvature is different for different width-to-thickness ratio of bare steel beam and composite beam.

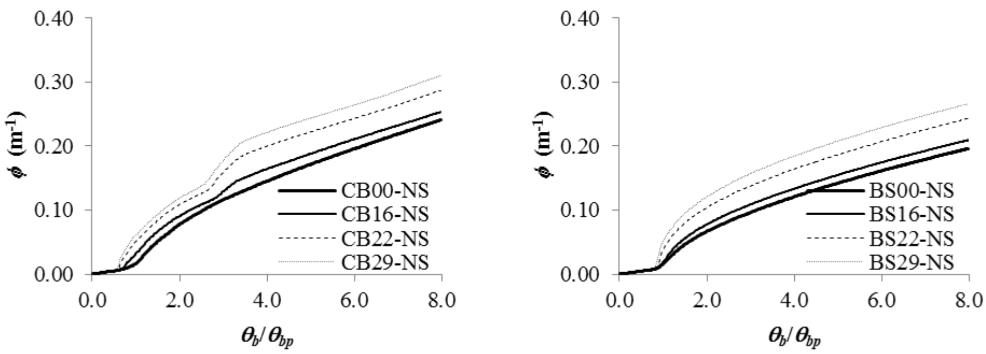

Fig. 5.7 Curvature versus beam rotation for different width-to-thickness ratios

In Figure 5.8 strain of beam flanges at the face of column is shown. Top two figures showing effect of width-to-thickness ratio in the bare and composite beam. Bellow two figures show comparison between bare and composite. Negative strain mean compression and positive strain corresponds to tension. Tension is appeared at lower flange and compression appeared at upper flange. In order to be in correspondence with actual geometrical condition, upper side is compression and lower side is corresponds to tension. Bold solid line is representing fixed connection, which all of section is effective section, without lack of section.

The model could show that regardless of composite or bare, in lower flange comparable effect of width-to-thickness ratio can be seen. Increase of width-to-thickness ratio results to increase of strain.

In the case of composite beam, upper flange show smaller strain than lower flange because of concrete constrain. Not only in lower flange, also in upper flange effect of width-to-thickness ratio can be seen.

In the case of lower flange, larger width-to-thickness ratio show higher strain. In the case of upper flange, smaller width-to-thickness ratio show higher strain. But when rotation reach to more than 2.0 θ_p , significant increase of the strain can be seen in the upper flange, and finally in larger than 3.0 θ_p, again larger width-to-thickness ratio show higher strain (no difference in slop). This is corresponding to concrete softening which is started from 1.0θ_p to 3.0θ_p.

The model could show the effect of composite action, and strain concentration on the lower flange can be seen by increasing of width-to-thickness ratio. Model is capable of showing effect of concrete damage. It can be seen that in both flanges strain condition change following to crush in the concrete.

Comparison of composite and bare can be conducted according to two bellow figures. Right side graph shows that, until 2θ_p upper flange strain is quite small. While lower flange strain is quite high, comparing with bare steel beam. After around 3.0θ_p some higher strain exist, but difference between difference of composite and bare become small (even if upper flange the strain of composite CB29 became a little more than bare BS29). But left side graph shows that reduction of width-to-thickness ratio resulted to reduction of lower flange strain, and increase of upper flange strain. CB00 representing fixed connection, and it can be seen that effect of composite action is quite limited comparing with CB29. So, the model could show that composite action is significantly affected by width-to-thickness ratio.

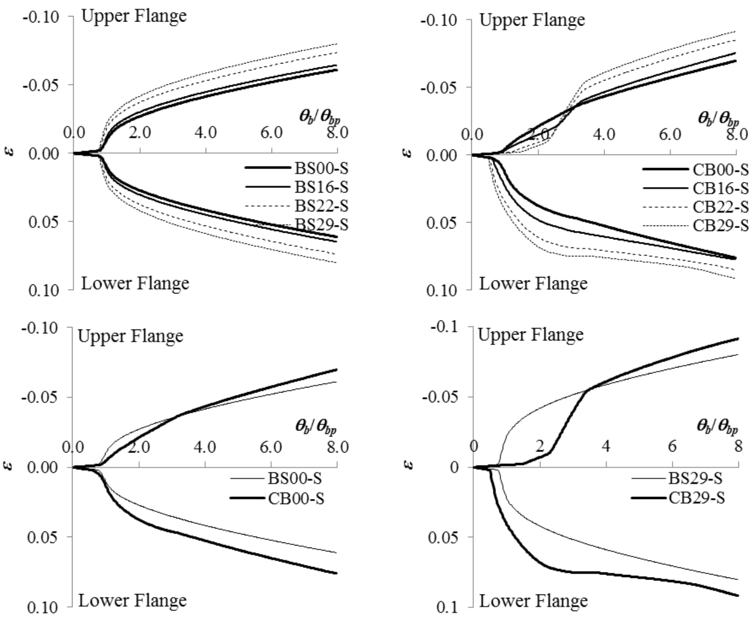

Fig. 5.8 Strain behavior

5.6 Estimation of relation of web and slab axial force

According to findings of chapter 2 and 3, effect of web axial force in the behavior of composite beam is considerable. The model is capable of estimation of relation between concert compression capacity and web axial force for different width-to-thickness ratios, shown in Figure 5.9.

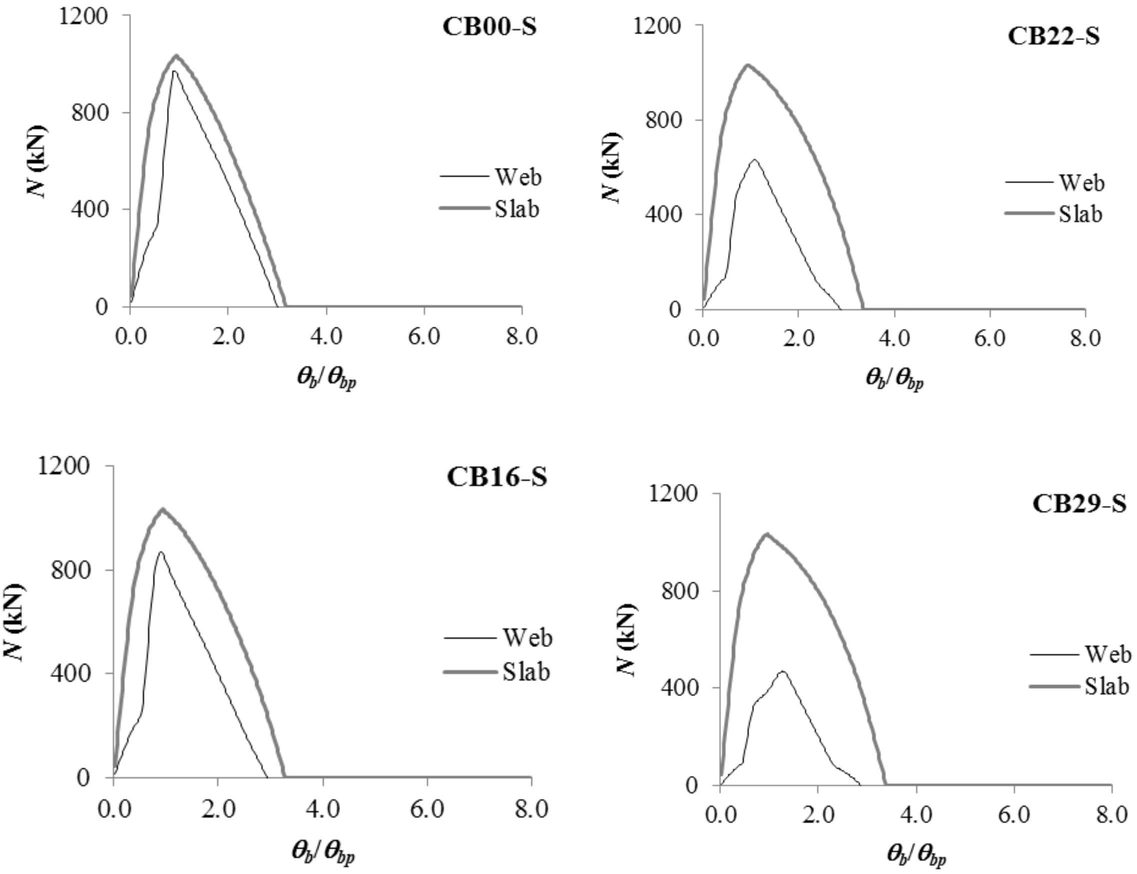

Fig. 5.9 Relation of web and slab axial force

5.7 Conclusions

Following to experimental test observations and findings of mechanical behavior investigated by FEA, a model is proposed to represent the restraining characteristics of composite beam connected to RHS column. The following conclusions are made:

1- In all specimens acceptable good correspondence of restraining characteristics obtained from conducted analysis by this model and experimental test results.

2- Effect of concrete bearing crush could be considered by the model. The model is also capable of estimation of each component moment in the composite beam.

3- Curvature distribution along the beam length and strain behavior obtained by the model has correspondance with the mechanical findings of finite element analysis in Chapter 3.

6. Conclusions

In this research, in order to investigate the elasto-plastic behavior of composite beam connected to the RHS column, cyclic loading test were conducted on T-shaped subassemblies of beam-to-RHS column connections with different width-to-thickness ratios. This study could show the effect of composite action on the elastic stiffness, strength and rotation capacity of composite beam comparing with the bare steel beam. Also it could clarify the effect of RHS width-to-thickness ratio and contribution of concrete slab on the strain condition of beam lower flange. Reasons of different rotation capacity are discussed through the detail study on the occurrence of different damages in the steel beam and concrete slab. It is shown that Occurrence of sever concrete bearing crush at the face of RHS column of specimen with width-to-thickness ratio of 22 resulted to considerable reduction of strain on the lower flange. Strain study showed that although in the early stages of loading the amount of strain was higher than bare steel beam with width-to-thickness ratio of 29, but concrete crush resulted to considerable reduction in the rate of strain increase. This resulted to delay in crack initiation and progress at the root of scallop. Finally higher cumulative rotation capacity was observed.

Following to experimental test observations, further research is conducted to clarify the structural condition of web connection. Finite element analysis study is conducted to understand the mechanical effects of composite action and out-of-plane deformation of RHS column on the elasto-plastic behavior of composite beam. Mechanism of stress transfer and strain concentration is shown by the means of FEA results. Finally, a model is proposed to represent the restraining characteristics of composite beam connected to RHS column.

The following conclusions are made by study the effect RHS column width-to-thickness ratio on the rotation capacity of composite beam in experimental tests:

- In all specimens regardless of existence of concrete slab or width-to-thickness ratio of RHS column, first crack initiation was occurred at the root of weld access hole (scallop). For the composite beam specimen CB-29 this occurred at earlier stage with higher progress, comparing with the bare steel beam connected to the RHS column with same *B/t* ratio (BS-29 specimen) and composite beam connected to RHS column with smaller *B/t* ratio (CB-22 specimen). Final failure pattern was determined by propagation of this crack.

- In the beam connected to RHS column with width-to-thickness ratio of 29, composite action resulted to 27% increase of actual plastic strength and 92% increase of stiffness in positive flexure, comparing with bare steel beam connected to RHS column with same with-to-thickness ratio. But cumulative rotation capacity of composite beam significantly reduced comparing with bare steel beam. Strain study in the first cycle of +2.0 θ_p showed that composite action increased the strain amount of lower flange 2.2 Times of bare steel beam. This strain condition resulted to early crack initiation with higher progress, and finally reduction of rotation capacity of composite beam.

- Reduction of RHS column width-to-thickness ratio in CB-22 specimen, did not result to considerable difference in the actual plastic strength and elastic stiffness in positive flexure comparing with CB-29, but %10 increase of beam ultimate strength observed. Also considerable improvement in the cumulative rotation capacity observed which was 4.2 times of CB-29. Experimental test results revealed another specific difference between composite specimens. It was observed that in the specimen with smaller width-to-thickness ratio severe concrete bearing crush happened at the vicinity of column face.

- Strain behavior study in CB-22 specimen, showed that in the first cycle of +2.0 θ_p , the amount of strain in the lower flange of CB-22 specimen was 55% smaller than CB-29 and 20% more than bare steel beam BS-29, but after the occurrence of sever crush in the concrete slab, sudden reduction in the tangent of strain in the lower flange happened. This resulted to smaller rate of strain increase, even comparing to the bare steel beam BS 29. Finally, this resulted to higher rotation capacity of CB-22 comparing with CB-29 and also BS-29.

- Occurrence of concrete crush can be considered as the start of removal of composite effect and start of closing to the bare steel beam condition. This showed that Further investigation about the mechanism of stress and strain transfer of composite beam is needed.

- It was observed that for same connection factor (α) cumulative rotation of composite beam (η) is reduced to almost less than half of bare steel beam.

The following conclusions are made from study of mechanism of elasto-plastic behavior of composite beam connected to RHS column:

- Derived equations obtained from limit analysis could show both effects of RHS column width-to-thickness ratio and axial force on reduction of composite beam web connection flexural strength, simultaneously.

- Adopted finite element model could show acceptable correspondence with test results. Finite element study showed that in both bare steel beam and composite beam effect of RHS column width-to-thickness ratios is considerable in the global behavior. But despite this similarity, different behavior in characteristics of strain hardening of composite beam can be seen. In the smaller width-to-thickness ratio of composite beam, by progress of rotation tendency of reaching to higher capacity exist. After that sudden strength reduction occur and keeping the constant strength after that reduction.

- In both bare steel beam and composite beam considerable effect of width-to-thickness ratio was shown in the strain behavior of flanges and web moment capacity. Finite element study showed that in the composite beam, effect of width-to-thickness is significant in the axial force of web, but slab force is less affected by width-to-thickness ratio.

- Mechanism of stress transfer is shown. It was found that start of concrete bearing crush is corresponding to start of stress increase of top flange. It was also found that maximum web axial force is not always happen at same time with start of softening of slab. In fact, in large width-to-thickness ratio reduction of axial force is first treated by flange. Top flange yield can be treated as a bench mark in the change of behavior. Sudden reduction in the total strength of M_b-θ_b curve corresponds to top flange yield.

- Mechanism of strain concentration is explained. It is shown that in the bare steel beam and composite beam difference between strain corresponding to reduction of web flexural capacity is small. However, this difference between strain condition of bare steel beam and composite beam is determined by the axial strain. It is shown that reduction of web flexural capacity does not result to further additional strain concentration, comparing to the bare steel beam. While axial strain due to movement of neutral axis result to more sever condition of strain in the composite beam.

- It is shown that effect of composite action to the curvature in not considerable. While effect of width-to-thickness ratio to the curvature and movement of neutral axis is considerable. So, the additional axial strain in the composite beam is depending on the width-to-thickness ratio of RHS column.

- By application of above findings a model proposed for evaluation of ultimate flexural strength of composite beam. This model prepared for the conditions which the neutral axis remain in the beam web. After the neutral axis exceeds the boundary of Mechanism II and enters the upper flange, modification in the stress condition of upper flange is needed. Accuracy of the model is verified by correspondence between the test results and model. Good agreement was observed for specimens which the web axial force did not exceed the boundary of Mechanism II.

The following conclusions are made from study the effect of slit and stud layout modification on the rotation capacity of composite beam:

- Experimental test results showed that existence of slit could reduce the strain on the lower flange. But improvement of behavior regarding rotation capacity could be obtained by the removal of studs at the vicinity of connection.

- Crack initiation in all specimens, regardless of bare steel or composite beam, happened at the root of scallop of beam lower flange. In bare steel beam specimen and both composite beam with slit specimens, crack initiation happened at almost similar cycle of loading, which was first cycle of +4.0 θ_p. But in the case of conventional composite beam specimen (CB-29), crack initiation occurred in much earlier cycle of loading (+2.0 θ_p). Also speed of crack opening was higher in this specimen.

- Regarding the rack pattern of concrete slab, considerable developments of cracks corresponding to compression force were just occurred in the specimen with conventional composite beam CB-29. In this specimen compression crack developed parallel to the loading beam. While In both composite beam specimens with slit, CBS-29 and CBS-29M, limited cracks corresponding to compression force appeared, which remained almost around the transverse beam.

- Finite element study showed that studs of transverse beam contribute in the composite action. It could be explained that these studs provide constraint condition for the slab and it may be the reason of contribution in the composite action. It is shown that roll of studs of transverse beam are similar to bearing stress transfer between slab and column face.

- Contribution of studs of transvers beam depends on location of stud. Due to torsional behavior of transvers beam, second stud shear is considerably smaller than the first stud. So number of studs can be kept according to calculations, and just movement of first stud away from the column face is recommended

- Considering the actual seismic loading, removal of studs at the vicinity of connection on both loading and transverse beam is recommended.

The following conclusions are made from the modeling of composite beam connected to RHS column:

- Following to experimental test observations and mechanical investigations by FEA, a model is proposed to represent the restraining characteristics of composite beam connected to RHS column.

- In all specimens acceptable good correspondence obtained from conducted analysis by this model and experimental test results.

- The model is capable of estimation of each component moment in the composite beam.

- Curvature distribution along the beam length and strain behavior obtained by the model has correspondance with the mechanical findings of finite element analysis in the Chapter 3.

References

Chapter 1:

1-1) AIJ, 1995d. “Performance of steel buildings during the 1995 Hyogoken-Nanbu earthquake”, Architectural Institute of Japan, *Tokyo* (1995)

1-2) AIJ, 1996. “Damage and Lessons of Steel Structures in the Hyogoken-Nanbu earthquake”, Architectural Institute of Japan, (1996)

1-3) “Recommendation for Design of Connections in Steel Structures”, Architectural Institute of Japan (AIJ) , pp. 139-141, Tokyo, Japan (2006)

1-4) Okada k. and S. Yamada; “Experimental Study on Deformation Capacity of Composite Beams With Conventional Type Beam-to-Column Connections (Evaluation of earthquake resistance of steel moment frames considering deformation capacity of composite beams, Part I)”, *J. Struct. Constr. Eng. ,AIJ,* No. 547, pp. 161–168, *Japan* (September 2001)

1-5) Okada K., T. Sang-Hoon and S. Yamada; “Tests On Ductility Capacity of Composite Beams,” *Proceedings of 7th Pacific Structural Steel Conference (PSSC).*, *USA* (2004)

1-6) Matsuo A., Y. Nakamura; “A Study on Strain and Plastic Deformation Capacity of Composite Beam-to-RHS Column with Thorough Diaphragm (Part1: Experimental Planning and Result)”, *Proceedings of Annual Meeting of Architectural Institute of Japan(AIJ)*, pp. 535–536, *Japan* (September 1999)

1-7) Tanaka T., K. Suita and N. Asakura; “Cyclic Loading Tests on Composite Beams with Scallops (Deformation Capacity Evaluation of Welded Beam to Column Connections Subjected to Repeated Plastic Strain, Part-15) ,” *Proceedings of Annual Meeting of Architectural Institute of Japan(AIJ), Japan*, pp. 745–746 (2013)

Chapter 2:

2-1) Okada k. and S.Yamada; "Experimental Study on Deformation Capacity of Composite Beams With Conventional Type Beam-to-Column Connections (Evaluation of earthquake resistance of steel moment frames considering deformation capacity of composite beams, Part I)", *J. Struct. Constr. Eng. ,AIJ,* No. 547, pp. 161–168, *Japan* (September 2001)

2-2) Okada K., T. Sang-Hoon and S. Yamada; "Tests On Ductility Capacity of Composite Beams," *Proceedings of 7th Pacific Structural Steel Conference (PSSC)., USA* (2004)

2-3) Matsuo A. and Y. Nakamura; "A Study on Strain and Plastic Deformation Capacity of Composite Beam-to-RHS Column with Thorough Diaphragm (Part1: Experimental Planning and Result)", *Proceedings of Annual Meeting of Architectural Institute of Japan(AIJ),* pp. 535–536, *Japan* (September 1999)

2-4) Tanaka, T., K. Suita and N. Asakura; "Cyclic Loading Tests on Composite Beams with Scallops (Deformation Capacity Evaluation of Welded Beam to Column Connections Subjected to Repeated Plastic Strain, Part-15) ," *Proceedings of Annual Meeting of Architectural Institute of Japan(AIJ), Japan*, pp. 745–746 (2013)

2-5) Beedle L.S.; "Plastic Design of Steel Frames", Lehigh University, 1st ed., pp.23-52, Bethlehem, US, (October 1958)

2-6) "Design Recommendations for Composite Constructions", Architectural Institute of Japan (AIJ), pp. 63-101, *Japan* (2010)

2-7) "Recommendation for Design of Connections in Steel Structures", Architectural Institute of Japan (AIJ), pp. 139-141, *Japan* (2006)

2-8) Chen S. and Y.C. Chao; "Effects of composite action on seismic performance of steel moment connections with reduced beam sections", *Journal of constructional steel research* , No.57 , pp. 417-434, *Japan* (2001)

Chapter 3:

3-1) Suita K. and T. Tanaka; “Flexural Strength of Beam Web to Square Tube Joints”, *Journal of Steel Construction Engineering,* Vol.7 No.26, pp. 51–58, *Japan* (June 2000)

3-2) “Recommendation for Design of Connections in Steel Structures”, Architectural Institute of Japan (AIJ), pp. 139-141, (2006)

3-3) Mansfield E. H.; “Studies in Collapse Analysis of Rigid-Plastic Plates with a Square Yield Diagram”, Proc. Of the Royal Society London, 241, Series A, pp.311-338, (August 1957)

3-4) Prager W.; “An Introduction to Plasticity”, Addison-Wesley Publishing Company, INC., (1959)

3-5) Design Recommendations for Composite Constructions”, Architectural Institute of Japan (AIJ), pp. 63-101, *Japan* (2010)

3-6) Tateyama E., K. Inoue and T. Arai; “Strength and Deformability of Composite Beam connected to Steel Column”, Proceedings of the Third International Conference on Steel-Concrete Composite Structures, pp.551-556, (September 1991)

3-7) Tsukada T., T. Tanaka and K. Suita; “Influence of Composite Slab on Strain Distribution of Beam Flanges, Part 11”, Summaries of technical papers of meeting of AIJ Kinki Branch, pp.1213-1214, (September 2012)

3-8) Okada K., T. Sang-Hoon and S. Yamada; “Tests On Ductility Capacity of Composite Beams,” *Proceedings of 7th Pacific Structural Steel Conference (PSSC)., USA* (2004)

3-9) Matsuo A. and Y. Nakamura; “A Study on Strain and Plastic Deformation Capacity of Composite Beam-to-RHS Column with Thorough Diaphragm (Part1: Experimental Planning and Result)”, *Proceedings of Annual Meeting of Architectural Institute of Japan(AIJ),* pp. 535–536, *Japan* (September

1999)

3-10) Tanaka T., K. Suita and N. Asakura; “Cyclic Loading Tests on Composite Beams with Scallops (Deformation Capacity Evaluation of Welded Beam to Column Connections Subjected to Repeated Plastic Strain, Part 15) ,” *Proceedings of Annual Meeting of Architectural Institute of Japan(AIJ), Japan*, pp. 745–746 (2013)

Chapter 4:

4-1) Matsuo A. and Y. Nakamura; “A Study on Strain and Plastic Deformation Capacity of Composite Beam-to-RHS Column with Thorough Diaphragm (Part1: Experimental Planning and Result)”, *Proceedings of Annual Meeting of Architectural Institute of Japan(AIJ),* pp. 535–536, *Japan* (September 1999)

3-1) Tagawa Y., I.Nishiyama and I. Yang; “*Elasto-Plastic Behavior of New Composite Beam System”, International Journal of Steel Structures*, Vol.3 , pp.45-52 (2003).

4-2) Yamashita T., M.Ohsaki, T. Miyamura, M. Kohiyama, Z. Jingyao; “Finite Element Model of Steel-Concrete Composite Beam for High-Precision Seismic Response Analyses of Four-Story Steel Frame”, *Proceedings of International Symposium on Disaster Simulation & Structural Safety in the Next Generation (DSII), Japan* (2011)

4-3) AISC 360-10; “Specification for Structural Steel Buildings”, American Institute of Steel Construction, pp. 16.1–xlviii, *Chicago, US* (22 June 2010)

4-4) AISC 341-10; “Seismic Provisions for Structural Steel Buildings” , American Institute of Steel Construction, June 2010, *Chicago, US* (2010)

Bibliography

1) Mansfield E. H.; "Studies in Collapse Analysis of Rigid-Plastic Plates with a Square Yield Diagram", Proc. Of the Royal Society London, 241, Series A, pp.311-338, (August 1957)

2) Beedle L. S.; "Plastic Design of Steel Frames", Lehigh University, 1st ed., pp.23-52, Bethlehem, US, (October 1958)

3) Prager W.; "An Introduction to Plasticity", Addison-Wesley Publishing Company, INC., (1959)

4) Tateyama E., K. Inoue and T. Arai; "Strength and Deformability of Composite Beam connected to Steel Column", Proceedings of the Third International Conference on Steel-Concrete Composite Structures, pp.551-556, (September 1991)

5) AIJ, 1995d. Performance of steel buildings during the 1995 Hyogoken-Nanbu earthquake, Architectural Institute of Japan, Tokyo (1995)

6) AIJ, 1996. Damage and Lessons of Steel Structures in the Hyogoken-Nanbu earthquake, Architectural Institute of Japan, (1996)

7) Matsuo A., Y. Nakamura; "A Study on Strain and Plastic Deformation Capacity of Composite Beam-to-RHS Column with Thorough Diaphragm (Part1: Experimental Planning and Result)", *Proceedings of Annual Meeting of Architectural Institute of Japan(AIJ),* pp. 535–536, *Japan* (September 1999)

8) Suita K. and T. Tanaka; "Flexural Strength of Beam Web to Square Tube Joints", *Journal of Steel Construction Engineering*, Vol.7 No.26, pp. 51–58, *Japan* (June 2000)

9) Okada k. and S. Yamada; “Experimental Study on Deformation Capacity of Composite Beams With Conventional Type Beam-to-Column Connections (Evaluation of earthquake resistance of steel moment frames considering deformation capacity of composite beams, Part I)”, *J. Struct. Constr. Eng. ,AIJ,* No. 547, pp. 161–168, *Japan* (September 2001)

10) Chen S. and Y.C. Chao; “Effects of composite action on seismic performance of steel moment connections with reduced beam sections”, *Journal of constructional steel research* , No.57 , pp. 417-434, *Japan* (2001)

11) Tagawa Y., I.Nishiyama and I. Yang (2003). “*Elasto-Plastic Behavior of New Composite Beam System”, International Journal of Steel Structures*, Vol.3 , pp.45-52 (2003)

12) Okada K., T. Sang-Hoon and S. Yamada; “Tests On Ductility Capacity of Composite Beams,” *Proceedings of 7th Pacific Structural Steel Conference (PSSC).*, *USA* (2004)

13) Recommendation for Design of Connections in Steel Structures, Architectural Institute of Japan (AIJ) , Tokyo (2006)

14) AISC 360-10; “Specification for Structural Steel Buildings”, American Institute of Steel Construction, pp. 16.1–xlviii, Chicago, US (22 June 2010)

15) AISC 341-10; “Seismic Provisions for Structural Steel Buildings” , American Institute of Steel Construction, June 2010, Chicago, US . (2010)

16) Design Recommendations for Composite Constructions, Architectural Institute of Japan (AIJ), pp. 63-101, *Japan* (2010)

17) Yamashita T., M.Ohsaki, T. Miyamura, M. Kohiyama, Z. Jingyao; “Finite Element Model of Steel-Concrete Composite Beam for High-Precision Seismic Response Analyses of Four-Story Steel Frame”, *Proceedings of International Symp. On Disaster Simulation & Structural Safety in the next generation (DSII), Japan* (2011)

18) Tsukada T., T. Tanaka and K. Suita, Influence of Composite Slab on Strain Distribution of Beam Flanges, Part 11, Summaries of technical papers of meeting of AIJ Kinki Branch, pp.1213-1214, (September 2012)

19) Tanaka T., K. Suita and N. Asakura; “Cyclic Loading Tests on Composite Beams with Scallops (Deformation Capacity Evaluation of Welded Beam to Column Connections Subjected to Repeated Plastic Strain, Part-15) ,” *Proceedings of Annual Meeting of Architectural Institute of Japan(AIJ), Japan*, pp. 745–746 (2013)